

University of Groningen

Rational Design in Photopharmacology with Molecular Photoswitches

Kobauri, Piermichele; Dekker, Frank J.; Szymanski, Wiktor; Feringa, Ben L.

Published in:
Angewandte Chemie - International Edition

DOI:
[10.1002/anie.202300681](https://doi.org/10.1002/anie.202300681)

IMPORTANT NOTE: You are advised to consult the publisher's version (publisher's PDF) if you wish to cite from it. Please check the document version below.

Document Version
Version created as part of publication process; publisher's layout; not normally made publicly available

Publication date:
2023

[Link to publication in University of Groningen/UMCG research database](#)

Citation for published version (APA):

Kobauri, P., Dekker, F. J., Szymanski, W., & Feringa, B. L. (2023). Rational Design in Photopharmacology with Molecular Photoswitches. *Angewandte Chemie - International Edition*, 62(30), Article e202300681. <https://doi.org/10.1002/anie.202300681>

Copyright

Other than for strictly personal use, it is not permitted to download or to forward/distribute the text or part of it without the consent of the author(s) and/or copyright holder(s), unless the work is under an open content license (like Creative Commons).

The publication may also be distributed here under the terms of Article 25fa of the Dutch Copyright Act, indicated by the "Taverne" license. More information can be found on the University of Groningen website: <https://www.rug.nl/library/open-access/self-archiving-pure/taverne-amendment>.

Take-down policy

If you believe that this document breaches copyright please contact us providing details, and we will remove access to the work immediately and investigate your claim.

Downloaded from the University of Groningen/UMCG research database (Pure): <http://www.rug.nl/research/portal>. For technical reasons the number of authors shown on this cover page is limited to 10 maximum.

Photoswitches

How to cite:

International Edition: doi.org/10.1002/anie.202300681

German Edition: doi.org/10.1002/ange.202300681

Rational Design in Photopharmacology with Molecular Photoswitches

Piermichele Kobauri, Frank J. Dekker, Wiktor Szymanski, and Ben L. Feringa**Angewandte
International Edition
Chemie

Abstract: Photopharmacology is an attractive approach for achieving targeted drug action with the use of light. In photopharmacology, molecular photoswitches are introduced into the structure of biologically active small molecules to allow for the optical control of their potency. Going beyond trial and error, photopharmacology has progressively applied rational drug design methodologies to devise light-controlled bioactive ligands. In this review, we categorize photopharmacological efforts from the standpoint of medicinal chemistry strategies, focusing on diffusible photochromic ligands modified with photoswitches that operate through *E-Z* bond isomerization. In the vast majority of cases, photoswitchable ligands are designed as analogs of existing compounds, through a variety of approaches. By analyzing in detail a comprehensive list of instructive examples, we describe the state of the art and discuss future opportunities for rational design in photopharmacology.

1. Introduction

Photopharmacology is an innovative discipline in medicinal chemistry and chemical biology that uses light to control the biological activity of molecules.^[1,2] The major goal of this emerging field is to solve the long-standing issue of on-target toxicity outside the disease location. On-target toxicity causes side (or adverse) reactions, which limits the application of, e.g., chemotherapeutics^[3,4] and statins.^[5] Such systemic effects occur outside the disease location, and ultimately threaten the safety of patients, thus reducing the benefits of the laborious processes of drug development, approval and pharmacovigilance.^[6,7]

In pursuit of Paul Ehrlich's "magic bullet" vision,^[8] established and clinically approved strategies to improve the therapeutic index^[9] of small molecule entities have been used for the development of drug delivery systems,^[10] antibody-drug conjugates,^[11] prodrugs,^[12] and soft drugs.^[13] To enhance the control over drug concentration at the site of action, or over spatially specific targeting, drug delivery nanotechnologies employ endo- or exogenous stimuli (e.g., pH, enzymatic activation, temperature, and ultrasound).^[14] On the other hand, antibody-drug conjugates provide targeted drug delivery by binding specific tumor-associated antigens.^[11]

With regard to small molecule design, prodrugs contain labile chemical modifications that temporarily silence their biological activity. The resulting changes in physicochemical

properties concurrently enhance the absorption, distribution, metabolism, excretion, and toxicity (ADMET) profile of the drugs.^[12] Conversely, soft drugs are designed to undergo metabolic conversion into non-toxic and inactive species.^[13] While both prodrugs and soft drugs feature metabolically liable sites, metabolism plays opposite roles, i.e., activating prodrugs and deactivating soft drugs.^[15]

Although the above-mentioned approaches represent great steps toward improved toxicity profiles, they mostly rely on endogenous metabolic conversions, which enable only limited and indirect control because they depend on localization and patient characteristics. In contrast, exogenous stimuli allow for a more direct control in terms of spatial and temporal resolution. Among other external triggers, such as magnetic field^[16] and acoustic waves,^[17] light has emerged as a non-invasive tool to achieve targeted drug action due to its high spatiotemporal precision and bi-orthogonality.^[18,19]

Alongside photodynamic therapy,^[20] light-mediated drug delivery,^[21] and optogenetics,^[22] photopharmacology has been evolving as a promising methodology for the optical control of biological processes.^[1,2,18,23–25] The incorporation of light-responsive moieties into the structure of drugs allows for irreversible or reversible modulation of their activity.^[26] When photocleavable protecting groups (or photocages) are introduced to mask pharmacophoric features, irradiation *irreversibly* removes the photolabile moiety, restoring the potency of the parent molecule. Conversely, when molecular photoswitches^[27] are introduced, irradiation triggers the *reversible* isomerization between two forms. These two isomers of the drug possess distinct structural and electronic features; hence, they are expected to show different potencies against the desired target.

In addition to its promising future prospects for drug discovery,^[25] reversible photopharmacology has showed great potential especially as a research tool for medicinal chemistry and chemical biology.^[24] When light, alone or in combination with thermal process, is able to switch between the drug forms with low and high potency, then both local drug activation (where needed) and inactivation (where potentially toxic) are possible. While the photoswitchable drug can be switched on locally for its on-target effect, it should be noted that the off-target toxicity profile^[5] will also be affected concurrently, albeit in an unpredictable way.^[1]

Since this review focuses on the development of photoswitchable small-molecule drugs (also known as diffusible photochromic ligands), the reader is referred to comprehen-

[*] Dr. P. Kobauri, Prof. Dr. W. Szymanski, Prof. Dr. B. L. Feringa
Stratingh Institute for Chemistry, University of Groningen
Nijenborgh 4, 9747 AG Groningen (The Netherlands)
E-mail: w.c.szymanski@rug.nl
b.l.feringa@rug.nl

Prof. Dr. F. J. Dekker
Chemical and Pharmaceutical Biology, Groningen Research Institute of Pharmacy, University of Groningen
A. Deusinglaan 1, 9713 AV Groningen (The Netherlands)

Prof. Dr. W. Szymanski
Department of Radiology, Medical Imaging Center, University of Groningen, University Medical Center Groningen
Hanzeplein 1, 9713 GZ Groningen (The Netherlands)
E-mail: w.szymanski@umcg.nl

© 2023 The Authors. Angewandte Chemie International Edition published by Wiley-VCH GmbH. This is an open access article under the terms of the Creative Commons Attribution License, which permits use, distribution and reproduction in any medium, provided the original work is properly cited.

sive reviews on the use of photocleavable protecting groups in biological contexts.^[28–30] Because a large number of references was necessary to categorize and identify trends within the field, the focus of the current analysis is on studies that report the use of molecular photoswitches that operate through the *E-Z* isomerization of a double bond. Regarding other photoswitches (e.g., spiropyrans, dithienylethenes, and donor-acceptor Stenhouse adducts), the interested reader is referred to previous extensive reviews.^[31–33] Finally, photochromic tethered ligands,^[18] photoswitchable peptides^[34] or nucleic acids^[35] are outside the scope of this review.

Molecular photoswitches are molecules that exist as two or more isomers that can be interconverted reversibly by means of light irradiation (Figure 1).^[27] The most common tools of reversible photopharmacology are *E-Z* photoswitches, which undergo isomerization between the (*E*)- and the (*Z*)-isomer upon irradiation with light. In particular, (heteroaryl)azobenzenes are the most frequently used switches, due to their robust photochemical behavior and synthetic accessibility.^[36] Irradiation with light of wavelength λ_1 promotes the photoisomerization of the thermally stable (*E*)-azobenzene to the metastable (*Z*)-azobenzene, which can revert to (*E*)-azobenzene either thermally or under irradiation with light of wavelength λ_2 (Figure 1). While (*E*)-azobenzene is planar, has an end-to-end distance of 9 Å and a dipole moment of 0 D, (*Z*)-azobenzene is bent, has an end-to-end distance of 6 Å and a dipole moment of 3 D.^[36]

Both isomers feature two hydrogen bond acceptors (HBAs) in the --N=N-- azo bond, although photoisomerization changes their directionality. In fact, (*E*)-azobenzene is able to engage in hydrogen bonds interactions on opposite sides of the azo bond, whereas (*Z*)-azobenzene is able to form interactions on the same side.

Among the heterocyclic variants of azobenzene,^[37] azopyrazole emerged as one of the most interesting photoswitches because of its quantitative photoisomerization in both directions and excellent solubility in water.^[32,38] The pyrazole ring provides an additional HBA in comparison to azobenzene. Hemithioindigo (HTI) is an emerging photoswitch that undergoes photoisomerization from the thermally stable (*Z*)-isomer to the metastable (*E*)-isomer upon irradiation with visible light.^[39] Both forms of HTI are nearly planar and show smaller changes in structure and electrostatics than azobenzene. In terms of hydrogen bonding capacity, HTI features a bidentate HBA.

All the photoswitches discussed above are T-type, because the isomerization from the metastable to the stable form can happen either thermally or photochemically. Conversely, for P-type switches, interconversion between the isomers is possible only with light. A typical example is stilbene, which undergoes *E*-to-*Z* and subsequent *Z*-to-*E* isomerization upon light irradiation. As compared to the previous photoswitches, stilbene does not contain any HBA.

For the majority of application scenarios,^[26] photopharmacology needs to design photoswitchable ligands that



Piermichele Kobauri studied chemistry at the University of Turin (Italy), where he received his MSc in 2016 under the supervision of Prof. Marco Lolli. He received his PhD at the University of Groningen (The Netherlands) in 2022 under the supervision of Prof. Ben L. Feringa and Prof. Wiktor Szymanski, on rational and computer-aided drug design approaches in photopharmacology. Currently, he is working at the pharma-tech company Aqemia in Paris (France). His research focuses on the development of computational workflows for the optimization of the drug discovery process.



Frank J. Dekker studied Pharmacy at Utrecht University, The Netherlands. He received his doctoral degree in Medicinal Chemistry in 2004 at Utrecht University. Subsequently, he did a postdoc in Chemical Biology at the Max Planck Institute for molecular physiology in Dortmund, Germany. In 2007, he moved to the university of Groningen, the Netherlands, to start his own research group on the development of chemical-biological methods for inhibition and detection of enzyme activity. In 2022 he became director of the master program Medical Pharmaceutical Sciences at the university of Groningen.



Wiktor Szymanski received his PhD degree from The Warsaw University of Technology, Poland. He then spent two years working on the use of biotransformations in organic chemistry with Prof. Ben L. Feringa and Prof. Dick B. Janssen at the University of Groningen. Since 2010 he has been working on the construction of photoactive protein-peptide- and DNA-bioconjugates and photopharmacology. In 2014, he joined University Medical Center Groningen, where he was appointed in 2015 as tenure track assistant professor and in 2019 as associate professor.



Ben L. Feringa obtained his PhD degree in 1978 at the University of Groningen in the Netherlands under the guidance of Prof. Hans Wynberg. After working as a research scientist at Shell he was appointed full professor at the University of Groningen in 1988 and as distinguished Jacobus H. van't Hoff Professor of Molecular Sciences in 2004. He is an elected foreign honorary member of the American Academy of Arts and Sciences and member of the Royal Netherlands Academy of Sciences. His research interests include stereochemistry, organic synthesis, asymmetric catalysis, molecular switches and motors, photopharmacology, self-assembly and nanosystems.

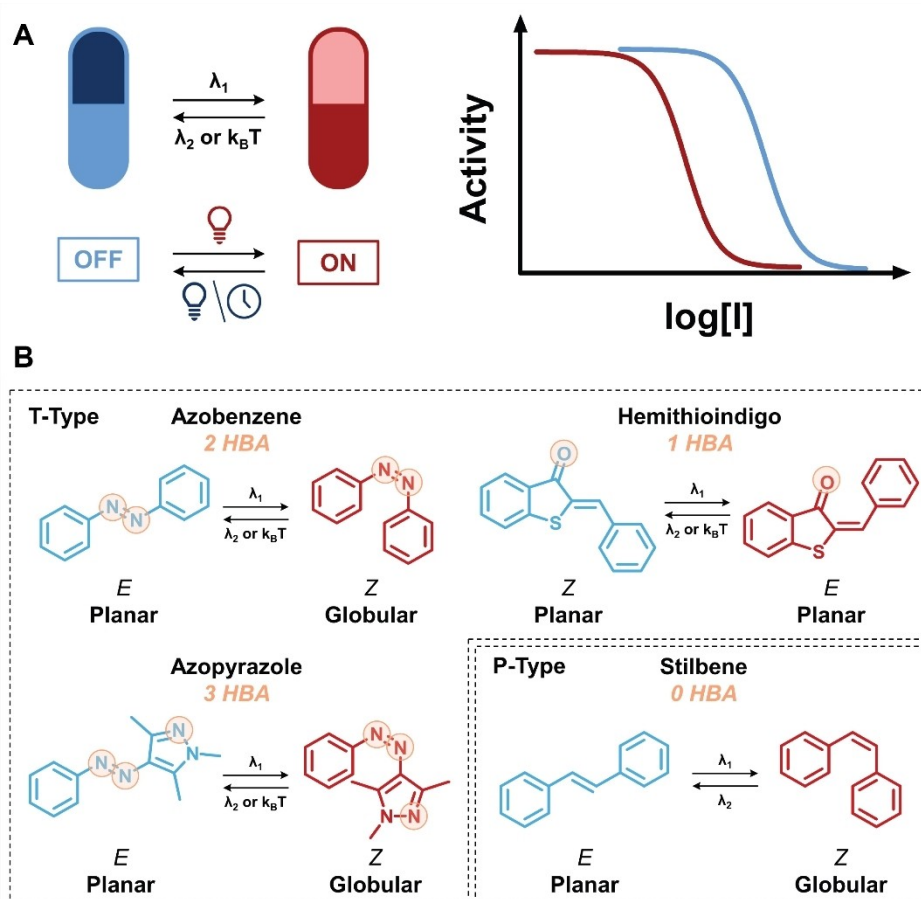


Figure 1. (A) Schematic representation of the principle of photopharmacology. In the ideal scenario, irradiation with light of wavelength λ_1 temporarily activates the drug by promoting photoisomerization to the metastable form, which loses its activity over time or upon irradiation with light of wavelength λ_2 . (B) Most common *E-Z* isomerization-based photoswitches used in photopharmacology. In general, photoisomerization promotes a reversible change from a planar to a globular structure, except for HTI. HBA are highlighted in orange.

are more potent in their metastable state, namely “(Z)-on” (or “*cis*-on”^[40]) for azobenzenes and “(E)-on” for HTIs. If the photoisomers of such “light-active” compounds also show large differences in potency, biological processes can be controlled effectively.^[1,23,24,26] Due to the strongly interdisciplinary nature of the field, the molecular design of photoswitchable agents combines elements of organic chemistry, photochemistry and medicinal chemistry.^[25] The resulting challenges go beyond typical molecular design for drug discovery:^[41] chemists have to design two forms, guided by the structures of known switches, and optimize the difference in potency, aiming at the thermally stable form to be less active.

Going beyond trial-and-error approaches, we believe that photopharmacology has enormous potential for assimilating rational drug design strategies. In this review, we analyze the state of the art in the rational design of photopharmacological agents and we outline the prospects for a more informed approach to photopharmacological design. We envision that the introduction of drug design approaches will help in the formal classification of photopharmacological efforts to date and in the recognition of opportunities for new design strategies, with the final aim of

translating photopharmacology from an academic setting to clinical applications.^[19]

2. Molecular Design in Photopharmacology

From a medicinal chemistry standpoint, photopharmacology is mainly concerned with analog design,^[42] using molecular photoswitches as building blocks (Figure 1). However, not only the potency of the original drug should be maintained or improved with the design of the new analog, but also the difference in potency between the photoisomers needs to be maximized, seeking activation upon irradiation.

The availability of prior knowledge determines the applicability of informed strategies in the design of photopharmacological agents. Two main rational drug design approaches can be distinguished, i.e., ligand-based and structure-based methods, both of which are usually supported by computational methods (Figure 2).^[43] Ligand-based methods are most suitable if there is limited structural information available about the target. They rely on affinity data of focused compound collections to reveal trends in qualitative or quantitative structure–activity relationships

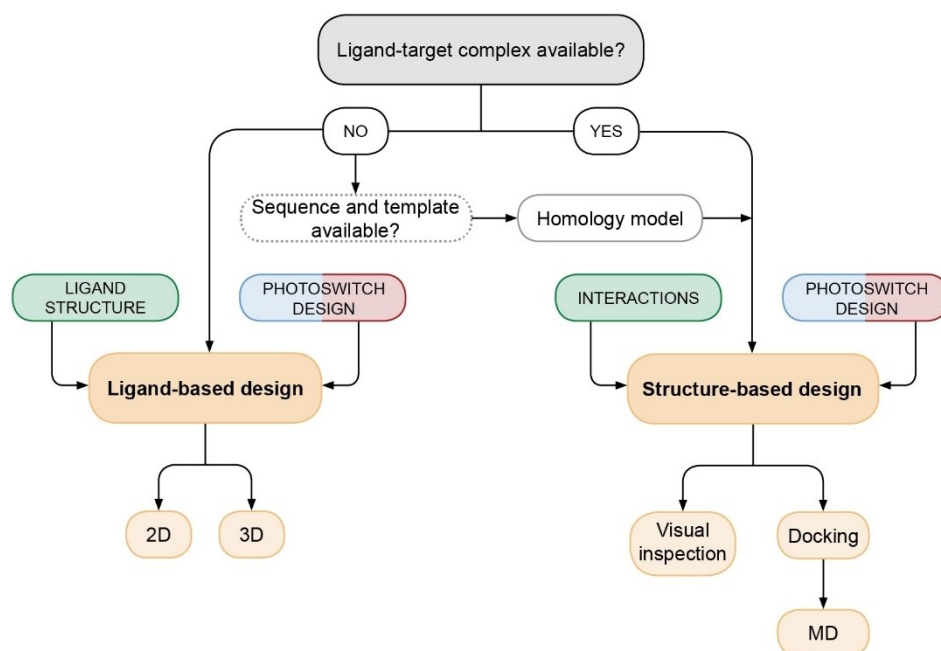


Figure 2. Decision tree for choosing between ligand- and structure-based design approaches for photopharmacology.

(SAR). Description of qualitative SAR can be achieved by 2D structures or descriptors^[44] (e.g., LogP, number of HBAs), or 3D considerations, such as shape^[45] or electrostatic potential (ESP) surface similarity,^[46] and pharmacophore modelling.^[47] SAR studies enable guided optimization of the affinity as well as the physico-chemical properties and *in vitro* ADMET properties of hit and lead compounds.

The use of structure-based drug design is preferred also for photopharmacological agents, if the structure of the desired target is available and if the site to which the ligand binds is known.^[48] Structural data allow for the visual inspection of the shape of a ligand-target complex or for computational exploration of hypotheses in ligand design.^[49] Knowledge about shape and electronic features of the binding pocket and the bioactive conformation support SAR analyses by enabling the identification of the most important ligand-protein intermolecular interactions. If the structure of the target has not been resolved, but the amino acid sequence and the 3D structure of a related target is available, then a homology model can be built to permit a certain degree of structure-based design.^[50]

The main computational techniques that drive structure-based drug design are molecular docking and molecular dynamics (MD) simulations.^[51] Molecular docking is a high-throughput method that predicts the binding mode of a ligand with the biological target.^[52] While docking calculations are static, MD simulations offer a time-dependent representation of the ligand-target complex.^[53] Both methods can be used *a priori*, i.e., to guide the hypothesis at the design phase, or *a posteriori*, i.e., to rationalize the results observed experimentally.^[48]

This review categorizes and critically discusses the design strategies used in photopharmacology, within the frame of ligand- and structure-based design approaches. In both

cases, a further distinction will be made if computer-aided drug design methods were used (e.g., density functional theory (DFT) calculations, pharmacophore modeling, molecular docking, MD), *a priori* or *a posteriori*.

To discuss the differences in potency between the photoisomers, we will use in this review the descriptor F , i.e., the ratio of the measures of drug efficacy (half-maximal inhibitory concentration (IC_{50}), inhibitory constant (K_i), minimum inhibitory concentration (MIC), etc.) of the two forms. For instance, in the case of (*Z*)-on ligands whose activity was quantified in terms of IC_{50} values, we use $F(E/Z)$, which is obtained by dividing the IC_{50} of the (*E*)-form by the IC_{50} of the (*Z*)-form. Analogously, we use $F(Z/E)$ for (*E*)-on ligands.

3. Analog Design

Except only a few isolated cases (see section 4), photo-switchable ligands have been devised as analogs of a known lead compound.^[42] *E-Z* photoswitches are usually introduced into the structure of existing bioactive compounds by applying the “azo-extension” and “azologization” approaches.^[1,2,54] In a nutshell, the first approach appends an azobenzene to the drug core after SAR evaluations, while the second approach identifies and substitutes bioisosteres of azobenzene (“azosteres”). In addition to these widespread rational design strategies, we make finer distinctions and expand the vocabulary in use in photopharmacology.

Starting from template ligands, photoswitches can be included by extension (see section 3.1), bioisosteric replacement (azologization, see section 3.2), or insertion (see section 3.3). Alternatively, they can act as spacers, thus connecting two identical or different pharmacophores (see

section 3.4). If a previously published compound containing a photoswitch was not studied in a light-dependent manner, it can be subjected anew to a photopharmacological investigation (“photo-repurposing”, see section 3.5). When a photoswitchable ligand is available, but reversed light-dependent behavior is needed, it is possible to apply the “sign inversion” strategy (see section 3.6).^[55]

3.1. Extension

A straightforward method to attain optical control of a bioactive molecule is the extension of its structure with an *E-Z* photoswitch in order to influence the affinity for the target upon photoisomerization. Finding the optimal position for this modification can be supported by SAR or structural considerations. Generally, photopharmacological studies use the umbrella term “azo-extension”,^[1,2] yet here we propose a finer distinction (Figure 3):

Extension from an aromatic ring that is already in the molecule and that is incorporated into the switch:

- Bona fide extensions (from an unsubstituted ring)
- Extension with the removal of substituents on the aromatic ring

Decoration:

- Direct decoration (single bond spacer)
- Decoration through a spacer (appendage)

When compared to the bioisosteric replacement strategy (see section 3.2), predicting the outcomes of a structure extension is more challenging. Starting from previous SAR data or structure-based observations, it is possible to assume

that certain extensions can be tolerated and can produce light-induced changes in affinity. However, hypothesis on the resulting (*E*)- or (*Z*)-on activity are more difficult to conceive, also because of the absence of predictive concepts such as (*E*)- and (*Z*)-like bioisosteres (see section 3.2).

3.1.1. Bona Fide Extensions

Bona fide extension is the design approach that takes an aromatic ring of the parent drug and extends it into an *E-Z* photoswitch without removing existing substituents (Table 1). Therefore, the analog features an extended π system that can protrude further in hydrophobic binding pockets, or can cause specific steric clashes only in one isomeric form.

The first applications of the *bona fide* extension strategy date back to the earliest reports of photopharmacology that introduced the field into the realm of science. Extending the aromatic rings of small parent compounds into azobenzenes led to the pioneering discovery in the 1960s of photopharmacological agents, such as (*Z*)-on chymotrypsin inhibitor **1**^[56] and (*E*)-on acetylcholine receptor (AChR) agonist **2**.^[57] More than 40 years later, during the renaissance of photopharmacology led by our group and the Trauner group,^[1,2] another simple aromatic structure was extended into an azobenzene. Modification of propofol, a positive allosteric modulator of γ -aminobutyric acid_A receptor (GABA_AR), resulted in a library of systematically substituted azo-derivatives.^[58] In contrast to the above-mentioned speculative design, here previous SAR data indicated that large substituents were tolerated at the *para*-position, and the pharmacophore was deemed to be compatible with azobenzene photochemistry. Compound **3** was characterized as an

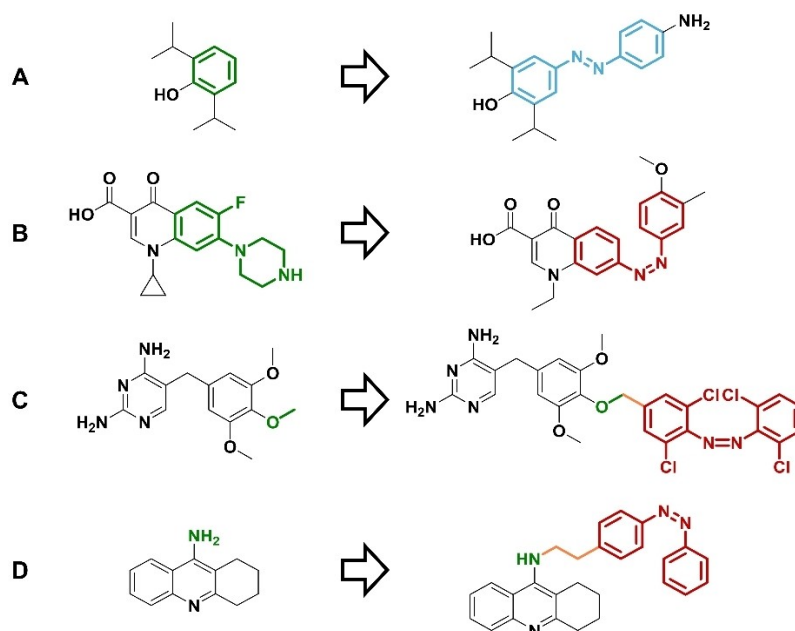
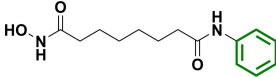
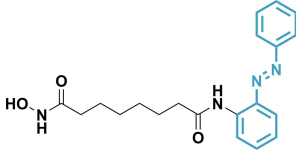
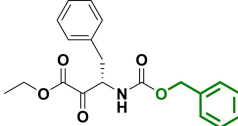
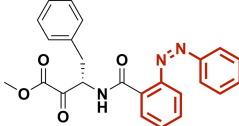
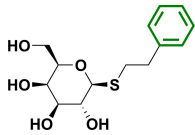
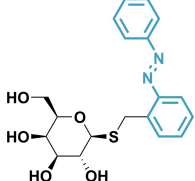


Figure 3. Examples of extension strategies. (A) *Bona fide* extension. (B) Extension with the removal of substituents on the aromatic ring. (C) Direct decoration. (D) Decoration through a spacer.

Table 1: Overview of *bona fide* extensions.

Entry	Compound	Target (ligand)	Parent compound	Photoswitchable derivative (active isomer)	Ref.
1	1	Chymotrypsin (inhibitor)			[56]
2	2	AChR (antagonist)			[57]
3	3	GABA _A R (potentiator)			[58]
4	4	MOR (agonist)			[59]
5	5	ENaC (blocker)			[60]
6	6	iGluR2 (agonist)			[61,62]
7	7	Microtubule polymerization (stabilizer)			[63]
9	8	Proteasome (inhibitor)			[65]
10	9	Proteasome (inhibitor)			[66]
8	10	TRPV6 (inhibitor)			[67]

Table 1: (Continued)

Entry	Compound	Target (ligand)	Parent compound	Photoswitchable derivative (active isomer)	Ref.
11	11	HDAC3 (inhibitor)			[68]
12	12	Chymotrypsin (inhibitor)			[69]
13	13	β -Galactosidase (inhibitor)			[70]

(*E*)-on potentiator of GABA-induced currents, thus acting as a photochromic anesthetic.

When more aromatic rings are available for extension, it is difficult to select one by considering only 2D structures and limited SAR data, and it is necessary to resort to a trial-and-error approach. For the ligand-based design of photo-switchable agonists of μ -opioid receptor (MOR), Trauner and co-workers applied *bona fide* azo-extension to both aromatic rings of fentanyl.^[59] Because of the absence of any agonistic activity, one of the screened compounds was discarded at the beginning of the study, whereas compound **4** was showed to be an (*E*)-on agonist of MOR. Conversely, if the available SAR studies are more informative, they can be translated to photopharmacological design ideas. Inspired by a series of homologs of phenamil, a blocker of the epithelial Na⁺ channel (ENaC), the Trauner group investigated the extension strategy on each of these closely related compounds.^[60] Electrophysiology experiments revealed that derivative **5** functioned as a (*Z*)-on ENaC blocker.

Thus far, all the discussed examples described *para*-substituted azobenzenes that were obtained through ligand-based considerations. However, visual inspection of X-ray structures (if available) can guide the direction in which the parent compound should be extended. During the development of photoswitchable agonists for the ionotropic glutamate receptor subunit 2 (iGluR2) found in α -amino-3-(5-methyl-3-hydroxyisoxazol-4-yl)propanoic acid receptors (AMPA), the X-ray structure of the complex (PDB ID: 2P2A) indicated that the benzene ring of the parent compound was pointing toward the solvent (Figure 4A).^[61] In particular, it also suggested that the gate of the binding pocket would accommodate a *meta*-substituted, rather than a *para*-substituted azobenzene. The biological results confirmed the structure-based hypothesis, as compound **6** was found to be an (*E*)-on agonist, while the derivative bearing a *para*-substitution pattern was inactive. A follow-up modeling study used molecular docking and MD to rationalize the behavior of compound **6**.^[62] In agreement with the experiments, the (*E*)-form displayed two possible binding modes,

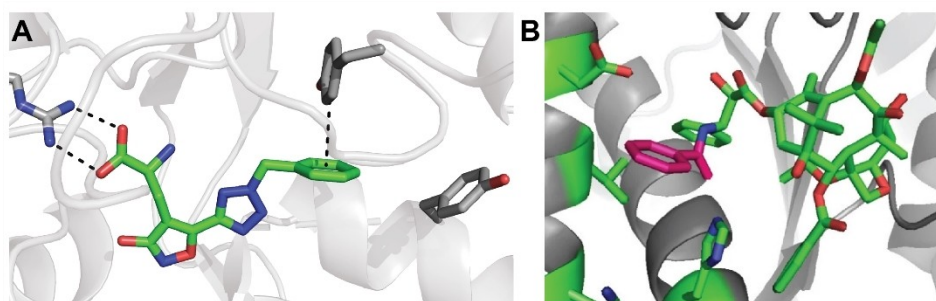


Figure 4. Visual inspection of ligand-target complexes for the formulation of extension hypotheses. (A) Crystal structure (PDB ID: 2P2A^[64]) of AMPA analog (green) bound to the iGluR2 ligand-binding domain (gray). The ligand has space to grow in the meta position. (B) Cryo-EM structure (PDB ID: 3J6G) of tubulin (gray cartoon, green residues) in complex with paclitaxel (green ligand, pink benzamide). Adapted with permission from ref. [63]. Copyright © 2020 Springer Nature.

while no docking poses were obtained for the (*Z*)-form. Subsequently, MD simulations of the conformational changes of iGluR2 upon ligand photoisomerization showed that (*Z*)-**6** adopted a metastable binding pose, which led to the ligand being liberated from the target. Similarly to the above-mentioned approach, examination of the available space in the paclitaxel-tubulin complex (Figure 4B) indicated that the benzamide substituent on a side-chain amine of paclitaxel could be extended with azobenzene.^[63] Furthermore, the authors postulated that the additional substituents on the outer ring of azobenzene could be used to modulate the photochemical features on the ligand, without being detrimental for the potency. In fact, a *para*-methoxyazobenzene could be installed in the *meta* position to generate compound **7**, a (*Z*)-on microtubule stabilizer.

Less common is applying the *bona fide* extension strategy to heteroaromatics, as in the case of light-controlled proteasome inhibitors.^[65] The antitumor agent bortezomib was extended into a canonical azobenzene, with a simultaneous replacement of the pyrazine ring with benzene. Visual inspection of the binding mode of bortezomib into the 20S proteasome (PDB ID: 2F16) aided the formulation of a structure-based hypothesis. The planar (*E*)-isomer was expected to fit into the active site, while the bulkier (*Z*)-isomer would cause steric clashes. Inhibition assays on cell lysates indicated that all compounds were (*E*)-active, with inhibitor **8** showing a $F(Z/E) > 2$. In a follow-up report by the Abell group, a different azo-extension was explored on the benzyl aniline ring to explore the S2 binding site.^[66] Interestingly, compound **9** acted as an (*E*)-on inhibitor on the isolated target, but as a (*Z*)-on drug on cancer cells. In a related example, a similar strategy was used for light-controlled inhibitors of transient receptor potential vanilloid 6 (TRPV6).^[67] The parent compounds featured two aromatic sites potentially suitable for extension, i.e., a methyl-substituted benzene and a pyridine. Since pre-existing SAR studies suggested that modifications on the benzene ring were detrimental for the activity, Raymond and co-workers extended the pyridine ring into an azoarene. Even though the pyridine ring was tentatively incorporated in the inner or the outer ring of azobenzene, only the classical azobenzene derivative **10** was determined to be a (*Z*)-on inhibitor, with a remarkable $F(E/Z) > 10$.

As an alternative strategy, if structural data are not available or not scrutinized, all regioisomers of azobenzene can be systematically explored to sample the space around

the original aromatic ring. After examining numerous variations in length, shape and substitution patterns, our group identified the *ortho*-extended vorinostat azo-derivative **11** as an (*E*)-on inhibitor with a $F(Z/E)$ of 10.^[68] However, the compounds that were designed through azologization showed more attractive light-induced differences in potency (see section 3.2.2.4). Abell and Harvey also reported a systematic analysis of regioisomers that led to a compound bearing an *ortho*-substituted azobenzene, i.e., **12**, a (*Z*)-active photoswitchable inhibitor of chymotrypsin.^[69] On closer inspection, such design concurrently incorporated the small modification of a benzyloxy group into a simple phenyl, before the extension took place. Similarly, β -galactosidase inhibitor **13** was obtained by extending 2-phenyl-ethyl β -D-thiogalactoside with simultaneous subtle modifications of the structure, as alkyl spacers with different lengths were examined.^[70] Despite its moderate $F(Z/E)$ of ≈ 5 , *a posteriori* ensemble docking poses suggested that the solvent-exposed binding pocket of β -galactosidase could accommodate both photoisomers of compound **13** (Figure 5).

3.1.2. Extension with the Removal of Substituents on the Aromatic Ring

Another design strategy is to extend a substituted aromatic ring (Table 2), as stated by the original definition of the azo-extension approach.^[2] In fact, the presence of a substituent can indicate that some variability is tolerated at a specific position. If the substituent does not play a crucial role in the pharmacophore, then a photoswitchable derivative should be active and its isomerization has the potential to result in light-induced differences in potency.

The extension approach frequently takes advantage of SAR studies indicating that the parent compounds could withstand variations on particular substituents. Illustrative cases can be found in the development of photoswitchable opener **14** for G-protein coupled inwardly rectifying K^+ (GIRK) channels,^[71] and in the development of photoswitchable antagonist TRPV1 channels based on capsazepine and BCTC, i.e., compounds **15** and **16**.^[72] After purely exploratory design hypotheses, the different (*E*)- and (*Z*)-active behaviors could not be rationalized in any way, hence they cannot be used as starting points for subsequent endeavors of rational design.

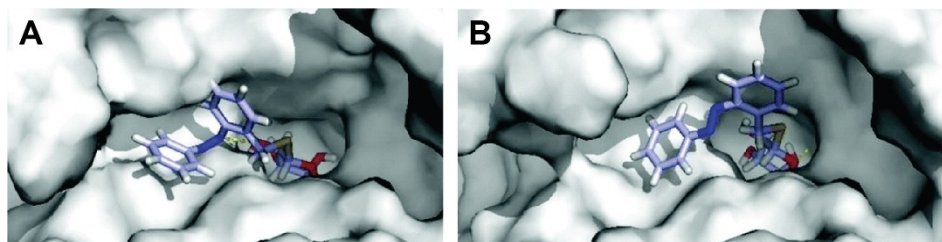


Figure 5. Docking poses of the (*Z*)-isomer (A) and the (*E*)-isomer (B) of compound **13** into β -galactosidase (gray surface). Adapted with permission from ref. [70]. Copyright © 2020 The Royal Society of Chemistry.

Table 2: Overview of extensions obtained after removing substituents.

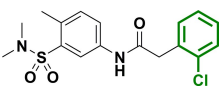
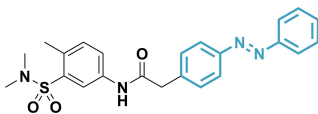
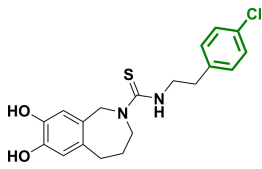
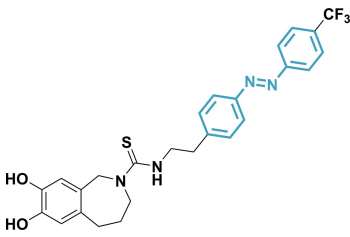
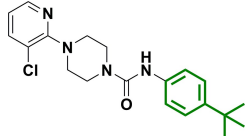
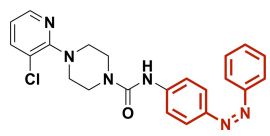
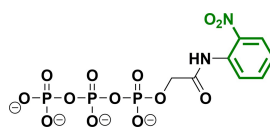
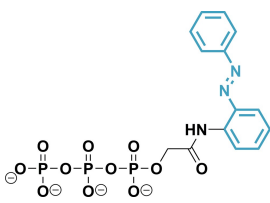
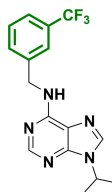
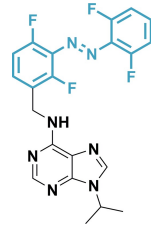
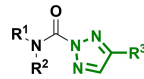
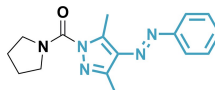
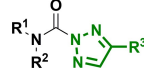
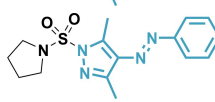
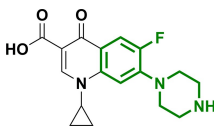
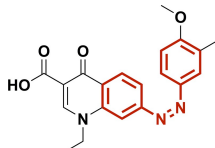
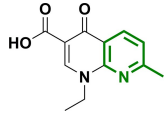
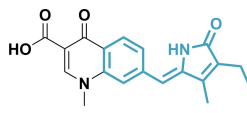
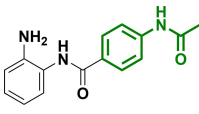
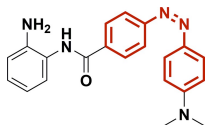
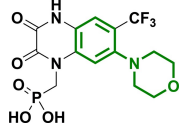
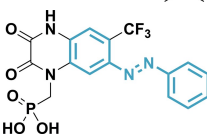
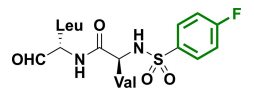
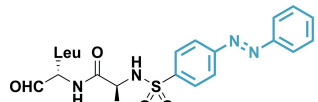
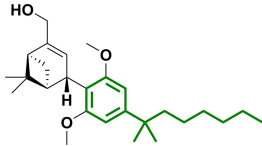
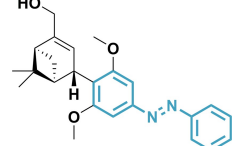
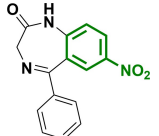
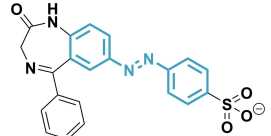
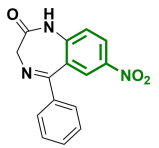
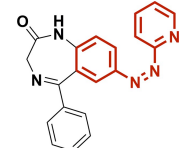
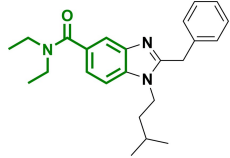
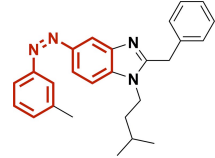
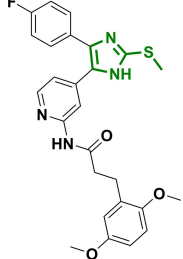
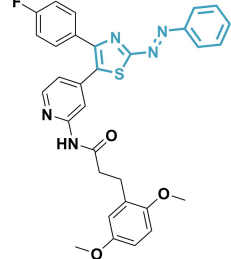
Entry	Compound	Target (ligand)	Parent compound	Photoswitchable derivative (active isomer)	Ref.
1	14	GIRK channels (opener)			[71]
2a	15	TRPV1 (antagonist)			[72]
2b	16	TRPV1 (antagonist)			[72]
3	17	Kinesin-microtubules (substrate)			[73]
4	18	CKI (inhibitor)			[74]
5a	19	CES (covalent inhibitor)			[75]
5b	20	CES (inhibitor)			[75]
6	21	DNA gyrase (inhibitor)			[76]
7	22	DNA gyrase (inhibitor)			[77]
8	23	HDAC (inhibitor)			[78]
9	24	AMPA (antagonist)			[79]

Table 2: (Continued)

Entry	Compound	Target (ligand)	Parent compound	Photoswitchable derivative (active isomer)	Ref.
10	25	m-Calpain (inhibitor)			[81]
11	26	CB ₂ R (agonist)			[82]
12	27	GABAR and GlyR (blocker)			[85,87]
13	28	GlyR (allosteric modulator)			[86]
14	29	CB ₂ R (agonist)			[88]
15	30	CK1δ/p38α MAPK (inhibitor)			[90]

On the other hand, essentially exploratory azo-extensions can also lead to bioisosteric replacements (see section 3.2) that were not easily recognizable through simple analysis of the molecular structure. For instance, a substrate for the actomyosin motor protein system was extended at the nitro-substituted *ortho*-position, resulting in derivative **17**.^[73] Since the (*E*)-isomer induced higher motility, the authors speculated that the flat (*E*)-azobenzene might be forming the same π - π stacking interactions of the adenosine ring in ATP, suggesting an intriguing bioisosterism between adenosine and (*E*)-azobenzene.

When previous SAR is not available for the template compound due to, e.g., its recent discovery, different regioisomers and substitution patterns can be screened to carry out a “photopharmacological SAR study”, as reported recently for visible-light photoswitchable circadian rhythm modulator **18**.^[74] Considering that the parent casein kinase I (CKI) inhibitor, longdaysin, had a hydrophobic substituent (a trifluoromethyl group) in the *meta* position, the best

inhibitory results were achieved with the (*E*)-isomer of the *meta*-substituted photoswitchable analog. In the case of *ortho*-substituted azobenzene, the (*Z*)-isomer was more active than the (*E*)-isomer, whereas *para*-substituted azobenzene displayed very little differences in potency before and after irradiation. These observations are in agreement with the substitution-dependent differences in potency between photoisomers that we discuss later, regarding the replacement of ambiguous bioisosteres (see section 3.2.2.3 and Figures 26 and 28). Subsequent photochemical optimization entailed the exploration of the azopyrazole switch, as well as *para*-methoxy, di- or tetra-*ortho*-fluoro substituents. The latter modification yielded compound **18**, a visible-light-responsive, (*E*)-on modulator of the circadian clock.

Going beyond benzene rings, extension also on hetero-aromatic rings has been described, e.g., for the optical control of carboxylesterase (CES) inhibitors.^[75] Even though the authors claimed to have conducted “de novo design”, we argue that their definition is inaccurate, because the design

started from known structures. In reality, a triazole group of the parent compound was effectively extended into an azopyrazole photoswitch. After the identification of the (*E*)-on covalent inhibitor **19** with a $F(Z/E)$ of 7, the urea moiety was further replaced with a less electrophilic sulfone, which yielded the (*E*)-on reversible inhibitor **20** with a $F(Z/E)$ of 3.

In addition to azo(hetero)arenes, aromatic cores can also be extended into less common *E-Z* photoswitches. Inspired by our work on photoswitchable antibiotics that applied the azo-extension approach to the aromatic core of quinolones (compound **21**),^[76] Sampedro and co-workers extended nalidixic acid with hydantoin and phytochrome.^[77] DFT calculations suggested that the (*Z*)-isomer would possess higher antimicrobial activity because of its planar geometry, which is better suitable for DNA intercalation than the twisted geometry of the (*E*)-isomer. As predicted, the photoswitchable fluoroquinolone **22** was determined to be a (*Z*)-on antibiotic, with a $F(E/Z)$ of 4. With a complementary approach, focusing on isomer-dependent electronic rather than structural effects, DFT studies also guided the design of (*Z*)-active histone deacetylase (HDAC) inhibitor **23**.^[78]

Compared to the ligand-based approaches outlined above, structure-based approaches allow the formulation of more elaborate design hypotheses. Such improvements are evident already in the case of straightforward visual inspection of X-ray (or cryo-EM) structures, as exemplified by the work of the Trauner group on the (*E*)-on AMPAR antagonist **24**.^[79] However, the most informative outcomes usually derive from computer-aided drug design efforts. For instance, Abell and co-workers performed early induced fit docking studies (IFD, useful method to account for protein mobility^[80]) to rationalize the biological activity of **25**, an (*E*)-on m-calpain inhibitor with a $F(Z/E) > 3$.^[81] The less potent (*Z*)-isomer was predicted to engage only in two out of the three expected hydrogen bonds. Structure-based considerations also enabled the development of photo-switchable agonists of cannabinoid receptor 2 (CB₂R).^[82] Herein, the extension strategy on a template agonist was evaluated by sampling several molecular designs: directly from the core after removal of the alkyl chain (compound **26**), and with a single-bond spacer (see section 3.1.3). *A posteriori* molecular docking corroborated the biological

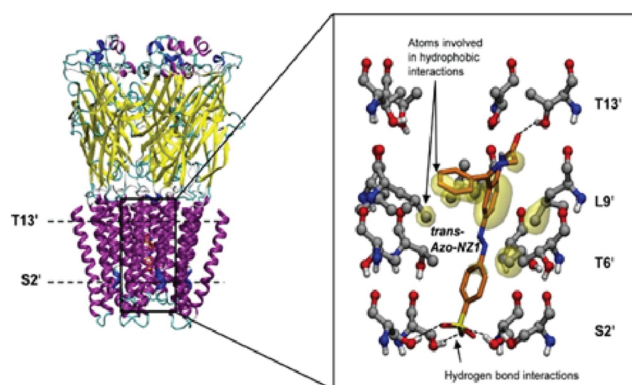


Figure 7. Docking of (*E*)-**27** in the transmembrane domain of $\rho 2$ GABA_cR (homology model). Adapted with permission from ref. [85]. Copyright © 2019 Wiley-VCH Verlag GmbH & Co. KGaA.

activity results, indicating that the elongated (*E*)-**26** might form more van der Waals contacts with the hydrophobic subpocket of the binding site (Figure 6). Nonetheless, docking scores were incorrectly discussed in detail, although they are known to be inaccurate predictions of binding affinities.^[83] In fact, the main purpose of docking scores is to help distinguishing between active and completely inactive molecules in the context of virtual screenings of large libraries.^[80,83,84] Therefore, we believe that docking scores are not suitable for detailed comparisons between photoisomers.

An alternative to such inaccurately quantitative analyses can be seen in more qualitative approaches, as demonstrated by the work of Bregestovski and co-workers.^[85] The azo-extended analog of nitrazepam **27** was found to be an (*E*)-on blocker of GABARs chloride-selective pore. To model the differences between the (*E*)- and the (*Z*)-form, molecular docking was carried out in a homology model of $\rho 2$ GABA_cR, after mutagenesis results guided the choice of the binding region (Figure 7). Subsequently, the authors enumerated the intermolecular interactions that were formed by each photoisomer with the transmembrane domain of the receptor, in terms of hydrogen bonds and hydrophobic contacts. In addition to engaging in more

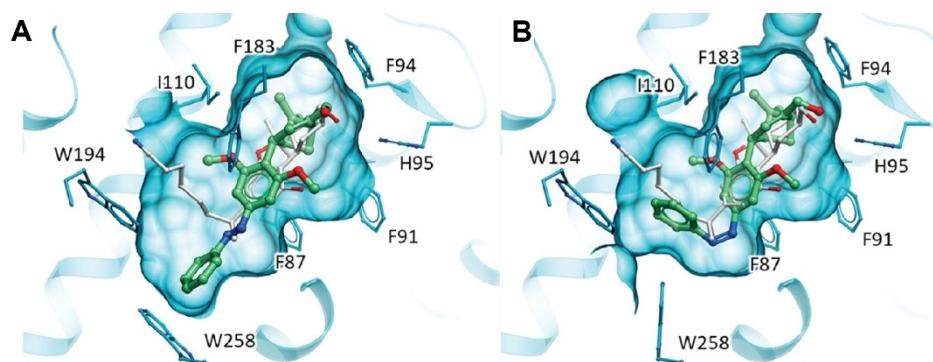


Figure 6. Docking poses of the (*E*)-isomer (A) and the (*Z*)-isomer (B) of compound **26** into CB₂R (blue). Adapted with permission from ref. [82]. Copyright © 2021 American Chemical Society.

interactions overall, (*E*)-**27** had an optimal length for placing its sulfonate group in the same region as the co-crystallized chloride ion. Further modifications on the benzodiazepine scaffold targeting GABARs led to the serendipitous discovery of **28**, a (*Z*)-on allosteric antagonist of glycine receptors (GlyRs).^[86] In an attempt to explain this unexpected behavior, blind molecular docking (i.e., with no prior definition of the binding site) suggested that the (*Z*)-**28** could interact deeper with the receptor, favoring the closed state. In an additional follow-up study, GABARs blocker **27** was also characterized as an (*E*)-on blocker of GlyRs, with the support of a similar computational workflow.^[87]

Besides counting specific interactions, a second alternative to quantitative analyses of docking scores is the qualitative evaluation of steric clashes between the ligand and the target. In this regard, Decker and co-workers published an elegant example of experimental and theoretical consensus during the development of a (*Z*)-on agonists for human CB₂R, i.e., compound **29**.^[88] Even though the authors defined their design approach as azologization, we categorize it rather as azo-extension, because aliphatic *N*-substituents on the benzamide had been previously shown to be tolerated.^[89] *A posteriori* docking calculations into a homology model were in very good agreement with the experimental results of a regioisomer screening. In particular, the light-induced differences could be rationalized through the comparison of steric clashes for *ortho*-, *meta*- or *para*-substitution with alkyl(oxy) or chloride. The largest light-activation was observed for *meta*-substituted **29**, possibly because substituents at the *meta* position would provoke steric clashes for the (*E*)-isomer, while they could be accommodated by the binding pocket in the (*Z*)-isomer (Figure 8).

Lastly, a structure-based “heteroazo-extension” was reported for the development of photoswitchable kinase inhibitors against p38 α mitogen-activated protein kinase (p38 α MAPK) and CK1 δ .^[90] Herges, Peifer and co-workers used *a priori* docking calculations to support the extension of the methylthioether-substituted 2-imidazole core into an heteroaromatic azobenzene bearing a thiazole ring, yielding

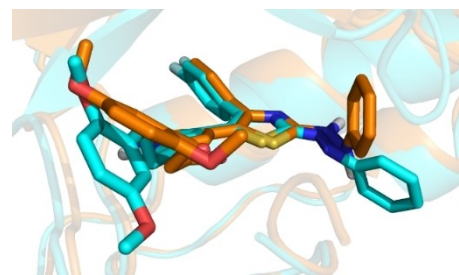


Figure 9. Crystal structures of p38 α MAPK in complex with compound **30** (cyan, PDB ID: 6HWU) and the reduced hydrazine by-product (orange, PDB ID: 6HWT^[90]).

compound **30**. Since the biological results did not match with the structure-based hypothesis of (*E*)-on activity, an X-ray structure of the ligand-enzyme complex was obtained (Figure 9). However, such structure revealed the presence of a reduced hydrazine instead of an azo bond (PDB ID: 6HWT), caused by the dithiothreitol (DTT) additive in the assay buffer. In fact, DTT-free crystallization conditions correctly afforded the (*E*)-isomer (PDB ID: 6HWU). These findings sparked an elaborate discussion on the pitfalls of photopharmacology, e.g., the risk of reduction of azo moieties, and the difficulty of rationally design *E-Z* inhibitory differences, which can be cancelled out by the conformational adaptations of proteins. Therefore, the authors proposed that azologization and scaffold hopping (see section 3.2.1) should be preferred over azo-extension. As mentioned later (see section 3.2), we also agree that bioisosteric replacement is a more promising approach for photopharmacology because it allows for more solid hypotheses on (*E*)- or (*Z*)-activity and for larger light-induced changes in potency.

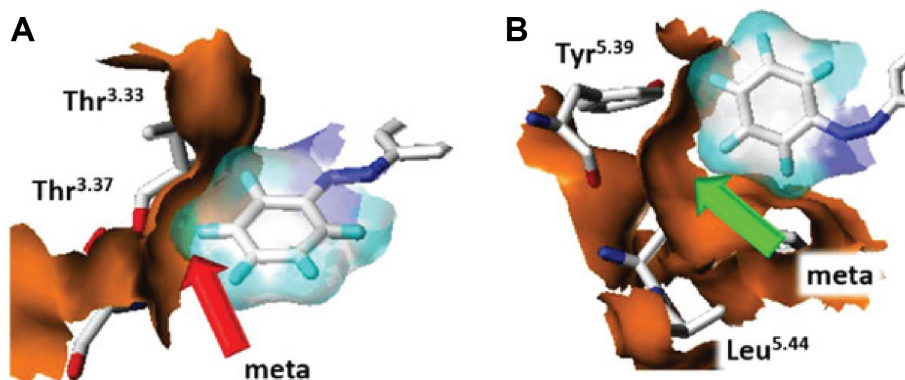


Figure 8. Docking of the (*E*)-isomer (A) and the (*Z*)-isomer (B) of the unsubstituted version of **29** in a homology model of CB₂R. While the red arrow indicates the potential steric clashes of the *meta*-substituted (*E*)-isomer, the green arrow indicates the available space for the *meta*-substituted (*Z*)-isomer. Adapted with permission from ref. [88]. Copyright © 2018 Wiley-VCH Verlag GmbH & Co. KGaA.

3.1.3. Direct Decoration

E-Z photoswitches have also been attached to bioactive molecules through a variety of linkers. Since such structural modification affects a region that is more distant from the pharmacophore, it is expected to retain the original activity and to generate more modest differences upon irradiation. Moreover, pre-existing aromatic rings are not needed, as the photoswitches can be introduced also in aliphatic portions of the molecule. In the following section, we focus on the shortest linker possible, i.e., a single bond (Table 3). For longer linkers, see section 3.1.4 and Table 4.

Although the presence of an aromatic ring in the template ligand is a perfect handle for direct extension (see sections 3.1.1 and 3.1.2), the insertion of a short spacer enables the photoswitch to protrude further in the available space, which can be highly beneficial for obtaining (*Z*)-on ligands. A clear example can be found in the already mentioned work on photoswitchable agonists of CB₂R by Carreira, Frank and co-authors.^[82] Whereas extension on the aromatic ring resulted in the (*E*)-active agonist **26** (Figure 6), attaching the azobenzene via a single bond extended the derivative further into the hydrophobic subpocket. Consequently, compound **31** was determined to be (*Z*)-active, because the (*E*)-isomer was too elongated to fit into the CB₂R binding pocket. When the aromatic ring of the parent ligand bears a substituent, it is also possible to attach the photoswitch directly at that moiety. For instance, our

group developed the (*Z*)-on, visible-light-responsive photo-switchable antibiotic **32** by appending an azobenzene to one of the methoxy groups of trimethoprim, after screening several linkers.^[91]

A second subgroup of direct appendages uses aliphatic anchoring points. This approach was introduced for the first time in pioneering studies on the photo-regulation of AChR with compound **33**,^[57] and it is still in use, as exemplified by the recent report on photoswitchable kinesin spindle protein (KSP, KIF11, or Eg5) inhibitors for the optical control of mitosis.^[92] Supported by SAR data and X-ray structures, a great number of extensions on different Eg5 inhibitors was systematically explored, leading to the (*Z*)-on azo-derivative **34**. Furthermore, Decker and co-workers demonstrated that quaternary ammonium cations are also suitable for the attachment of azobenzene.^[93] The potent muscarinic AChR (mAChR) agonist iperoxo was extended with regular and tetra-*ortho*-fluoroazobenzene through a single bond spacer. Simultaneously, the authors investigated the light-induced effects of both univalent and bivalent photoswitchable ligands, i.e., with only one or two repeating units of the iperoxo pharmacophore. Compound **35** acted as a full AChR agonist, albeit with no significant differences upon irradiation. However, since azobenzene played the role of a spacer in the bivalent ligands, the reader is referred to the dedicated discussion for more details (see section 3.4).

Table 3: Overview of direct decorations.

Entry	Compound	Target (ligand)	Parent compound	Photoswitchable derivative (active isomer)	Ref.
1	31	CB ₂ R (agonist)			[82]
2	32	DHFR (inhibitor)			[91]
3	33	AChR (antagonist)			[57]
4	34	Eg5 (inhibitor)			[92]
5	35	mAChR			[93]

Table 4: Overview of decorations by means of a spacer (green = linking group; orange = spacer).

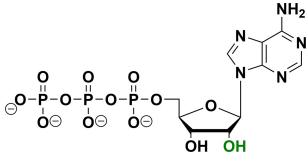
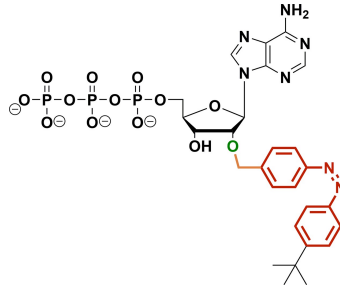
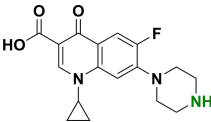
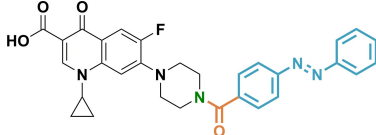
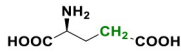
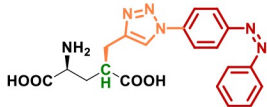
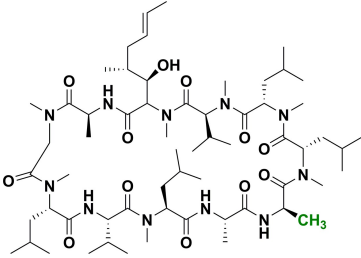
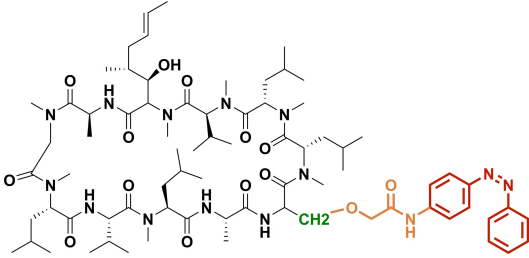
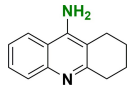
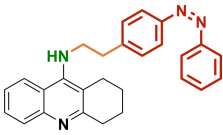
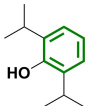
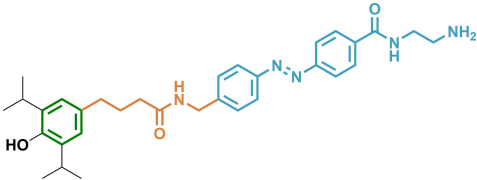
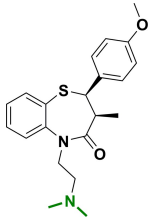
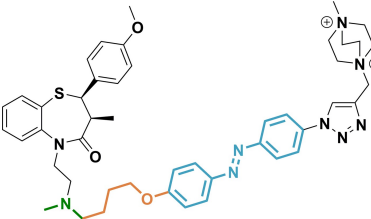
Entry	Compound	Target (ligand)	Parent compound	Photoswitchable derivative (active isomer)	Ref.
1	36	Kinesin-microtubules (substrate)			[94]
2	37	DNA gyrase (inhibitor)			[95]
3	38	NMDAR (agonist)			[96]
4	39	Calcineurin (inhibitor)			[97]
5	40	AChE (inhibitor)			[98]
6	41	GABA _A R (potentiator)			[99]
7	42	LTCC (blocker)			[100]

Table 4: (Continued)

Entry	Compound	Target (ligand)	Parent compound	Photoswitchable derivative (active isomer)	Ref.
8	43	NMDAR (antagonist)			[101]
9	44	CB ₁ R (inhibitor)			[103]
10	45	Tubulin (modulator)			[104, 105]

3.1.4. Decoration through a Spacer

While only a limited amount of photopharmacological agents were obtained by means of direct attachment (see section 3.1.3), peripheral decoration is prevailing. This widespread design strategy appends *E-Z* photoswitches to the template ligand via longer spacers (Table 4).

Several spacers of varying length have been used for the appendage of *E-Z* photoswitches to known ligands. Examples of short spacers include the minimal methylene bridge of compound **36**, (*Z*)-on substrate of ATPase kinase,^[94] and the amide linker of compound **37**, an (*E*)-on antibiotic based on the DNA gyrase inhibitor ciprofloxacin.^[95] The choice of the linker can be dictated purely by the available synthetic methodologies, e.g., click chemistry for the triazole spacers of (*E*)-on agonist **38** for *N*-methyl-D-aspartate receptor (NMDAR).^[96] In the case of ligand **39**, azo-derivative of the peptide immunosuppressant cyclosporin A, a flexible amide spacer was used.^[97] This compound was further improved using a “protein borrowing” strategy, employing the azobenzene itself as a spacer (see section 3.4).

With regard to the strength of the design hypotheses, ligand-based considerations are often surpassed by the evaluation of Protein Data Bank (PDB) structural data. For instance, simple visual inspection of the tacrine-acetylcholinesterase (AChE) complex (PDB ID: 1ACJ) indicated that the attachment of azobenzene to the aniline nitrogen of tacrine could be tolerated because it protruded toward the

solvent.^[98] In fact, decoration with an ethylene-linked azobenzene generated the (*Z*)-on AChE inhibitor **40**. When longer and more flexible linkers are introduced through ligand-based design, they can hinder the interpretation of biological results, as in the development of the (*E*)-active allosteric GABA_AR agonist **41**.^[99] On the other hand, structure-based computational methods are able to shed light on the molecular details of differential binding also when extended linkers are involved. To explain the observed behavior of compound **42** as an (*E*)-on L-type calcium channel (LTCC) blocker, Trauner and co-workers performed *a posteriori* molecular docking into a homology model.^[100] The linear structure of the (*E*)-form was beneficial for the achieving an elongated binding mode, while the steric bulk of the (*Z*)-form hindered optimal contacts with the pore.

The level of detail that is provided by the availability of determined target structures enables more profound comparisons between different design approaches. Ellis-Davies and co-workers used *a priori* docking calculations to evaluate two possible modifications of the NMDAR antagonist ifenprodil, i.e., photocaging of the phenol group and attachment of azobenzene via a long linker.^[101] The docking poses suggested that the both strategies could result in favorable light-induced effects. The azo-decorated inhibitor **43** was predicted to be (*E*)-active, because the (*Z*)-form showed an unfavorable conformation with potential steric clashes with the target (Figure 10). However, both isomers

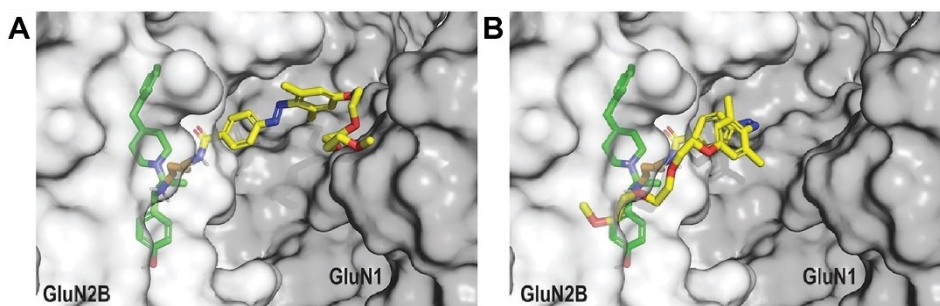


Figure 10. Docking poses of the (*E*)-isomer (A) and the (*Z*)-isomer (B) of compound **43** (yellow) into the NMDAR (gray surface, PDB ID: 3QEL). Adapted with permission from ref. [101]. Copyright © 2021 Wiley-VCH Verlag GmbH & Co. KGaA.

were found to be completely inactive, whereas the photocage-based design strategy yielded a light-activatable inhibitor. Based on these results, the authors concluded that the photocaging approach is more promising in the context of NMDAR antagonists. Besides the well-known higher rate of success of irreversible photopharmacology,^[28,29,102] the additional polyethylene glycol chain of ligand **43** (presumably introduced for solubility reasons) was not object of any comment, although such structural alteration might have greatly influenced the bioactivity outcome.

Analogously, Decker and co-workers compared the application of azo-extension and azologization (see section 3.2) for the development of photoswitchable CB₁R antagonists based on rimonabant.^[103] While the azologization strategy resulted in loss of original affinity and modest differences between the photoisomers, decorating rimonabant with azobenzene after removing a piperidine ring led to a (*Z*)-on antagonist (**44**) with a $F(E/Z) > 15$. *A posteriori* molecular docking suggested that its (*Z*)-form could engage in hydrogen bonds with Ser123, whereas solvent exposure of the (*E*)-form could account for its lower potency (Figure 11). Such visual evaluation of solvent-exposed hydrophobic groups in docking poses is commonly exploited in structure-based drug design.^[80]

As an alternative to structure-based approaches, prior SAR data on closely related modifications are also valuable for guiding the first phases of design. This is exemplified by the report of Arndt, Trauner and co-workers on photo-switchable F-actin modulators.^[104] Starting from jasplakinolide, a potent inducer of actin polymerization, the choice of a handle for the azo-attachment was supported by previous conjugates bearing bulky fluorophores in that position.

Compound **45** showed (*Z*)-on cytotoxicity, with a $F(E/Z) > 10$. In an important follow-up characterization, cryo-EM structures were reported for both isomers (Figure 12).^[105] (*Z*)-**45** (PDB ID: 7AHN) fitted into a cavity in F-actin, triggering a conformational change that was in agreement with the results. Moreover, the (*Z*)-azo bond occupied a similar region to the hydroxyl group of the parent compound. As an additional correlation with the biological outcomes, the complex with the more potent (*Z*)-isomer was resolved with better resolution, as opposed to the structure with the (*E*)-isomer (PDB ID: 7AHQ). Overall, the binding mode of (*Z*)-**45** was demonstrated to be highly similar to another actin stabilizer, i.e., phalloidin. These groundbreaking results enhance our fundamental understanding of photopharmacology and have the potential to guide subsequent structure-based optimization efforts.

With long spacers, structure-based design proved crucial for identifying solvent-exposed areas either for at the design phase (compound **40**) or for the interpretation of experimental observations (compound **44**). In both cases, the ligands displayed (*Z*)-on behavior, because of the unfavorable exposure of the higher hydrophobic surface of the (*E*)-azobenzene substructure.

3.2. Bioisosteric Replacement

Another strategy in the medicinal chemists' toolbox for the design of drug analogs is bioisosteric replacement, which identifies and exchanges substructures that are sterically or electronically similar.^[106] In photopharmacology, certain moieties can be replaced with photoresponsive bioisosteres

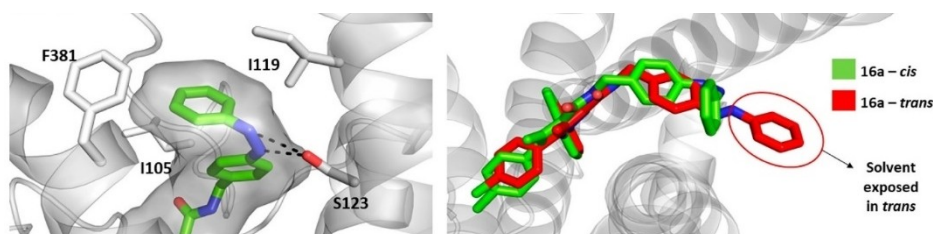


Figure 11. Docking poses of the (*E*)-isomer (red) and the (*Z*)-isomer (green) of compound **44** into the NMDAR (gray, PDB ID: 5TGZ). Adapted with permission from ref. [103]. Copyright © 2021 American Chemical Society.

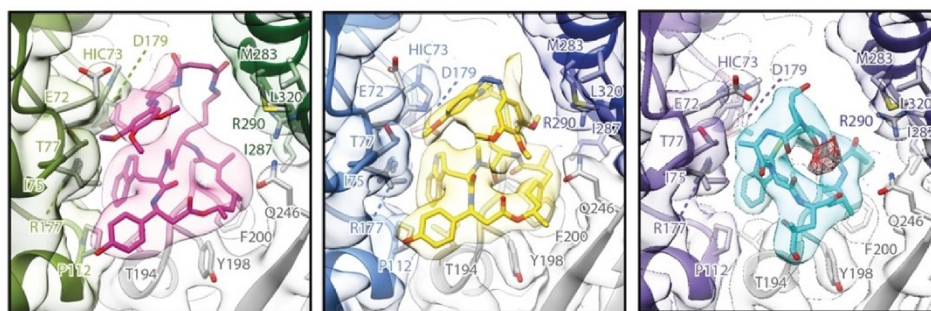


Figure 12. Crystal structures of F-actin in complex with (*E*)-**45** (magenta, PDB ID: 7AHQ), (*Z*)-**45** (yellow, PDB ID: 7AHN), and phalloidin (cyan, PDB ID: 6T1Y). Adapted with permission from ref. [105]. Copyright © 2021 Wiley-VCH Verlag GmbH & Co. KGaA.

to enable the optical control of the biological activity of drugs. When specifically the azobenzene photoswitch is incorporated into the structure, the bioisosteric replacement is referred to as “azologization” and the bioisosteres as “azosteres”.^[54]

According to the seminal definition by Thornber,^[107] bioisosteres are evaluated in terms of the following parameters: size, shape, electronic density distribution, polarizability, dipole moment, lipophilicity, polarity, and pKa. Generally speaking, bioisosteric replacement can involve substructures that play one or more of these roles in a drug:

1. Scaffold: the moiety is a structural element that holds other functional groups in a certain geometry for optimal binding to the target. The key parameters of such substructure are size and shape, and its replacement belongs to the category of scaffold hopping.^[108–110]
2. Molecular interactions: the moiety is a functional element that interacts with the target. Here, size, shape, electronic properties, pKa, chemical reactivity and hydrogen bonding are the key parameters.
3. Pharmacokinetics/metabolism: the moiety is introduced in the parent drug to optimize its ADMET properties, rendering lipophilicity, hydrophilicity, hydrogen bonding and pKa the important parameters. If the moiety specifically contributes to blocking or assisting metabolism, its chemical reactivity is the key parameter.

With the above classification in mind, we offer a few considerations on the prospects of bioisosteric replacement in photopharmacology. Irradiation of *E-Z* photoswitches results in distinct structural (i.e., size and shape) and electronic (i.e., electronic distribution and dipole moment) changes. Therefore, *E-Z* photoswitches can serve as scaffolds with light-controllable size and geometry (role 1), or as interacting moieties with photoresponsive size, shape, electronic properties, and hydrogen bonding (role 2). On the other hand, the introduction of a photoswitch might be detrimental to the optimized ADMET of the parent drug (role 3), especially in the case of azobenzenes. In fact, their susceptibility to reduction in hypoxic environments has been also used for azobenzene-containing prodrugs.^[111] Molecular design in photopharmacology often overlooks the role of the targeted bioisostere, yet we believe that the field would benefit from a deeper understanding of the structural,

functional and pharmacokinetic implications of bioisosteric replacements.

The introduction of the “azologization” concept by the Trauner group was grounded on considerations of simple 2D similarity.^[54] An azobenzene bioisostere (“azostere”) was defined as a substructure containing two aromatic rings connected by a two-atom linker, i.e., stilbene, 1,2-diphenyl ethane, 1,2-diphenyl hydrazine, *N*-benzyl aniline, benzyl phenyl ether, benzyl phenyl thioether, biaryl ester, *N*-aryl benzamide. In contrast to “classical” bioisosteres, which comprise simple atoms, groups or ring equivalents, the azosteres are mostly akin to “nonclassical” bioisosteres,^[112] because they include more complex substructures with distinct steric and electronic properties.^[113] A typical example of such replacement outside photopharmacology is the bioisosterism between a carboxylic acid and a tetrazole moiety.

Subsequently, the Trauner group further expanded the conceptualization of the approach with 3D data on molecular geometries taken from the PDB and the Cambridge Structural Database (CSD), as well as with bioactivity data from the DrugBank and ChEMBL databases.^[114] To map the space available for azologization, the dihedral angles of the C–X–Y–C linkers were used as a criterion to categorize the ligands into (*E*)-azologs (around 180°) and (*Z*)-azologs (0°). In addition to the dihedral angle comparison, the authors used the shape similarity of known ligands with their (*E*)- or (*Z*)-azologs to find candidates for azologization (see sections 3.2.1.1.2 and 3.2.2.1.4). The systems with a *gauche* conformation (dihedral angles around 60°) were deemed less suitable for azologization. In our opinion, this strict requirement for an ideal (*Z*)-like geometry dismisses fragments that have great potential for the design of (*Z*)-on photoswitchable drugs (see sections 3.2.1.2 and 3.2.2.2), e.g., biaryl sulfonamides and *N*-benzylanilines.

Overall, expansion of the current chemical space available for bioisosteric replacement in photopharmacology would require deeper considerations on the conformational preferences of the azosteres, both as isolated molecules and in complex with the target. Furthermore, the electronic similarities should also be evaluated, in terms of, e.g., dipole moment and electrostatic potential surface.

In accordance with the medicinal chemistry literature,^[115] we will make an important distinction in this section of the

review. Since bioisosteres of *E-Z* photoswitches can play different roles in the parent compound, their replacement can affect either the scaffold or the periphery of a ligand:

1. The scaffold is the molecular core that keeps the functional groups in position for crucial interactions (role 1 of a drug element) and/or is engaged in these interactions (role 2). Bioisosteric replacements of the core belong to the well-studied scaffold hopping strategy.^[108–110] This is a high-risk/high-gain approach in photopharmacology, because structural and electronic changes should have greater impact on binding. The *E*-to-*Z* photoisomerization should result in the correct positioning of functional groups only in one isomer, especially if the compound has an extended structure.
2. The periphery comprises regions of the drug that form important additional interactions (role 2) but are not essential for the pharmacological activity. When the bioisosteric replacements take place in these parts, they are examples of the “terminal substitution” strategy. Such modifications are expected to have less pronounced effects on the original potency, but also to result in smaller light-induced differences in bioactivity.

In addition to the above classification, a second distinction is necessary to outline the intricacies of molecular design in photopharmacology. Depending on their preferred conformation, the azosteres can be defined as (*E*)-like, (*Z*)-like or ambiguous. At the design phase, the photoswitchable analog is often expected to be more potent in one form based on the similarity between the parent fragment and this form. With its planar and flat geometry, an (*E*)-like azostere can be mimicked by (*E*)-azobenzene. On the other

hand, the bent geometry of a (*Z*)-like azostere is better approximated by (*Z*)-azobenzene.^[116] In some rare cases, (*Z*)-like azosteres also have electronic properties more similar to (*Z*)-azobenzene, which has a dipole moment of 3 D compared to the 0 D observed for (*E*)-azobenzene.^[36] Finally, some substructures remain ambiguous in this respect because they can act as both (*E*)- or (*Z*)-like, depending on their substitution pattern.

Besides the obvious substructure with two aromatic rings separated by a two-atom linker, less evident azosteres have also been explored. As we present in the next sections, these can span from diverse aromatic moieties (such as one-atom linked systems, biaryls, and fused rings) all the way to alkyl chains and atypical systems. Inspired by a recent categorization,^[117] we propose to classify the bioisosteric replacement approaches in photopharmacology as follows (Figure 13):

- Class 1: -X-Y- linker;
- Class 2: -Z- linker;
- Class 3: - linker (single bond);
- Class 4: no linker (fused rings);
- Class 5: aliphatic chains;
- Class 6: atypical systems.

In summary, we categorize here the bioisosteric replacements (Figure 14) depending on the affected region of the parent drug (scaffold versus periphery), the conformation and electronic properties of the azostere ((*E*)-like versus (*Z*)-like) and its molecular structure (class 1–6).

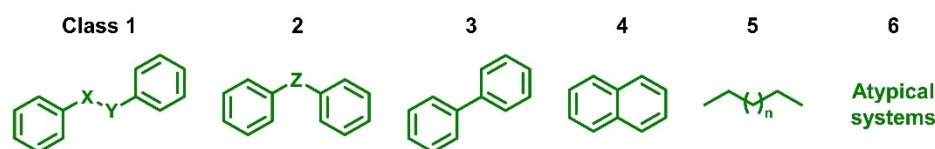


Figure 13. Classification of azosteres.

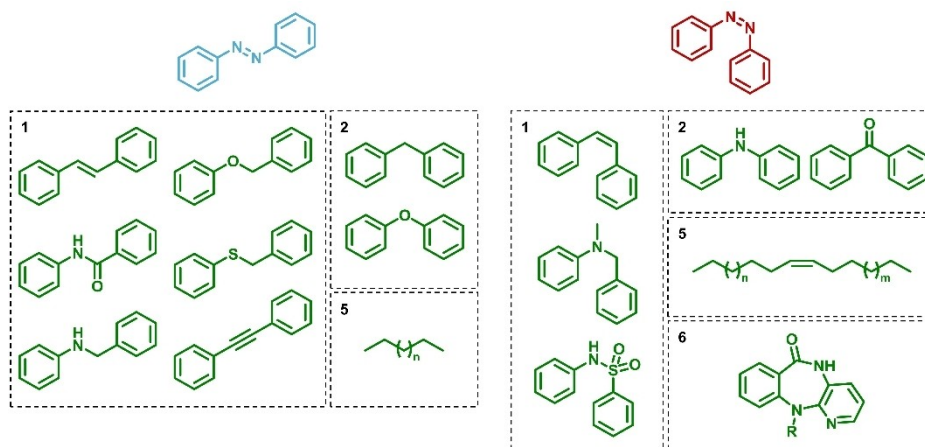


Figure 14. Overview of (*E*)-like and (*Z*)-like azosteres, subdivided into classes 1–6 (see section 3.2 and Figure 13).

3.2.1. Scaffold Hopping

In general, scaffold hopping appears to be more challenging for photopharmacological endeavors than terminal substitutions (see section 3.2.2), but it also has the potential to be more rewarding.^[116] Despite the ongoing debate on the exact definition of scaffolds,^[118] they can be divided into two broad categories:^[109]

1. A *structural* scaffold ensures the proper orientation (“exit vectors”) of the key interacting groups (role 1).
2. A *functional* scaffold comprises the elements that form crucial interactions, akin to a pharmacophore (role 2);

The most promising approach for photopharmacology is arguably the replacement of structural scaffolds (role 1), to exploit the significant geometrical changes caused by *E-Z* photoisomerization. In particular, the differences in end-to-end distance result in amplified structural changes when the photoswitch is incorporated in the center of an extended molecule. At the same time, unsubstituted *E-Z* photo-switches are inherently endowed with several pharmacophore features, and can also able to act as functional scaffolds (role 2). Azobenzene itself has two HBAs in the azo bond as well as two benzene rings that can form hydrophobic contacts and π interactions. The ideal strategy for designing successful photopharmacological agents would be embedding a photoswitch within the pharmacophore, exploiting both scaffold roles simultaneously. In addition, further decoration of the photoswitch with interacting groups offers the chance to toggle between interacting/non-interacting orientations of these groups.

3.2.1.1. (E)-Like Scaffolds

(*E*)-like bioisosteres are endowed with a flat, planar geometry that resembles (*E*)-azobenzene, and more generally (*E*)-photoswitches. Therefore, scaffold hopping of these substructures is expected to yield (*E*)-on photoswitchable ligands (Table 5).

3.2.1.1.1. (E)-Stilbene (Class 1)

Even when evaluated solely on the basis of its 2D structure, stilbene is the most obvious azostere. In fact, $-\text{CH}=\text{CH}-$ is a classical bioisostere of $-\text{N}=\text{N}-$,^[112,113] and the replacement of a $-\text{CH}$ group with an N atom in (hetero)aromatic systems is often highly beneficial for multiparameter optimizations.^[119] Moreover, stilbene is itself a bistable (P-type) *E-Z* photo-switch, which can undergo *E*-to-*Z* and *Z*-to-*E* isomerizations only upon irradiation with light (see section 1 and Figure 1). By contrast, azobenzene is a T-type photoswitch, hence its introduction in the place of stilbene makes the (*Z*)-form of the ligand metastable. As an additional improvement over stilbenes, azobenzenes are not prone to UV-promoted electrocyclicization, thus lowering the chances of undesired side-reactions upon photoisomerization. With regard to hydrogen bonding, the replacement of the $-\text{CH}=\text{CH}-$ bond with an $-\text{N}=\text{N}-$ azo bond introduces two HBA. Overall, scaffold hopping of (*E*)-stilbene with azobenzene allows a robust optical control of biological activity with concurrent small alterations of the parent ligand. This can be exemplified by the work of Trauner and co-workers, who changed the (*E*)-stilbene core of resveratrol into azobenzene for the structure-based design of (*E*)-on ATP synthase inhibitor **46**.^[120]

When there is some discrepancy between the design hypothesis and the outcome, *a posteriori* molecular docking can offer a valuable rationalization, as shown for photo-switchable inhibitors of sirtuin 2.^[121] The moderate differences in potency of compound **47** could be explained by the unfavorable positioning of the carbamate in a hydrophobic region. Furthermore, the intrinsic flexibility of the ligand was probably able to level off the differences. The surprising (*Z*)-on inhibition of compound **48** (*F*(*E/Z*) of 23) was tentatively explained with the additional interactions formed by the (*Z*)-isomer with Arg97 and Glu116 (Figure 15). The authors also associated such unexpected light-activation with the known improvement of aqueous solubility of azobenzene upon irradiation.^[122] Despite their high degree of similarity, scaffold hopping of (*E*)-stilbene with azoben-

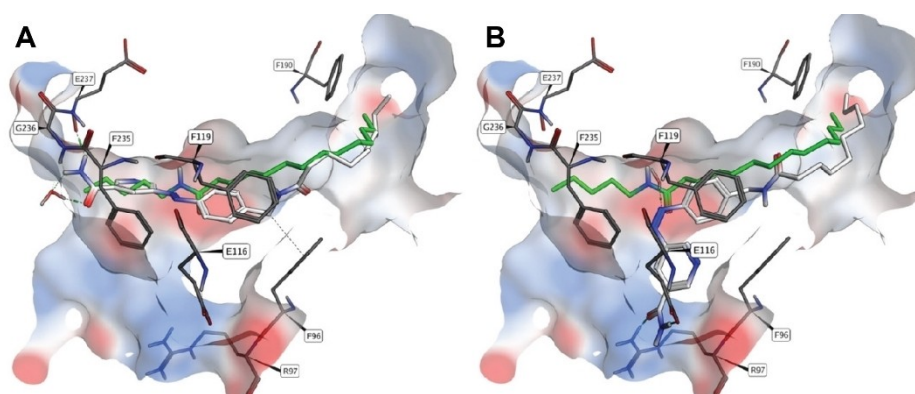


Figure 15. Docking poses of (*E*)-**48** (A) and (*Z*)-**48** (B) into sirtuin 2 (PDB ID: 4Y6L). The (*Z*)-isomer engages in two charge-assisted hydrogen bonds with Arg97 and Glu116. Adapted with permission from ref. [121]. Copyright © 2020 Wiley-VCH Verlag GmbH & Co. KGaA.

Table 5: Overview of replacements of (E)-like scaffolds.

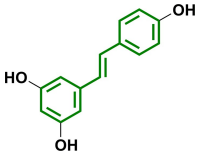
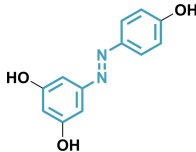
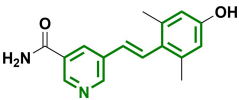
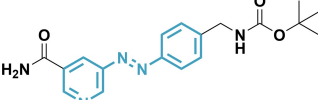
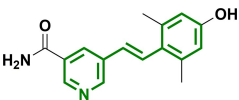
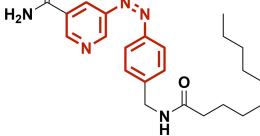
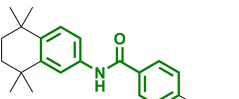
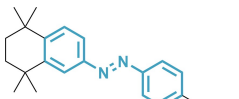
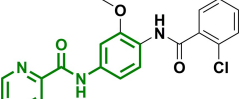
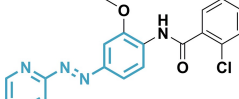
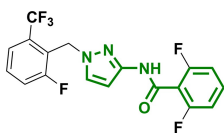
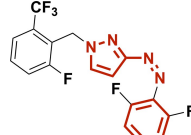
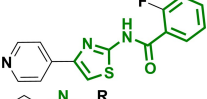
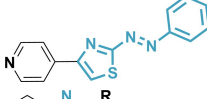
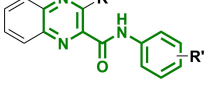
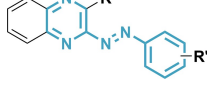
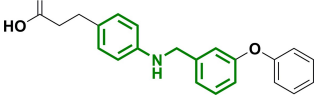
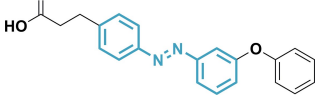
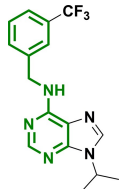
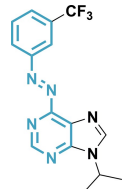
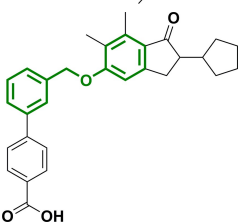
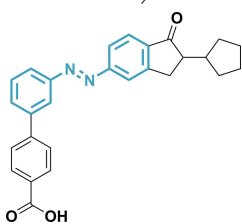
Entry	Compound	Target (ligand)	Parent compound	Photoswitchable derivative (active isomer)	Class ^[a]	Ref.
1	46	F ₁ F ₀ -ATP synthase (inhibitor)			1	[120]
2a	47	Sirtuin 2 (inhibitor)			1	[121]
2b	48	Sirtuin 2 (inhibitor)			1	[121]
3	49	RAR α (agonist)			1	[114]
4	50	mGluR5 (modulator)			1	[124,125]
5	51	CRAC (inhibitor)			1	[126]
6	52	ROCK (inhibitor)			1	[127]
7	53	5-HT ₃ R (antagonist)			1	[128]
8	54	GPCR40 (agonist)			1	[129]
9	55	CKI α (inhibitor)			1	[130]
10	56	mGluR2 (allosteric agonist)			1	[131]

Table 5: (Continued)

Entry	Compound	Target (ligand)	Parent compound	Photoswitchable derivative (active isomer)	Class ^[a]	Ref.
11	57	5-HT ₃ R (inhibitor)			1	[128]
12	58	RET kinase (inhibitor)			1	[134]
13	59	RET kinase (inhibitor)			1	[135]
14	60	12/15-LOX (inhibitor)			6	[136,137]
15	61	17βHSD3 (inhibitor)			6	[138]

[a] Azostere class: 1–6 (see section 3.2).

zene was only described twice, with one challenging example.

3.2.1.1.2. N-Aryl Benzamide (Class 1)

N-Aryl benzamide underwent numerous bioisosteric replacements in photopharmacology. Replacing this substructure with (*E*)-azobenzene exchanges one HBD and two HBA of the amide linker with two acceptors of the $\text{N}=\text{N}$ -azo bond. Therefore, substitution with the azo bond is expected to cause moderate losses of potency compared to the parent ligand.^[114] On the other hand, the amide bond has a non-zero dipole moment, in contrast to the 0 D dipole moment of (*E*)-azobenzene.

Interestingly, the 3D bioisosterism between *N*-aryl benzamide and (*E*)-azobenzene (as well as (*E*)-stilbene) has been recognized also outside of the photopharmacology field, e.g., in the context of minor groove binders for DNA.^[123] Similar yet deeper considerations on the 3D structure of bioactive compounds were used for the ligand-based design of agonist **49** for retinoic acid receptor α (RAR α).^[114] Even though this work focused on the shape similarity of whole ligands, it represents a step toward the use of pharmacophore screening in photopharmacology. Rational replacement of the *N*-aryl benzamide fragment

resulted in an (*E*)-on agonist. Since compound **49** had already been tested previously without studying its light-dependent behavior, this bioisosteric replacement also constitutes an example of photo-repurposing (see section 3.5). Arguably, the rather straightforward structural similarity between (*E*)-azobenzene and a *N*-aryl benzamide did not need such computational analysis.

At times, the parent compound can contain two identical azosteres that seem equally crucial for binding, as was the case in the development of ligand **50**, a photoswitchable modulator for metabotropic GluR5 (mGluR5).^[124] The two *N*-aryl amide bridges on both sides of an anisole core were separately replaced with an azo bond to identify the best site for azologization. By substituting the *N*-phenyl picolinamide with an azopyridine, Gorostiza and co-workers obtained compound **50**, an (*E*)-on negative allosteric modulator that was later co-crystallized bound to mGluR5 in a follow-up study.^[125] Analysis of the binding mode of the (*E*)-isomer led to the hypothesis that photoisomerization would displace the azobenzene group from a hydrophobic pocket, disrupting their shape complementarity.

In addition to the azopyridine described above, multiple heterocyclic azobenzenes derived from other *N*-heteroaryl benzamides. For instance, the bioisosteric replacement of an *N*-pyrazolyl benzamide allowed the convenient inclusion of an azopyrazole into compound **51**.^[126] This inhibitor of

calcium release-activated channel (CRAC) showed an unexpected (*Z*)-on behavior and a $F(E/Z)$ of 150, which were not rationalized. Incidentally, the biological results might indicate that it is easier to achieve large differences in potency between photoisomers when the photoswitchable ligand exhibits activities in the micromolar range (see also section 3.2.2.1.2). In another heterocyclic azolog, molecular docking guided the structure-based design of (*E*)-on kinase inhibitor **52** through the substitution of *N*-thiazolyl benzamide with an unusual phenylazothiazole.^[127] Despite being generally an effective bioisosteric replacement, in rare occasions the azologization of *N*-aryl benzamides can also generate inactive compounds, as in the case of antagonist **53** for the 5-hydroxytryptamine receptor (5-HT₃R).^[128]

3.2.1.1.3. *N*-Benzyaniline (Class 1)

N-Benzyaniline can adopt both (*E*)- and (*Z*)-like conformations,^[114] and *N*-methylation biases the conformational distribution toward the (*Z*)-like (see section 3.2.1.2.2).^[116] The $-NH-$ group is both a HBD and a HBA, thus the replacement of the $-NH-C-$ linker with an $-N=N-$ azo bond causes the overall exchange of a HBD with a second HBA.

The first example of such scaffold hopping is the azologization of *N*-benzyaniline in a G protein-coupled receptor (GPCR) ligand, which yielded **54**, an (*E*)-on agonist for GPCR40.^[129] Even though the design was based on a simple comparison of 2D structures, optical control of GPCR40 was achieved in HeLa cells. In a second example, the *N*-benzylaminopurine core of the CKI α inhibitor longdaysin was replaced with a heterocyclic azobenzene.^[130] Compound **55** underwent reduction in the presence of DTT, which is a common constituent of assay buffers. Therefore, irradiation did not result in reversible photocontrol of biological activity, but it rather promoted the irreversible conversion to the more potent hydrazine. Altogether, although *N*-benzyl anilines are common motifs in medicinal chemistry,^[114] their substitution is underrepresented in

photopharmacology, possibly due to their typical *gauche* conformation, which makes successful bioisosteric replacements less straightforward.^[114]

3.2.1.1.4. Benzyl Phenyl Ether (Class 1)

Dihedral angle analysis indicates that benzyl phenyl ether is mostly an (*E*)-like azostere.^[114] However, some benzyl ethers in the azolog space^[114] have a bent conformation, which could be exploited for the design of (*Z*)-on photoswitchable drugs (see section 3.2.1.2). With respect to hydrogen bonding, the ether oxygen atom is a bidentate HBA. Therefore, the replacement of a $-O-CH_2-$ linker with the $-N=N-$ azo bond results in the displacement of two HBA sites from one oxygen atom to two nitrogen atoms, thus modifying the spatial orientation of these HBA lone pairs.

As mentioned before, a structural scaffold is responsible for the spatial arrangement of key interacting groups. The bioisosteric replacement of such scaffolds with azobenzene should allow to target particular interactions only in one form, as recently demonstrated by the Trauner group for their photoswitchable allosteric mGluR₂ agonist **56**.^[131] In a remarkable application of structure-based design, *a priori* molecular docking suggested that (*E*)-**56** adopted a similar binding mode to the parent compound (biphenylindanone A), while the (*Z*)-azobenzene scaffold did not place the carboxylic acid in place for the hydrogen bond with Arg635 (Figure 16). Biological evaluation confirmed this computational hypothesis, suggesting that targeting an isomer-specific interaction through a photoresponsive scaffold is a feasible strategy for significant light-induced effects.

3.2.1.1.5. Benzyl Phenyl Sulfide (Class 1)

Benzyl phenyl sulfide is an underexplored bioisostere of azobenzene, in line with its lower incidence also in medicinal chemistry. Nevertheless, the fact that benzyl phenyl sulfide was introduced into the structure of antibacterial agents in

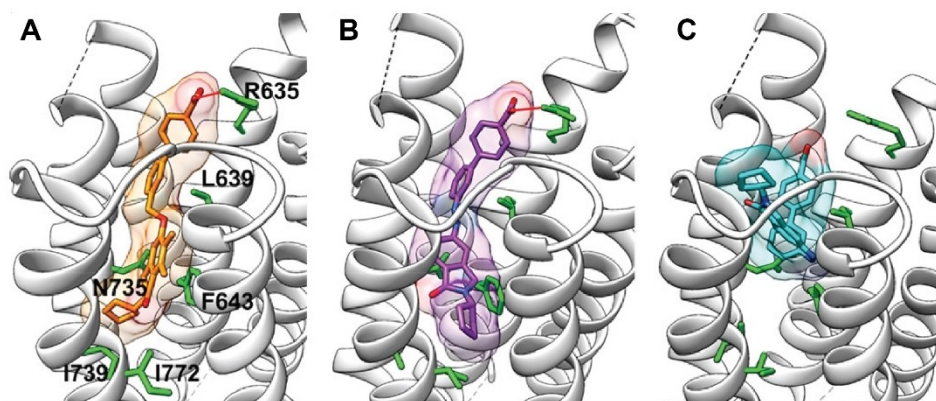


Figure 16. Docking poses of biphenylindanone A (A), (*E*)-**56** (B), and (*Z*)-**56** (C) into a homology model of mGluR₂. In a similar way to the parent compound, only the (*E*)-isomer forms a salt bridge with Arg635 and hydrophobic contacts within the binding pocket (green residues). Adapted with permission from ref. [131]. Copyright © 2021 American Chemical Society.

place of (*E*)-stilbene^[132] hints at a certain degree of similarity between this thioether and (*E*)-azobenzene. In terms of hydrogen bonding, the sulfur atom of the thioether linker has also some unconventional, lesser known HBA character.^[133] Hence, replacing a $-S-CH_2-$ linker with the $-N=N-$ azo bond introduces two classical HBA sites. This scaffold hopping strategy was explored only by the König group for the development of 5-HT₃R antagonists.^[128] Compound **57** was expected to be (*E*)-active based on considerations of previous docking into a homology model of the receptor. In addition, this study also reported the replacement of a *N*-benzyl amide group with azobenzene (compound **53**). The replacement of benzyl phenyl sulfide needs to be explored further, as only one candidate was shown to be active in this study, albeit with no significant difference between the photoisomers.

3.2.1.1.6. Diarylacetylene (Class 1)

Because it features a linear and rigid linker, diarylacetylene has a clear shape similarity with (*E*)-azobenzene, as confirmed by several studies reviewed herein. Nevertheless, some minor discrepancies lie in the length and the spatial orientation of the $-C\equiv C-$ linker when compared to the $-N=N-$ azo bond, while the latter contributes two HBA in terms of pharmacophore features.

As a clear example of the potential of substituting a structural scaffold, the Grøtli group recently reported the kinase inhibitor **58**, using REarranged during Transfection (RET) kinase as a model target.^[134] The replacement of a core diphenylacetylene with (*E*)-azobenzene was envisioned

to produce an (*E*)-on inhibitor (Figure 17). This structure-based hypothesis was supported by molecular docking calculations into a homology model, which suggested that the (*E*)-isomer could be more active than the (*Z*)-isomer because it formed key hydrogen bonds with the hinge region. Conversely, the (*Z*)-azobenzene scaffold placed the substituents far from these residues. The original heterocyclic head was replaced with a 7-azaindole because of its excellent hinge-binding and photophysical properties. Enzymatic and cellular assays showed that compound **58** was an (*E*)-on inhibitor with a F(Z/E) of 17 and 11, respectively.

In addition to their structural role, photoswitches can also be used as functional scaffolds. By incorporating an azoheteroarene into the pyrazolopyrimidine core, again Grøtli and co-workers designed the first photoswitchable kinase inhibitor **59**.^[135] With a structure-based hypothesis that was supported by prior docking calculations, the RET kinase was expected to tolerate only the (*E*)-form in its binding pocket. This scaffold hopping led to (*E*)-on inhibitor with a F(Z/E) > 3, indicating that the substitution of diarylacetylene scaffolds with *E-Z* photoswitches is an effective approach to design dark-active photopharmaceuticals.

3.2.1.1.7. Atypical Systems (Class 6)

With atypical systems, we refer to bioisosteres that elude classification in the other five classes because they do not feature simply two adjacent aromatic rings nor aliphatic chains. The first bioisosteric replacement of an atypical (*E*)-like scaffold was described in 2006 by the Kuhn group.^[136] A photoswitchable inhibitor of 12/15-lipoxygenase was ration-

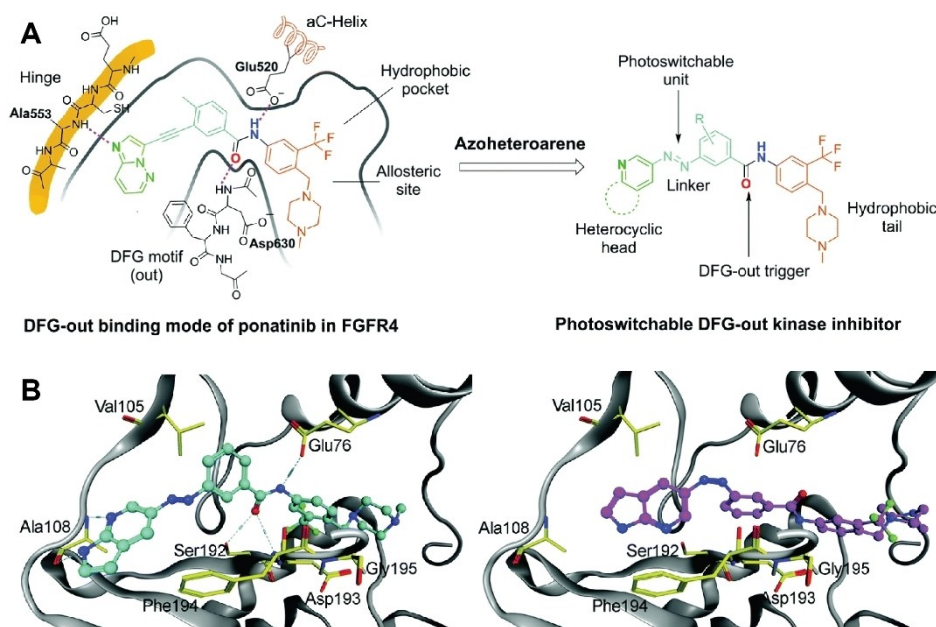


Figure 17. Structure-based design of compound **58**. (A) 2D interaction model of ponatinib in FGFR4 kinase and scaffold hopping of diarylacetylene with an azoheteroarene. (B) Docking poses of (*E*)-**58** (left) and (*Z*)-**58** (right) into a homology model of the DFG-out RET kinase. Hydrogen bonding between the headgroup of the inhibitor and the hinge region is predicted exclusively for the (*E*)-isomer. Adapted with permission from ref. [134]. Copyright © 2021 The Royal Society of Chemistry.

ally designed through the substitution of the entire core of ebselen with the strikingly similar HTI. Manual modification of a PDB complex followed by simple energy minimization suggested that the (*E*)-isomer could overlap with ebselen, while isomerization to the (*Z*)-form caused steric clashes with the target. Although the computational approach was simplistic and did not take protein flexibility into account, the (*E*)-on photoswitchable inhibitor **60** showed an impressive $F(Z/E)$ of 33. A follow-up computational study investigated the binding of compound **60** in detail, with a combination of molecular docking, MD, quantum mechanics/molecular mechanics (QM/MM) and molecular mechanics Poisson–Boltzmann surface area (MM-PBSA) calculations.^[137] The (*Z*)-isomer was predicted to have a shorter residence time in regions where it could compete with the ligand for binding. This successful example highlights the potential of the scaffold hopping strategy, especially if only minor modifications are required to make the core photoresponsive.

A second example of scaffold hopping of an atypical (*E*)-like core has been reported very recently for the optical control of 17 β -hydroxysteroid dehydrogenase type 3 (17 β HSD3).^[138] A series of tetrahydrodibenzazocine inhibitors inspired the design of diazocine analogs due to their striking similarity. Overlap of the the ligand structures showed that the metastable (*E*)-isomer could adopt a similar spatial arrangement to the parent compound, while the out-of-plane geometry of the (*Z*)-isomer was different. *A priori* docking simulations into a homology model reinforced the hypothesis that compound **61** would be light-active. Nevertheless, DTT- and glutathione-mediated reduction of the –N=N– azo bond into a ring-opened dianiline hindered any application. These results further highlight the possible risks of introducing azo bonds into bioactive compounds with regard to ADMET properties (see section 3.2).

3.2.1.2. (*Z*)-Like Scaffolds

(*Z*)-like bioisosteres feature a bent geometry that resembles (*Z*)-azobenzene. Therefore, scaffold hopping of these substructures is expected to generate (*Z*)-on photoswitchable ligands (Table 6).

3.2.1.2.1. (*Z*)-Stilbene (Class 1)

As mentioned earlier, stilbene is an evident azostere. The same considerations hold true here, as this replacement introduces two HBA of the azo bond, which are arguably more exposed and reachable in the (*Z*)-configuration. In contrast to (*E*)-stilbene (section 3.2.1.1.1), this bioisosteric replacement involved only cases of scaffold hopping, with no examples of terminal substitutions. Moreover, all the following examples revolve around the tubulin polymerization inhibitor combretastatin A-4 (CA-4), which has been the object of multiple azologization efforts because of its ideal similarity with azobenzene (Table 6).^[139–145]

With a significantly more potent *cis*-isomer, CA-4 is a highly promising starting point for scaffold hopping with (*Z*)-azobenzene. In a report that focused on the shape and electrostatics of the ligands, QM calculations suggested that CA-4 and its (*Z*)-azolog have very similar geometry and charges.^[139] Besides such ligand-based 3D considerations, another design approach taken by Thorn-Seshold et al. conceived an analogous core replacement by analyzing 2D SAR and visually inspecting the binding mode of CA-4 and colchicine.^[140] This approach stemmed from the evaluation of CA-4 pharmacophore, which required two methoxy-substituted, aromatic rings in a (*Z*)-configuration to be biologically active. Compound **62** has been reported independently times by three groups,^[139–141] confirming the (*Z*)-on character of this cytotoxic inhibitor, albeit with some variance in the light-promoted activation ($F(E/Z)$ of 35,^[139] 76,^[140] and >200^[141]). The reproducibility of such scaffold hopping indicates that it is an obvious but reliable design strategy for (*Z*)-on chemotherapeutic agents.

In an effort toward the improvement of compound **62**, a subsequent SAR study evaluated several modifications, but identified one of them as optimal, i.e., an ethoxy group instead of a methoxy group.^[145] To rationalize the striking $F(E/Z) > 550$ of compound **63**, the binding mode similarity of (*Z*)-photostatins and CA-4 was explored by molecular docking. However, not only the computational results were not able to provide an explanation of the biological data, but the docking scores were also improperly treated as predictions of binding affinities (see section 3.1.2 for our comments on such practice).

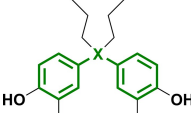
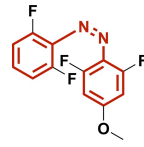
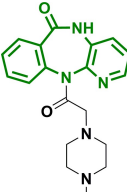
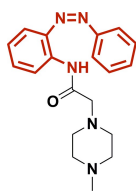
As a different strategy to optimize photoswitchable tubulin polymerization inhibitors in terms of metabolic stability and photochemical behavior in aqueous media, azobenzene was replaced with HTI via an additional scaffold hopping.^[142] Since the parent inhibitor had a relatively simple structure, analog design used a rough 2D pharmacophore model. In our opinion, 3D considerations would have enabled a clearer visualization of the molecular geometries and the collocation of the substituents. However, the authors examined the binding mode of tubulin inhibitors in the colchicine pocket. Guided by SAR data of colchicine-like binders such as CA-4, they were able to design dark-active (**64**, **65**) or light-active ligands (**66**) through the rearrangement of phenolic and methoxy moieties. Despite the planarity of both (*E*)- and (*Z*)-isomers, the asymmetrical geometry of HTI enabled to place the substituents as in the pharmacophore model. Interestingly, this report also introduced the idea of “intentional negative controls” to probe the SAR understanding in photopharmacology. Three compounds were intentionally designed to be inactive, according to the expected requirements for activity. Remarkably, *in vitro* and *in cellulo* assays confirmed the effectiveness of their design ideas in most cases, with a $F(E/Z)$ of 4 for compound **64**.

A follow-up report took inspiration for the inhibitor design from indanocine, an analog of colchicine that contains yet another scaffold, i.e., indanone.^[143] Initially, Thorn-Seshold and collaborators compared the parent CA-4 and HTI with regard to end-to-end distances and the torsion

Table 6: Overview of replacements of (Z)-like scaffolds.

Entry	Compound	Target (ligand)	Parent compound	Photoswitchable derivative (active isomer)	Class ^[a]	Ref.
1	62	Tubulin polymerization (inhibitor)			1	[139–141]
2	63	Tubulin polymerization (inhibitor)			1	[145]
3a	64	Tubulin polymerization (inhibitor)			1	[142]
3b	65	Tubulin polymerization (inhibitor)			1	[142]
3c	66	Tubulin polymerization (inhibitor)			1	[142]
4	67	Tubulin polymerization (inhibitor)			1	[143]
5a	68	Tubulin polymerization (inhibitor)			1	[147]
5b	69	Tubulin polymerization (inhibitor)			1	[147]
6	70	Tubulin polymerization (inhibitor)			1	[144]
7	71	<i>E. coli</i> and human DHFR (inhibitor)			1	[40,148]
8	72	Lp-PLA ₂ (inhibitor)			1	[116]
9	73	α_2 -AR (agonist)			2	[150]

Table 6: (Continued)

Entry	Compound	Target (ligand)	Parent compound	Photoswitchable derivative (active isomer)	Class ^[a]	Ref.
10	74	ER α (antagonist)			2	[151]
11	75	M ₁ mAChR (antagonist)			4	[152]

[a] Azostere class: 1–6 (see section 3.2).

angle between the aryl rings. Then, the substituents were chosen to match the substitution pattern of indanocene. The necessity of a *para*-hydroxy group further prevented the use of azobenzene, as *para*-hydroxyazobenzenes undergo extremely fast thermal (*Z*)-to-(*E*)isomerization.^[146] After a thorough SAR exploration, the dark-active compound **67** was obtained as a complementary tool for the study of tubulin inhibition.

To further expand the toolbox available for the optical control over the microtubule cytoskeleton, a third round of scaffold hopping led to the recent implementation of styrylbenzothiazole in CA-4 analogs.^[147] This photoswitch is geometrically similar to azobenzene but it features a bulkier benzothiazole ring on one side. At the design stage, the authors envisioned that this ring could mimic either of the two methoxy-containing benzene rings of CA-4. Such strategy resulted in (*Z*)-on derivatives **68** and **69**, with a $F(E/Z)$ of 20. The intentional negative controls were designed by permuting the substituents to double-check their hypothesis (Figure 18A), following a smart method introduced by this group earlier (vide supra).^[142] X-ray crystal structures (PDB IDs: 6ZWC and 6ZWB) demonstrated the perfect overlap between the novel benzothiazole and the parent benzene rings in the binding pocket of tubulin (Figure 18B).

With the most recent study in this series of sequential scaffold hoppings, the Thorn-Seshold group developed

another photoswitchable tubulin polymerization inhibitor.^[144] After styrylbenzothiazole, the authors investigated a pyrrole HTI scaffold, which has great potential for photopharmacological applications. In fact, this photoswitch is responsive to light of bio-compatible wavelengths, and shows quantitative photoisomerization in both directions. Furthermore, it is resistant to reduction by glutathione. The compounds were rationally designed to place an ethyl instead of a methoxy substituent as a spacefilling group in the binding pocket. Antiproliferative assays confirmed such hypothesis and determined a $F(E/Z) > 10$ for derivative **70**.

Overall, the work by Thorn-Seshold offers a successful example of “photoswitchable scaffold hopping”. Over the years, several combinations of photoswitchable scaffolds were explored, guided by the spatial arrangement of the methoxy and phenolic groups of CA-4 and colchicine.

3.2.1.2.2. N-Benzyl-N-Methylaniline (Class 1)

Although CSD and PDB structural queries indicated that *N*-benzylanilines can feature both (*E*)- and (*Z*)-like conformations,^[114] we found that *N*-methylation biases the conformational distribution toward the (*Z*)-like form.^[116] Almost all entries in the PDB were embedded in the core of methotrexate, a dihydrofolate reductase (DHFR) inhibitor

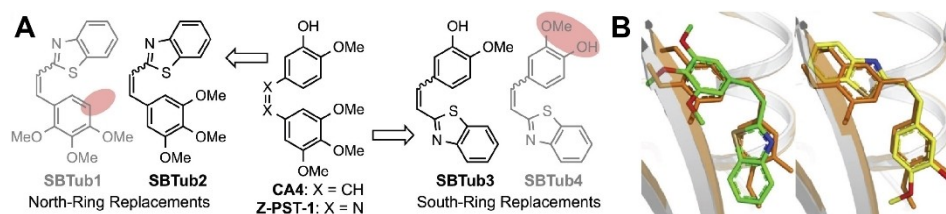


Figure 18. Scaffold hopping of (*Z*)-azobenzene with styrylbenzothiazole. (A) The inhibitors were designed to mimic the CA-4 pharmacophore in their (*Z*)-form, while the intentional negative controls (transparent structures) were designed to mismatch it (red circles). (B) Binding mode of (*Z*)-**68** (green, PDB ID: 6ZWC) and (*Z*)-**69** (yellow, PDB ID: 6ZWB) superposed with CA-4 (orange, PDB ID: 5LYJ). Adapted with permission from ref. [147]. Copyright © 2021 Elsevier Ltd.

that inspired the following examples of scaffold hopping. On the other hand, such moiety has not been involved in cases of terminal replacement, so far.

The potential of *N*-benzyl-*N*-methylaniline as a (*Z*)-like core was recognized in two identical molecular designs of photoswitchable DHFR inhibitors (compound **71**). With the *Escherichia coli* (*E. coli*) enzyme as target, visual inspection of the protein-ligand complex (PDB ID: 4P66) suggested that the bent geometry of the parent scaffold would support the replacement with (*Z*)-azobenzene.^[148] Compared to the linear and extended (*E*)-azobenzene, the (*Z*)-isomer showed an excellent overlap with the binding conformation of methotrexate. In fact, the inhibitor contains a heterocyclic variation of *N*-benzyl-*N*-methylaniline, with a pyrazine (belonging to a pteridine ring) in the place of the benzyl substituent. The azologization of such system required its simplification to quinazoline ring for synthetic accessibility, together with the substitution of the $-\text{CH}_2-\text{N}(\text{CH}_3)-$ linker with an $-\text{N}=\text{N}-$ azo bond. The authors tested *in vitro* their rational, structure-based hypothesis, which resulted in the light-activatable DHFR inhibitor **71** with a $F(E/Z)$ of 13.

In a slightly earlier report, the Gorostiza group designed an identical photoswitchable inhibitor (**71**) for human DHFR through a more detailed structure-based strategy.^[40] Using the same assumptions as in the previous report of the same compound, the bent shape of the *N*-aryl-*N*-benzylaniline group in methotrexate was anticipated to be mimicked only by (*Z*)-azobenzene. Molecular docking calculations further supported the striking similarity between the binding modes of (*Z*)-**71** and methotrexate (Figure 19), albeit with inaccurate comparisons of docking scores (see section 3.1.2 for a discussion on this practice). The azolog (named “phototrexate”) proved to be a (*Z*)-on inhibitor that was effective *in vitro*, *in cellulo* and *in vivo* on zebrafish larvae.

3.2.1.2.3. Biaryl Sulfonamide (Class 1)

Biaryl sulfonamide is an underrepresented yet promising (*Z*)-like azostere. In fact, this substructure shows poor shape similarity with (*E*)-azobenzene,^[114] while its bent geometry is more similar to (*Z*)-azobenzene.^[116] Furthermore, the magnitude (≈ 6 D) and the direction of the dipole moment of biaryl sulfonamide are better mimicked by (*Z*)-azobenzene.^[116] In terms of hydrogen bonding capacity, the

$-\text{SO}_2\text{NH}-$ linker features two sulfonyl oxygens (i.e., two bidentate HBAs) and one nitrogen atom (i.e., a HBD). Thus, their replacement with two HBAs of the $-\text{N}=\text{N}-$ azo bond is expected to cause a decrease in potency.

The only example of such scaffold hopping was described by our group.^[116] First, CSD and PDB data indicated that biaryl sulfonamides and (*Z*)-azobenzenes have similar distributions of centroid angles and ring distances. Additionally, DFT calculations revealed their electronic similarity with regard to dipole moments and electronic potential surfaces. To examine the bioisosteric replacement of a biaryl sulfonamide core, we chose an inhibitor of lipoprotein-associated phospholipase A₂ (Lp-PLA₂). *A priori* IFD and MD calculations suggested that the bent (*Z*)-isomer of azolog **72** would mimic the binding mode of its template compound, as opposed to the linear (*E*)-isomer. Nevertheless, (*Z*)-**72** did not engage in the key hydrogen bonds formed by the sulfonamide bridge with the oxyanion hole of Lp-PLA₂. Such predictions were confirmed experimentally, as compound **72** showed a $F(E/Z) > 10$ but also a 100-fold lower potency than the parent inhibitor. Since the biaryl sulfonamide moiety interacted with buried residues of the target, its azolog suffered a larger loss of activity. Concurrently, a larger difference in activity between the photoisomers was achieved, suggesting that a (*Z*)-like substructure was strictly required for biological activity. Overall, ligand- and structure-based considerations offered critical insights on the azologization of a biaryl sulfonamide scaffold (for its terminal substitution, see section 3.2.2.1).

3.2.1.2.4. Diarylamine and Diarylmethylene (Class 2)

The bioisosteric replacement of two aromatics linked by a one-atom bridge is extremely rare in photopharmacology, both in the scaffold and at the periphery. However, we believe that especially diarylamines and benzophenones (see section 3.2.2.2.2) might be a source of inspiration for the rational design of (*Z*)-on ligands, because the two facing aryl rings have an intrinsically (*Z*)-like arrangement.^[106,149]

An unusual 2D azologization of a diarylamine substructure led to the light-dependent modulation of α_2 -AR.^[150] Starting from the known adrenergic agonist clonidine, the $-\text{NH}-$ nitrogen linker was replaced with an $-\text{N}=\text{N}-$ azo group, while the parent cyclic

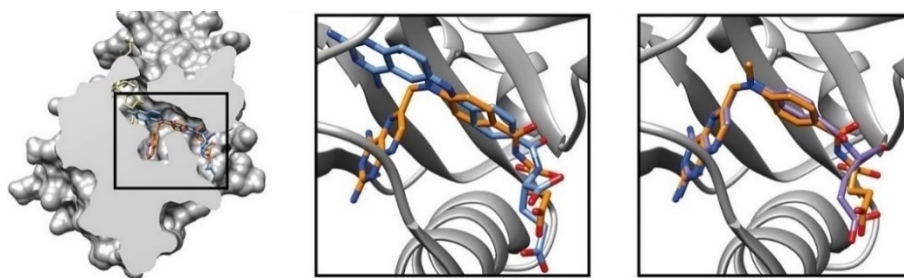


Figure 19. Docking poses of (*E*)-isomer (blue) and (*Z*)-isomer (purple) of compound **71** into human DHFR, compared to the experimental binding mode of methotrexate (PDB ID: 1U72). Adapted with permission from ref. [40]. Copyright © 2018 American Chemical Society.

amidine was converted into its aromatic counterpart, i.e., imidazole. In accordance with their ligand-based hypothesis, Gorostiza and co-authors obtained the (*Z*)-on adrenergic agonist **73**, which enabled *in vivo* optical control of locomotion in zebrafish and pupillary responses in mice.

On the other hand, diarylmethanes defy a more rigid categorization, as they were shown to be both (*Z*)- and (*E*)-like azosteres. Using a scaffold hopping strategy, the $-C-$ methylene linker of a estrogen receptor α (ER α) antagonist was replaced with an $-N=N-$ azo bond.^[151] Such replacement implied the introduction of two HBA in the place of a lipophilic bridge, resulting in compound **74**, a (*Z*)-on ER α ligand, with a $F(E/Z) > 4$. In this case, the presence of two additional substituents on the methylene linker probably increased the (*Z*)-like character of this otherwise (*E*)-like bioisostere (see section 3.2.2.1.6).

3.2.1.2.5. Atypical Systems (Class 6)

Atypical tricyclic azosteres were explored very recently for the first time, during the development of photoswitchable antagonists of M₁ mAChR.^[152] The design stemmed from a ligand-based hypothesis, i.e., the shape similarity between (*Z*)-azobenzene and the fused tricyclic scaffold of pirenzepine. Such hidden bioisosteric replacement was termed “crypto-azologization”, because a bond needed to be broken to carve the (*Z*)-like azostere out of the scaffold (Figure 20). In addition to the 3D overlap of substructures, the authors performed molecular docking studies into M₁ mAChR to explore the scaffold hopping in silico. The computational results revealed that the (*Z*)-form adopted a binding mode comparable to pirenzepine, with the same end-to-end distance. On the other hand, only flipped poses were obtained for the planar (*E*)-form, conflicting with antagonism activity. This innovative design strategy resulted in the (*Z*)-on antagonist **75**, which displayed a 200-fold lower potency than the parent compound. We speculate that such a large decrease in activity might be due to a higher entropic cost for the binding of compound **75**, as compared to pirenzepine with its conformationally preorganized tricyclic core.

3.2.1.3. Ambiguous, (*E/Z*)-Like Scaffolds

Ambiguous bioisosteres (i.e., biaryl, naphthalene, phenanthrene, adamantyl) can be regarded as both (*E*)- and (*Z*)-like, depending on their substitution pattern. As a result, scaffold hopping can potentially generate both (*E*)- and (*Z*)-on photoswitchable ligands. While terminal substitution of these ambiguous substructures is more common (see section 3.2.2.3), only one example involved them as scaffolds. In this case, the naphthalene core of histamine H₃ receptor (H₃R) antagonists was replaced with azobenzene.^[153] After preparing a library of compounds, the Leurs group identified two ligands with the largest light-induced changes in affinity. In line with the spatial arrangement of substituents on the parent 2,6-naphthalene scaffold, the biological results showed a clear dependency on the pattern of the disubstituted azobenzene core. Whereas the *para-meta* compound (**76**) was (*E*)-active, the *meta-meta* compound (**77**) showed (*Z*)-on antagonism. *A posteriori* docking and subsequent MD calculations aided the interpretation of such opposite effects in terms of solvent exposure of apolar surface areas and conformer focusing^[154] (Figure 21). One of the two photoisomers displayed higher H₃R affinity when it was predicted to bury the hydrophobic region of the binding site. Concurrently, a lower affinity was observed when the isomer had reduced conformational freedom upon binding. Despite the ambiguous nature of the naphthalene core, a detailed computational analysis facilitated the rationalization of the observed H₃R modulation.

3.2.2. Terminal Substitution

Bioisosteric replacements at the periphery of drug structures are likely to be more tolerated but are concurrently likely to result in smaller differences between the photoisomers. In other words, there is often a trade-off between preservation of original potency and amplitude of light-induced changes in potency.

3.2.2.1. (*E*)-Like Bioisosteres

(*E*)-Like bioisosteres have been the object of terminal substitutions with *E-Z* photoswitches (Table 7) much more frequently than (*Z*)-like bioisosteres (see section 3.2.2.2 and Table 8). In the context of the classical azosteres (i.e., two



Figure 20. 2D structure of a generic fused tricyclic scaffold, and 3D superposition of (*E*)- and (*Z*)-azobenzene (orange) scaffold onto such tricyclic core (gray). Adapted with permission from ref. [152]. Copyright © 2021 American Chemical Society.

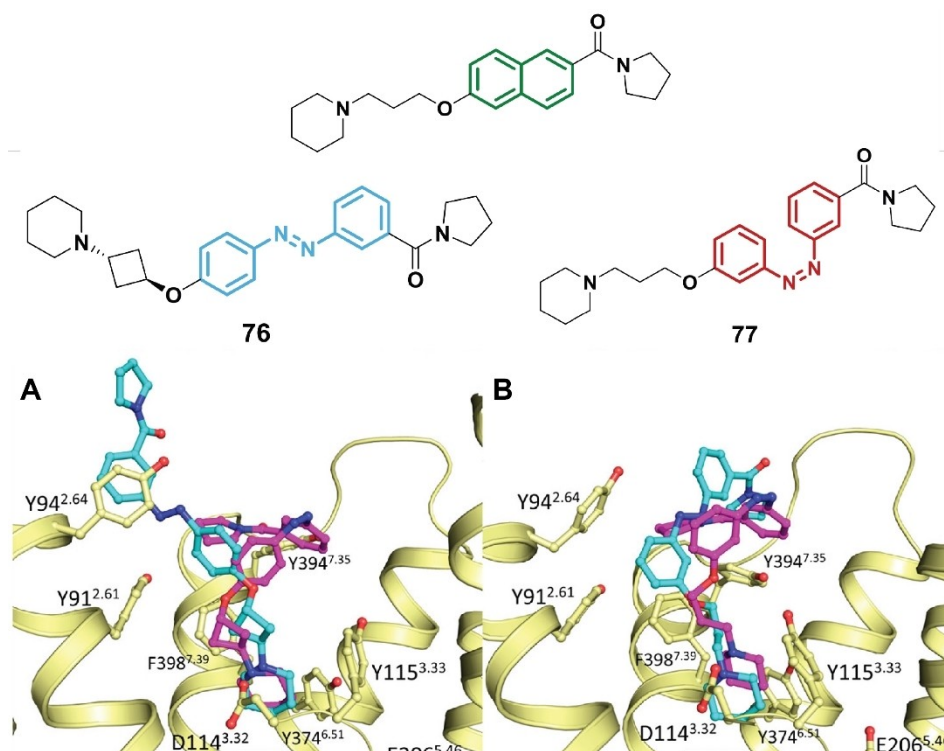


Figure 21. Scaffold hopping of the naphthalene core (green) of a H₃R antagonist. Predicted binding poses of compounds **76** (A) and **77** (B). Adapted with permission from ref. [153]. Copyright © 2018 American Chemical Society.

aromatic rings separated by a two-atom linker), this bias toward (*E*)-like substructures was also supported by the higher frequency of azosteres with (*E*)-like dihedral angle distributions.^[114]

3.2.2.1.1. Aza-Stilbene (Class 1)

Aza-stilbene has the closest similarity to (*E*)-azobenzene. In fact, this classic bioisosteric replacement requires the substitution of only one carbon in the –CH=N– linker, thus introducing one HBA with the nitrogen atom. In line with the scarce representation of aza-stilbenes in bioactive ligands, only in one study such moiety was replaced with azobenzene for the design of photoswitchable inhibitor **78**, targeting AChE.^[155] To amplify the light-induced changes in end-to-end distances, the authors also repeated the flexible alkyl chain on the other side of the photoswitch. In the dual inhibitor **130**, azobenzene is better defined as a linker (see section 3.4). Both design approaches led to a mixed library of (*E*)- and (*Z*)-on inhibitors, although the parent compound was in its (*E*)-form.

3.2.2.1.2. (*E*)-Stilbene (Class 1)

After the rare aza-stilbene, (*E*)-stilbene is the most evident bioisostere of azobenzene, as discussed earlier (see section 3.2.1.1.1). The obvious similarity between (*E*)-stilbene and

(*E*)-azobenzene was exploited for example in the ligand-based design of photoswitchable AChR antagonist **79**.^[156]

Going beyond 2D considerations, structure-based design allows for more informed hypotheses and more meaningful interpretations. Existing crystallographic data of the protein-ligand complex guided the design of compound **80**, a photoswitchable inhibitor of the human serotonin transporter (hSERT).^[157] Although such ligand was devised by azologization of the (*E*)-stilbene of escitalopram, it was counterintuitively activated with light, resulting in an impressive F(*E*/*Z*) of 43. *A posteriori* IFD calculations suggested that the (*Z*)-form resembled the binding mode of the parent compound in 75 % of the predicted poses, while that was the case only for 32 % of (*E*)-poses (Figure 22).

To prevent unexpected outcomes, hypotheses can be initially evaluated in silico, as reported in the structure-based design of light-controlled modulator **81** for the farnesoid X receptor (FXR).^[158] *A priori* molecular docking indicated that the (*E*)-isomer could approximate the parent binding mode better than the (*Z*)-isomer. Pharmacological evaluation confirmed the (*E*)-on agonism profile of the photohormone, which showed a high F(*Z*/*E*) of ≈ 100 (dark EC₅₀ = 1.1 μ M, irradiated EC₅₀ = 95 μ M). As we already commented (see section 3.2.1.1.2), such large differences in potency seem more likely to emerge from photoswitchable ligands that are active in the high-micromolar range. In general, terminal substitution of (*E*)-stilbenes is a straightforward yet effective strategy for the rational design of (*E*)-on photopharmaceuticals.

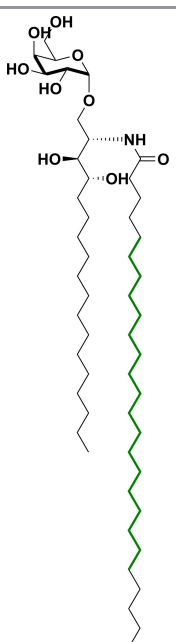
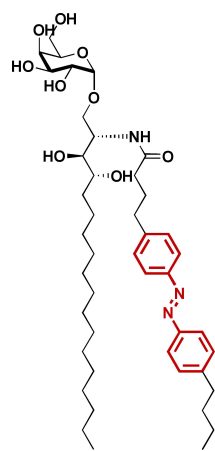
Table 7: Overview of terminal replacements of (E)-like bioisosteres.

Entry	Compound	Target (ligand)	Parent compound	Photoswitchable derivative (active isomer)	Class ^[a]	Ref.
1	78	AChE (inhibitor)			1	[155]
2	79	nAChR (agonist)			1	[156]
3	80	hSERT (inhibitor)			1	[157]
4	81	FXR (agonist)			1	[158]
5	82	Sirtuin 2 (inhibitor)			1	[121]
6	83	EAAT2 (inhibitor)			1	[159]
7	84	GltTk (inhibitor)			1	[160, 161]
8	85	Na _v (blocker)			1	[54]
9	86	GABA _A R (antagonist)			1	[162]
10	87	GLP-1R (modulator)			1	[164]
11	88	GlyT2 (inhibitor)			1	[163]

Table 7: (Continued)

Entry	Compound	Target (ligand)	Parent compound	Photoswitchable derivative (active isomer)	Class ^[a]	Ref.
12	89	LTA ₄ H (inhibitor)			1	[114]
13	90	PPAR γ (inhibitor)			1	[166]
14	91	H ₃ R (agonist)			1	[167]
15	92	NMDAR (antagonist)			2	[169]
16	93	GAT1 (inhibitor)			2	[171]
17a	94	LasR (activator)			5	[173]
17b	95	LasR (activator)			5	[173]
18	96	LasR (activator/inhibitor)			5	[174]
19a	97	CB ₁ R (agonist)			5	[175]
19b	98	CB ₁ R (agonist)			5	[175]
20	99	S1PR (agonist)			5	[176]
21	100	Lipid rafts			5	[177]

Table 7: (Continued)

Entry	Compound	Target (ligand)	Parent compound	Photoswitchable derivative (active isomer)	Class ^[a]	Ref.
22	101	CD1d and NKT cell receptor (activator)			5	[178]

[a] Azostere class: 1–6 (see section 3.2).

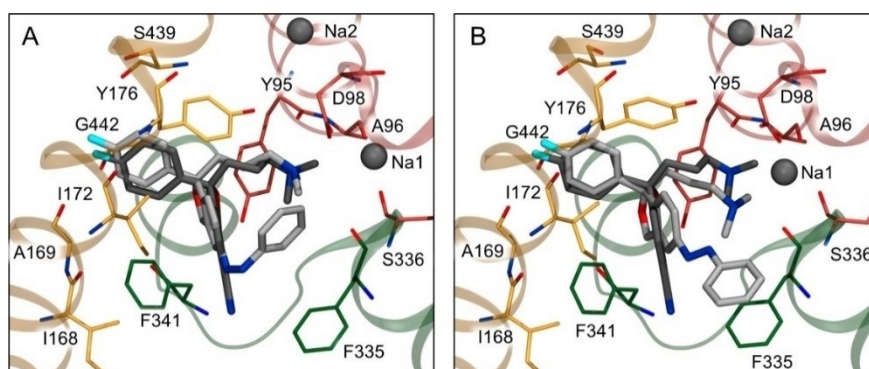


Figure 22. IFD poses of (Z)-isomer (A) and the (E)-isomer (B) of compound **80** (light gray) into hSERT (PDB ID: 5171), superposed with the co-crystallized parent inhibitor, escitalopram (dark gray). Adapted with permission from ref. [157]. Copyright © 2020 American Chemical Society.

3.2.2.1.3. N-Aryl Benzamide (Class 1)

For general comments on *N*-aryl benzamide substructure, see section 3.2.1.1.2. Along with scaffold hopping endeavors, also terminal azologization of *N*-aryl benzamides is a popular strategy in photopharmacology and it has generated several photoswitchable ligands for a variety of targets.

In line with its planar geometry, the substitution of an *N*-phenyl benzamide moiety enabled the design of the sirtuin 2 inhibitor **82**^[121] and of two strongly related, dark-active glutamate transporter inhibitors, **83**^[159] and **84**.^[160] In a recent follow-up study by our group, the binding modes of both photoisomers of compound **84** were elucidated by X-ray crystallography (PDB ID: 6ZLH for the (E)-isomer; PDB

ID: 6ZL4 for the (Z)-isomer).^[161] The experimental data suggested that compound **83** is an (E)-on inhibitor (with a F(Z/E) of 3.6) probably because of an additional hydrogen bond between the azo group and the backbone amide of Gly360 (Figure 23). These pioneering results are of vital importance for photopharmacology, as they provide key insights on the light-induced differences in binding at the molecular level.

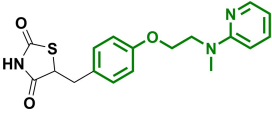
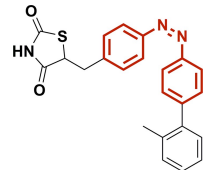
3.2.2.1.4. Benzyl Phenyl Ether (Class 1)

In addition to one successful example of scaffold hopping (see section 3.2.1.1.4), bioisosteric replacement of benzyl

Table 8: Overview of terminal replacements of (Z)-like bioisosteres.

Entry	Compound	Target (ligand)	Parent compound	Photoswitchable derivative (active isomer)	Class ^[a]	Ref.
1	102	BRAF ^{V600E} (inhibitor)			1	[179]
2	103	HDAC2 (inhibitor)			1	[116]
3	104	CRY1 (stabilizer)			2	[180]
4	105	TRPV1 (agonist)			5	[181]
5	106	PKC (agonist)			5	[182]
6	107	mTOR and Hippo (agonist)			5	[183]
7	108	LPA1–5 (agonist)			5	[184]
8	109	KATP channel (blocker)			6	[185]
9	110	HDAC (inhibitor)			6	[68]
10	111	HDAH (inhibitor)			6	[186]

Table 8: (Continued)

Entry	Compound	Target (ligand)	Parent compound	Photoswitchable derivative (active isomer)	Class ^[a]	Ref.
11	112	PPAR γ (agonist)			6	[166]

[a] Azostere class: 1–6 (see section 3.2).

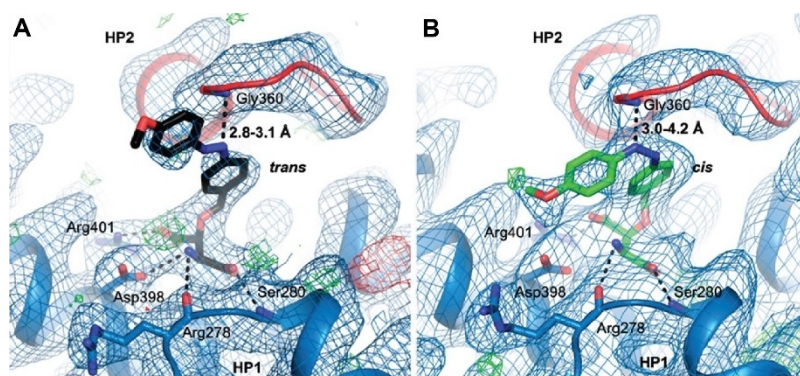


Figure 23. X-ray structures of the (*E*)-isomer (A, PDB ID: 6ZLH) and the (*Z*)-isomer (B, PDB ID: 6ZL4) of compound **84** bound to the glutamate transporter homologue from *Thermococcus kodakarensis* (Glt_{Tk}). Hydrogen bonds are depicted as black dashed lines. Adapted with permission from ref. [161]. Copyright © 2021 American Chemical Society.

phenyl ether generated (*E*)-on ligands in almost all cases involving the periphery. Moreover, this substructure inspired the first application of the azologization strategy. In fact, with a fundamental contribution to rational design in photopharmacology, Trauner and co-workers introduced the term “azologization” in the literature and provided the first definition of “azosteres” using exactly this approach.^[54] Replacing the benzyl phenyl ether tail of fomocaine with azobenzene yielded compound **85**, an (*E*)-on photoswitchable blocker for voltage-gated Na⁺ channels (Na_v), which enabled the optical control of action potential firing of mouse hippocampal neurons.

A similar design approach led to the development of other (*E*)-on ligands: compounds **86**, antagonist of the GABA_AR,^[162] **87**, glycine transporter T2 (GlyT₂) inhibitor,^[163] and **88**, allosteric modulator for glucagon-like peptide 1 receptor (GLP-1R).^[164] In a follow-up report on compound **88**, it was envisioned that because benzyl phenyl ether is flexible, structural preorganization in an (*E*)-like conformation might give a boost in activity.^[165] Therefore, the above-mentioned azolog was subjected to a further substitution of the azo bond into an olefinic bond. This approach represents a great example of intercommunication between medicinal chemistry, photopharmacology and back to medicinal chemistry again: photopharmacological insights supported the design of a tool that was not light-responsive, but had improved potency compared to the original compound.

Besides suggesting a scaffold hopping strategy on *N*-aryl benzamide for compound **52** (see section 3.2.1.1.2), 3D overlap of promising azosteres prompted the terminal substitution of benzyl phenyl ether for **89** (Figure 24).^[114] Such rare 3D-aware azologization resulted in an (*E*)-on inhibitor of leukotriene A₄ hydrolase (LTA₄H). However, the definition of an azolog space provided little additional knowledge, because it led to the identification of already known azosteres, such as *N*-phenyl benzamide and benzyl phenyl ether.

Moving from ligand- to structure-based approaches, a priori molecular docking guided the design of compound **90**, a modulator for peroxisome proliferator-activated receptor γ (PPAR γ).^[166] Trauner and co-workers left the polar head-group unchanged and replaced the benzyl phenyl ether in an aromatic tail that affects function and potency of the ligand (effector module). Such terminal substitution resulted in a lack of biological activity, whereas better outcomes were obtained by replacing a more extended hydrophobic group (see section 3.2.2.2.4). Except for the last case, benzyl phenyl ether is an established azostere for rational photopharmacology, whether at the core or at the periphery of a bioactive compound.

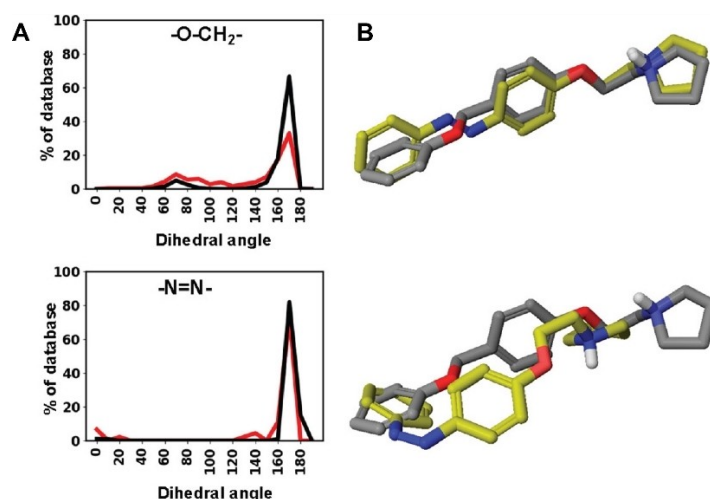


Figure 24. (A) Dihedral angle distribution from the CSD and the PDB for benzyl phenyl ethers and azobenzenes. (B) 3D overlap of template compound (gray) and (E)- and (Z)-isomers of azolog **89** (yellow). Adapted with permission from ref.[114]. Copyright © 2019 American Chemical Society.

3.2.2.1.5. Diarylacetylene (Class 1)

The only example of terminal substitution of a diphenylacetylene moiety was reported for the development of photo-switchable agonists for the human H_3R .^[167] The SAR-informed design kept the key imidazole core and replaced the flanking diphenylacetylene group with azobenzene, as the strict requirements for this side chain suggested that any deviation could greatly influence the original potency. The lead compound **91** displayed (*E*)-on agonism, with a $F(Z/E)$ of 20. Both scaffold hopping (see section 3.2.1.1.6) and terminal bioisosteric replacement of diarylacetylene with azobenzene proved to be effective strategies for the design of (*E*)-on photoswitchable ligands.

3.2.2.1.6. Diaryl Ether and Diarylmethylene (Class 2)

Azologization of aromatic systems that feature two rings and a one-atom linker is still an atypical strategy in photopharmacology. In contrast to diarylamines (see section 3.2.1.2.4) and benzophenones (see section 3.2.2.2.2), diaryl ethers and diarylmethylenes appear more suitable as (*E*)-like bioisosteres. For instance, diaryl ether has been reported as a convenient bioisostere of (*E*)-stilbene.^[168] The only photopharmacological example involved the replacement of a diaryl ether with azobenzene to generate **92**, an (*E*)-on antagonist of NMDARs.^[169] Although diaryl ether is widely used in medicinal chemistry,^[170] its underexplored azologization deserves more attention and could provide great inspiration for the design of dark-active photoswitchable ligands.

By contrast, substituting diarylmethylene moieties can lead to variable outcomes, depending on the steric bulk on the methylene bridge (see section 3.2.1.2.4). With a ligand-based strategy, photoswitchable inhibitors of GABA transporters were designed through the azologization of an

diarylmethylene with an unsubstituted $-CH_2-$ linker.^[171] To screen different designs, the authors explored *ortho*-, *meta*-, and *para*-substituted azobenzenes as well as a larger naphthyl outer ring. The most potent derivative was the naphthalene-containing **93**, which showed (*E*)-on inhibition of murine GABA transporter 1 (GAT1). Taking the results from scaffold hopping (see section 3.2.1.2.4) and this terminal replacement into account, it appears that an aryl-C-aryl substructure is a (*Z*)-on azostere when it features a $-C(XY)-$ linker, while it is an (*E*)-on azostere with a $-CH_2-$ linker.

3.2.2.1.7. Saturated Aliphatic Chains (Class 5)

Aliphatic chains are somewhat surprising azosteres, because they do not include any aromatic rings. However, it is their lipophilicity that makes them appropriate for replacement with the hydrophobic azobenzene, in spite of the cost in terms of flexibility loss. The classification of saturated aliphatic chains as (*E*)-like azosteres is not obvious, except if they are compared to unsaturated chains (see section 3.2.2.2.3). The bioisosterism between aliphatic chains and azobenzene was recognized as early as 1971, in one of the first photopharmacological studies by Erlanger and co-workers.^[172] They obtained compound **127**, an (*E*)-on agonist of muscle-type nicotinic AChR (nAChR), by replacing the alkyl spacer of decamethonium with an azobenzene (see section 3.4).

The lipophilic character of azobenzene inspired more recent efforts to substitute aliphatic chains. A representative case is the design of photoswitchable quorum sensing autoinducers, through the azologization of the saturated alkyl chain of an analog of *N*-butyryl-L-homoserine lactone.^[173] Bioluminescence activity assays indicated that a methylene bridge between the lactone head group and the photoswitch influenced the light-dependent behavior. While

the absence of such methylene bridge generated the (*E*)-on inducing agent **94**, its presence led to the (*Z*)-on compound **95**. In a follow-up study, the alkyl chain of a slightly different autoinducer, *N*-3-(oxo-dodecanoyl)-L-homoserine lactone, was replaced with an azobenzene moiety, exploring different lengths of a hydrophobic tail in the *para* position.^[174] The screening of this parameter proved to be crucial, as **96** showed an astonishing $F(E/Z) > 700$ on LasR, due to an optimal four-carbon-atom tail. Remarkably, further characterization revealed that in reality this derivative is an efficacy switch, displaying opposite behaviors (quorum-sensing inhibition versus activation) before and after irradiation.

In the examples described above, the bioisosteric replacement of aliphatic substructures produced a mixture of (*E*)- and (*Z*)-on ligands, with no attempt to rationalize the light-induced changes. However, computational methods can provide valuable insights into the reasons behind experimental observations, as demonstrated by the following report on CB₁R agonists.^[175] Starting from the alkyl group of Δ^9 -tetrahydrocannabinol, structure-based considerations aided the design of photoswitchable derivatives. By exploring different regioisomers, the authors found that the substitution pattern of the azobenzene moiety affected the activity. Whereas compound **97**, bearing a *meta*-substituted azobenzene, was a (*Z*)-on agonist, the *ortho*-substituted **98** was determined to be an (*E*)-on ligand. The interpretation of these results was based on the spatial arrangement of azobenzene in molecular docking calculations. The active isomers occupied the same hydrophobic channel as the aliphatic chain of the co-crystallized CB₁R agonist (Figure 25). The only weak point of this computational rationalization lies in the problematic comparison of docking scores, which are known not to be suitable for this type of discussion (see section 3.1.2).^[80,83,84]

Arguably, the azologization of aliphatic groups offers the most interesting outcomes when applied to photoswitchable lipids. The body of work of the Trauner group clearly proves the potential of this branch of photopharmacology. An illustrative case may be found in the design of compound **99**, azolog of sphingosine-1-phosphate (S1P), which was inspired by the fact that S1P receptor (S1PR) activation depends on

sphingoid base chain length.^[176] To maximize the changes in length upon irradiation, the azobenzene photoswitch was incorporated in the center of the lipid tail. Interestingly, compound **99** was determined to be either an (*E*)-on or a (*Z*)-on agonist, depending on the S1PR subtype. *A posteriori* docking into homology models suggested that interactions between the polar headgroup and the receptor play a critical role in the activation.

Finally, a distinct approach is exploiting the structural differences between saturated and unsaturated aliphatic chains. In fact, bioisosteric replacement with azobenzene allows the geometry of a lipid tail to be toggled between linear (saturated chain and (*E*)-azobenzene) and bent (unsaturated chains and (*Z*)-azobenzene). This is exemplified by the development of the sphingolipid ceramide azolog **100**^[177] and of the photoswitchable galactosylceramide **101**.^[178] However, such strategy was shown to give more predictable and consistent results when unsaturated, (*Z*)-like aliphatic chains are targeted as bioisosteres of *E-Z* photoswitches (see section 3.2.2.3).

3.2.2.2. (*Z*)-Like Bioisosteres

With their bent geometry, (*Z*)-like bioisosteres are suitable candidates for terminal substitution with (*Z*)-photoswitches (Table 8). Despite their less frequent application, such substitutions are highly promising for the rational design of (*Z*)-active ligands.

3.2.2.2.1. Biaryl Sulfonamide (Class 1)

The azostere character of biaryl sulfonamide was discussed in detail earlier (see section 3.2.1.2.3). When a ligand features more sites amenable to bioisosteric replacement with azobenzene, it is always advisable to visually inspect the protein-ligand complex (if available). In the structure-based design of BRAF^{V600E} inhibitors by our group, the parent compound contained both an amide and a sulfonamide linker.^[179] While azologization of *N*-aryl amides usually generates (*E*)-on ligands (see section 3.2.1.1.2), a (*Z*)-on

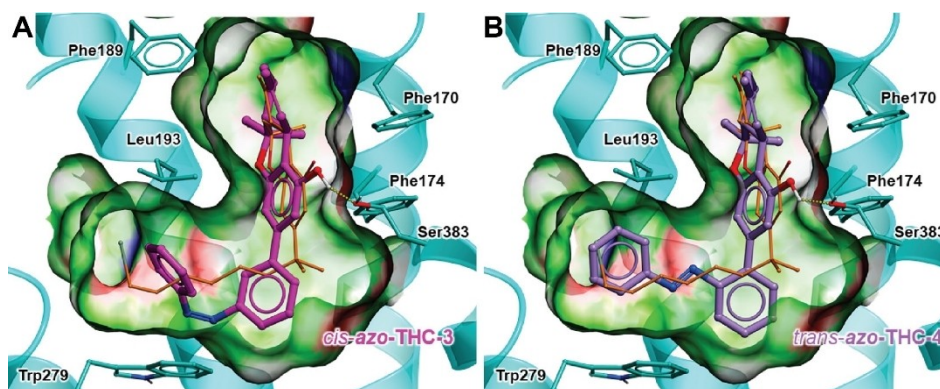


Figure 25. Docking poses for (*Z*)-**97** (A) and (*E*)-**98** (B) into CB₁R (PDB ID: 5XRA). The azobenzene moieties fill a hydrophobic subpocket, overlapping with the co-crystallized alkyl chain (orange). Adapted with permission from ref. [175]. Copyright © 2017 American Chemical Society.

inhibitor was expected after azologization of biaryl sulfonamide, because of its bent conformation observed in the bound state. Compound **102** displayed a substantial $F(E/Z)$ of 10, which could be rationalized by a striking overlap between the docking poses of the (*Z*)-form and the parent inhibitor.

The high degree of similarity between (*Z*)-azobenzene and biaryl sulfonamide was further studied by us, as discussed earlier (see section 3.2.1.2.3).^[116] Besides performing scaffold hopping on a Lp-PLA₂ inhibitor (**72**), we also designed an azolog of belinostat (**103**) by replacing a terminal biaryl sulfonamide that was not directly involved in important interactions. The latter photoswitchable derivative was confirmed to be a (*Z*)-on HDAC2 inhibitor, with a $F(E/Z)$ of 2 and a 12-fold decrease in potency compared to belinostat. In this case, the sulfonamide moiety served only as a solvent-exposed linker to guarantee optimal contacts between the capping group and the target. Thus, **103** showed a smaller loss of original activity, with a less distinct difference between photoisomers, as compared to **72**. The biological results of both design strategies suggested that the pharmacophoric role of the biaryl sulfonamide influenced the outcome of the azologization, with a trade-off between losing the original activity and achieving a large difference in activity between the photoisomers.

3.2.2.2.2. Benzophenone (Class 2)

Together with diarylamine (see section 3.2.1.2.4), benzophenone is another one-atom-linked diaromatic system that is attractive for designing (*Z*)-on ligands, because of its rigid, bent conformation.^[149] Bioisosteric replacement with azobenzene exchanges a bidentate HBA of the $-C(=O)-$ linker with two HBAs of the $-N=N-$ azo bond, resulting in the same number of HBAs but with different orientation. The structural and electronic similarity between benzophenone and (*Z*)-azobenzene was recognized only recently by our group for the optical regulation of the circadian clock.^[180] Comparison of conformational distributions from the CSD and the PDB indicated that (*Z*)-azobenzene is similar to benzophenone with regard to angles and distances between the aromatic rings. Moreover, both substructures have an identical dipole moment of 3.0 D, as opposed to the null dipole moment of (*E*)-azobenzene. Next, the azologization of a benzophenone-containing cryptochrome-1 (CRY1) stabilizer was explored in silico with molecular docking (PDB ID: 7D19). To achieve optical control with visible light, the benzophenone substructure was replaced with tetra-*ortho*-fluoroazobenzene. The computational results suggested that (*Z*)-**104** could mimic the experimental binding mode of the parent compound. In fact, biological evaluation of **104** confirmed the (*Z*)-on character of this visible-light-responsive circadian period modulator.

3.2.2.2.3. Unsaturated Aliphatic Chains (Class 5)

The bioisosteric replacement of unsaturated aliphatic chains with (*Z*)-azobenzene takes advantage of their similarity with respect to hydrophobicity and bent geometry. As mentioned earlier (see section 3.2.2.1.7), the photoisomerization of azobenzene enables the control of the straightness of lipid tails. The (*E*)-isomer of an azobenzene-containing chain is linear, whereas its bent (*Z*)-isomer features a structure closer to an (poly)unsaturated chain. Examples of this design strategy for (*Z*)-active fatty acids include compounds **105**, an agonist of TRPV1,^[181] **106** for protein kinase C (PKC),^[182] and **107**, a modulator of mammalian target of rapamycin (mTOR) and Hippo signaling pathways.^[183] In the case of photoswitchable analogs of lysophosphatidic acid (LPA), computational studies supported the structural similarity between (*Z*)-**108** and its monounsaturated parent compound.^[184] *A posteriori* molecular docking into the crystal structure of LPA₁ receptor (PDB ID: 4Z34) and homology models of LPA₂₋₅ receptors suggested that the (*Z*)-form could mimic the binding mode of LPA. On the other hand, the (*E*)-form needed to adopt an out-of-plane conformation to fit into the binding pocket, which might explain its lower activity. Overall, these studies illustrate the potential of emulating unsaturated carbon chains with (*Z*)-azobenzene, with light-induced differences that are amplified by the incorporation of the photoswitch in the middle of the chain.

3.2.2.2.4. Atypical Systems (Class 6)

The peculiar azologization of an atypical substructure, i.e., a benzene ring with an extended substituent in glimepiride, led to the design of ATP-sensitive K⁺ (K_{ATP}) channel blocker **109**.^[185] Prior to the biological studies, the authors compared the crystal structures of the parent compound and its azo-derivative, which is an extremely rare yet valuable practice in photopharmacology. This analysis highlighted the similarity between glimepiride and (*E*)-**109**. Nevertheless, the original alkyl chain is obviously free to rotate in solution, while azobenzene can only alternate between two binding conformations. In fact, the compound was found to be a (*Z*)-on K_{ATP} channel blocker.

Additional (*Z*)-like atypical systems for rational design in photopharmacology are aliphatic chains that end with an aryl group. These flexible substructures have inspired several terminal substitutions with *E-Z* photoswitches for the development of (*Z*)-on ligands. For instance, our group incorporated an azobenzene in place of an atypical substructure, i.e., an aliphatic chain with a benzamide cap, of HDAC inhibitor vorinostat.^[68] Compound **110** showed a high $F(E/Z)$ of 39. Alternatively, a strongly related series of compounds was designed for the inhibition of two bacterial HDAC homologs.^[186] The azopyrazole derivatives displayed a miscellaneous behavior of (*E*)- and (*Z*)-on inhibition against histone deacetylase-like amidohydrolases (HDAHs) and acetylpolymine amidohydrolases (APAHs). The crystal structure of HDAH in complex with (*E*)-**111** (PDB ID:

5G14) revealed that the binding mode is comparable to vorinostat, also with regard to π - π stacking interactions with two phenylalanine residues.

If structural data are available beforehand, structure-based approaches should be preferred for the informed design of (*Z*)-on ligands. During the development of photo-switchable PPAR γ agonists, *a priori* molecular docking supported the atypical azologization of benzyl ether chains with an aromatic tail end.^[166] After the first biological evaluation, a subsequent cycle of design explored additional hydrophobic contacts between a trifluoromethyl or a phenyl substituent and a lipophilic subpocket. Such structure-based optimization resulted in the (*Z*)-on photohormone **112**.

3.2.2.3. Ambiguous, (*E/Z*)-Like Bioisosteres

Substructures belonging to class 3 (biaryls), class 4 (fused rings) and class 6 (only adamantyl moiety) exhibit an ambiguous bioisosterism with *E-Z* photoswitches (Table 9). Due to their intrinsic lack of flexibility, the replacement of these moieties shows a certain degree of correlation with the substitution pattern on the photoswitch (Figure 26 and 28). Especially in the case of aromatic classes 3 and 4, understanding such spatial dependence can pave the way for more conscious azologizations.

3.2.2.3.1. Biaryl (Class 3)

Biaryl motifs have the potential to serve as a great source of structural inspiration for photopharmacology, as they contain two aromatic rings and are popular in drug discovery.^[187] The exchange of a single bond spacer with an --N=N-- azo bond introduces two HBAs in the drug structure, often resulting in additional interactions with the target. Since the aryl rings are connected by a very short linker, they are inherently not able to explore a wide conformational space. Therefore, biaryls are ambiguous bioisosteres because they can be mimicked by either (*E*)- or (*Z*)-photoswitches, depending on the substitution patterns. In fact, the outcomes of the replacement of biaryls are influenced by the

substitution patterns of both the biaryl itself and of the photoswitch, with the spatial arrangement of the outer ring being the key parameter (Figure 26).

This correlation is exemplified by the work of the Leurs group on photoswitchable modulators for the peptidergic chemokine CXCR3 receptor.^[188] Inspired by series of ligands that showed either antagonism or agonism depending on the position and size of a halogen substituent, the authors envisioned that an azobenzene photoswitch could be used to control the efficacy around this hotspot. In fact, compound **113** was found to be an (*E*)-on antagonist and a (*Z*)-on agonist, demonstrating that a *para*-substituted biphenyl could be mimicked by a *meta*-substituted (*Z*)-azobenzene (Figure 26). Follow-up considerations on the 3D structure of the ligands further supported such “regiospecific” azologization.^[189] Prompted by the successful control over efficacy hotspots, it is tempting to imagine a similar optical control over activity cliffs,^[190] where photoisomerization could toggle between completely inactive and highly active isomers.

If one of the two rings of the biaryl system is a heterocycle, similar regioisomeric considerations (Figure 26) seem to be valid for the introduction of heterocyclic photoswitches such as azopyrazoles. Tamaoki and co-workers demonstrated that a *para*-substituted biaryl substructure in centromere-associated protein E (CENP-E) inhibitors could be resembled by *para*-substituted (*E*)-azopyrazole (compound **114**^[191]) or *meta*-substituted (*Z*)-azopyrazole (compound **115**^[192]). On the other hand, the interpretation of the consequences of replacing biaryls is not always so straightforward, as in the case of protein arginine deiminases (PAD₁₋₄) inhibitors.^[193] After the replacement of a *para*-substituted biphenyl moiety with azobenzene, the photo-switchable derivatives displayed mixed behavior. Compound **116** was determined to be a (*Z*)-on covalent inhibitor, whereas compound **117** showed (*E*)-on reversible inhibition.

In addition to being a bioisostere of *para*-substituted biphenyls, *meta*-substituted (*Z*)-azobenzene can also be a good mimic for *ortho*-substituted systems (Figure 26). During the structure-based development of photoswitchable GABA uptake inhibitors, *a priori* molecular docking into homology models of GAT1 guided the design of (*E*)-on

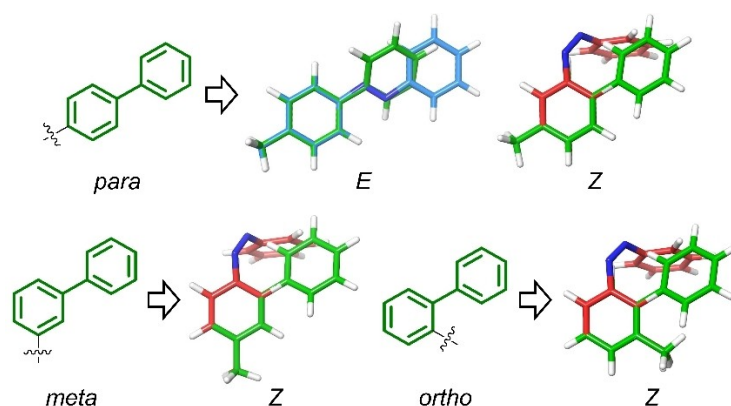


Figure 26. Qualitative trends observed in the azologization of biaryl systems.

Table 9: Overview of terminal replacements of (*E/Z*)-like bioisosteres.

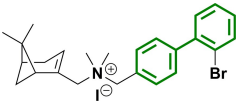
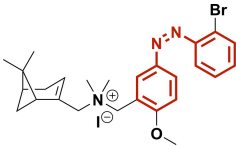
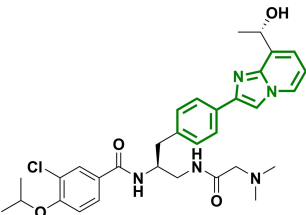
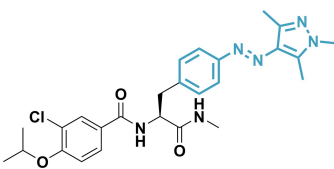
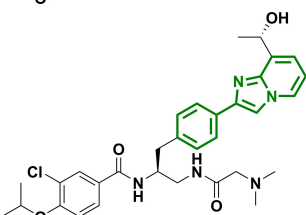
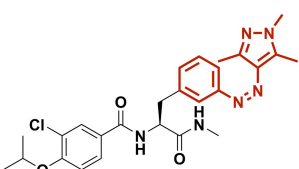
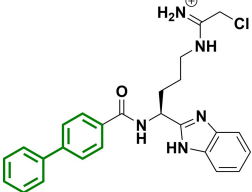
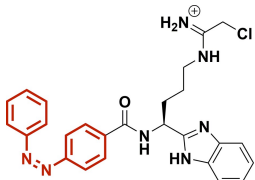
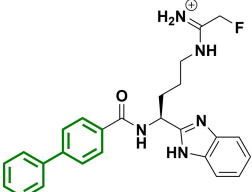
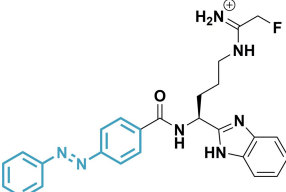
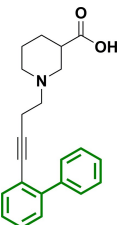
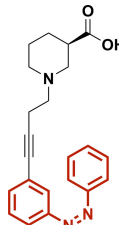
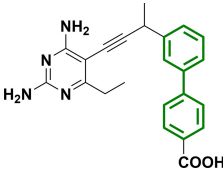
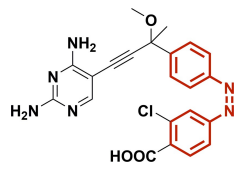
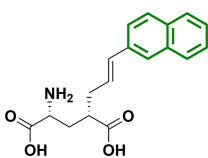
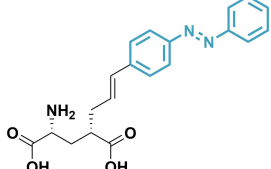
Entry	Compound	Target (ligand)	Parent compound	Photoswitchable derivative (active isomer)	Class[a]	Ref.
1	113	CXCR3 (agonist/antagonist)			3	[188,189]
2	114	CENP-E (inhibitor)			3	[191]
3	115	CENP-E (inhibitor)			3	[192]
4a	116	PAD ₁₋₄ (covalent inhibitor)			3	[193]
4b	117	PAD ₁₋₄ (inhibitor)			3	[193]
5	118	GAT1 (inhibitor)			3	[194]
6	119	<i>E. coli</i> DHFR (inhibitor)			3	[195]
7	120	iGluR5-6 (agonist)			4	[196–198]

Table 9: (Continued)

Entry	Compound	Target (ligand)	Parent compound	Photoswitchable derivative (active isomer)	Class[a]	Ref.
8a	97	CB ₁ R (agonist)			4	[175]
8b	98	CB ₁ R (agonist)			4	[175]
9a	121	β ₂ -AR (antagonist)			4	[199]
9b	122	β ₂ -AR (antagonist)			4	[199]
10	123	NMDAR (antagonist)			4	[169]
11a	97	CB ₁ R (agonist)			6	[175]
11b	98	CB ₁ R (agonist)			6	[175]
12	124	CB ₂ R (antagonist)			6	[117]

[a] Azostere class: 1–6 (see section 3.2).

ligands.^[194] The calculations suggested that the (*Z*)-isomer of compound **118** could engage in more interactions with GAT1, including a hydrogen bond between the azo bond and Arg69 (Figure 27). Consistent with these “substitution-activity relationships”, a very recent study by our group showed that a *meta*-substituted biphenyl group could be replaced with a *para*-substituted (*Z*)-azobenzene in the photoswitchable *E. coli* DHFR inhibitor **119**.^[195]

Broadly speaking, the examples in this section indicate that photopharmacological endeavors can greatly benefit

from replacing biaryl groups. Considering the limited mobility of the single bond and the introduction of two pharmacophore features with the HBAs of the –N=N– azo bond, we believe that many opportunities still lie in the scaffold hopping of biaryl systems.

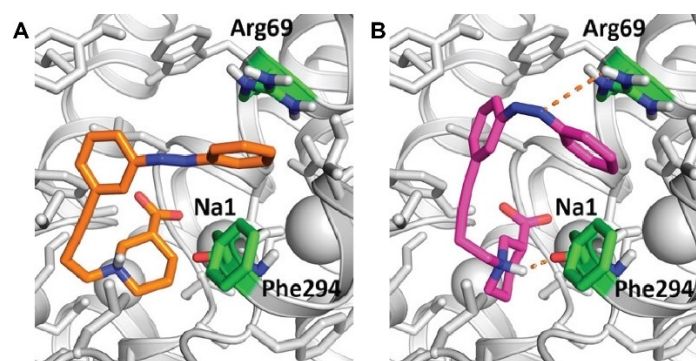


Figure 27. Docking poses of (*E*)-**118** (A) and (*Z*)-**118** (B) into a homology model of GAT1. The (*Z*)-isomer engages in more hydrogen bonds (orange dotted lines) with the specific residues (green) of the target. Adapted with permission from ref. [194]. Copyright © 2018 American Chemical Society.

3.2.2.3.2. Fused Rings (Class 4)

Due to their flat, aromatic structure, naphthalene and phenanthrene groups are clearly suitable for azologization. Compared to them, azobenzene is more extended and can make further hydrophobic contacts as well as engage in hydrogen bonds with the two HBAs of the $\text{N}=\text{N}$ azo bond. In an analogous way to biaryl systems (see section above), the categorization of fused ring systems as (*E*)- or (*Z*)-like bioisosteres depends on the substitution pattern of both the parent fused rings and the azobenzene derivative (Figure 28). Also in this case, the critical feature is the placement of the outer ring in space. In fact, early azologization efforts led to the identification of 2-substituted naphthalene as a bioisostere of *para*-substituted (*E*)-azobenzene.^[196] Follow-up studies on this photoswitchable agonist of iGluRs (compound **120**) shed light on the structural basis of its (*E*)-on partial agonism. The X-ray structure of (*E*)-**120** bound to the ligand-binding domain of a dimeric kainite receptor subunit (GluK2) (PDB ID: 4H81) revealed that the azobenzene moiety is engaged in hydrophobic interactions, and provided an explanation for the observed partial agonistic behavior.^[197] In contrast to the full agonist glutamate, the bulky azobenzene group protrudes from an exit tunnel of the receptor, causing a more open

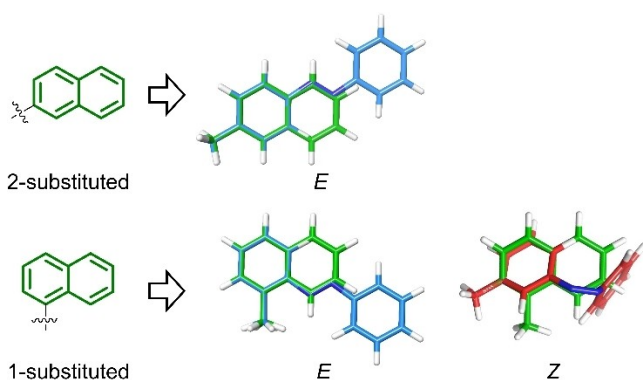


Figure 28. Qualitative trends observed in the azologization of fused ring systems.

conformation of the clamshell. Rigid molecular docking calculations on the (*Z*)-isomer were in agreement with the experimental results, as (*Z*)-**120** did not fit in the crystal structure without steric clashes. However, protein flexibility was taken into account only in a second follow-up computational study, which performed MD simulations to evaluate the effects of the *E-Z* photoisomerization on the binding to the receptor.^[198] During the MD trajectories of GluK2 in complex with the less potent (*Z*)-**120** the channel showed a lower degree of opening because of weaker ligand-receptor and intradomain interactions, compared to the full agonist glutamate or the more active (*E*)-isomer.

Similar tendencies (Figure 28) have been observed for the azologization of 1-substituted naphthalene, in the case of the structure-based design of photoswitchable agonists of CB₁Rs (see section 3.2.2.1.7)^[175] and antagonist of β_2 -AR.^[199] While ligands containing *ortho*-substituted azobenzenes (**98**^[175] and **122**^[199]) were (*E*)-active, the ones containing *meta*-substituted azobenzenes were (*Z*)-active (**97**^[175] and **121**^[199]). In line with these SAR results, compounds with *para*-substituted azobenzenes from both studies did not show any activity.

Finally, the only case of azologization of phenanthrene (compound **123**) did not yield an active photoswitchable modulator for NMDARs, probably because it was accompanied by the removal of a carbonyl group for synthetic accessibility.^[169] Nevertheless, we believe that phenanthrene still holds potential as an azostere, but the replacement should be studied without other modifications on the structure to allow for direct comparison with the parent compound.

3.2.2.3.3. Adamantyl (Class 6)

Despite being underrepresented in bioactive compounds, the adamantyl moiety has displayed great value as a multi-functional group for drug design.^[200] This group can increase the lipophilicity of a drug and interact with hydrophobic residues such as Val, Leu, Phe and Tyr, besides improving the general drug-likeness of a compound. Although the adamantyl group is not aromatic as the ambiguous bioisostere

teres discussed before, its lipophilic character and its compact structure render such moiety suitable for replacement with azobenzene. For instance, the design of photo-switchable agonists of CB₁R_s (see sections 3.2.2.1.7 and 3.2.2.3.2) can be described also through the lens of an azologization of an adamantyl group.^[175] Starting from a Δ^9 -tetrahydrocannabinol analog, the 2-substituted adamantyl moiety was mimicked by an *ortho*-substituted (*E*)-azobenzene in compound **98**, and by a *meta*-substituted (*Z*)-azobenzene in compound **97**.

The importance of adamantane as a hydrophobic azostere has been studied in detail only recently by Tao and co-workers.^[117] In a pioneering approach, they investigated which are the most common interactions usually formed by azosteres. Statistical analysis of PDB data indicated that known azosteres are more likely to engage in hydrophobic contacts with Leu and π - π interactions with Phe. Inspired by such analysis and by the crystal structure of a CB₂R-antagonist complex (PDB ID: 5ZTY), the authors designed photo-switchable analogs of this antagonist through the azologization of its 1-substituted adamantyl group, which was located in a lipophilic subpocket. Compound **124**, bearing an *ortho*-substituted methylene-linked azobenzene, was identified as a (*Z*)-on antagonist with a high *F*(*E*/*Z*) of 44. *A posteriori* docking studies suggested that only the (*Z*)-isomer could occupy the targeted lipophilic subpocket (Figure 29). Because of its hydrophobic and bulky structure, the

adamantyl group is suitable for bioisosteric replacements with both isomers of azobenzene, depending on the substitution patterns of parent compounds and azologs.

3.3. Insertion into the Bioactive Molecule

While we used the term *extension* for the attachment of an *E*-*Z* photoswitch (see section 3.1) and the term *bioisosteric replacement* for the substitution of a substructure with an *E*-*Z* photoswitch (see section 3.2), we define *insertion* as the introduction of azobenzene between two atoms of the parent compound. In other words, it can be seen as an “internal extension”, and it is not a bioisosteric replacement because all the atoms of the parent compound are still there. Such rare approach is exemplified by the work of Groschner and co-workers on short transient receptor potential channel (TRPC3) agonists.^[201] The insertion of an azobenzene photoswitch into the aliphatic chain of the parent ligand led to compound **125**, a (*Z*)-active TRPC3 agonist that enabled the optical control of neuronal firing and cellular Ca²⁺ signaling (Figure 30).

Despite being an uncommon strategy, the insertion of azobenzene was elegantly applied in the design of photo-switchable inhibitors of mitochondrial complex I.^[202] Inspired by an activity cliff^[190] previously observed in two regioisomers bearing either a *para*- or *ortho*-alkyl-substi-

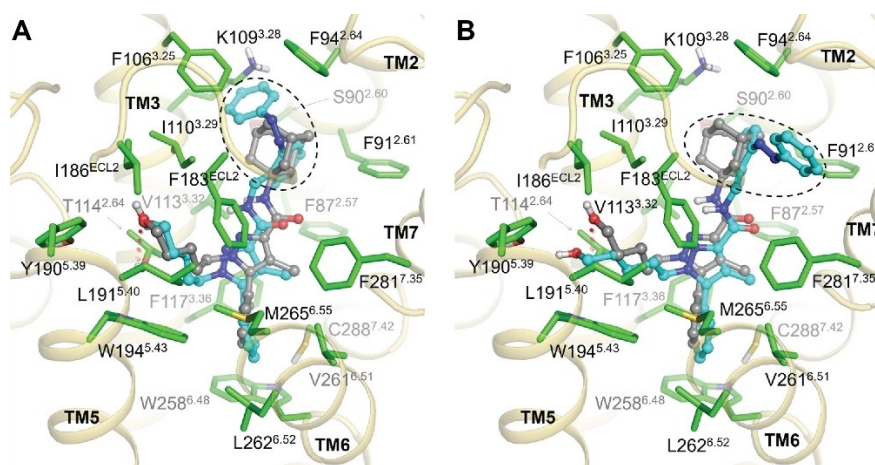


Figure 29. Docking poses for (*Z*)-**124** (A) and (*E*)-**124** (B) into CB₂R (PDB ID: 5ZTY), superposed with the co-crystallized parent ligand (gray). Adapted with permission from ref. [117]. Copyright © 2021 American Chemical Society.

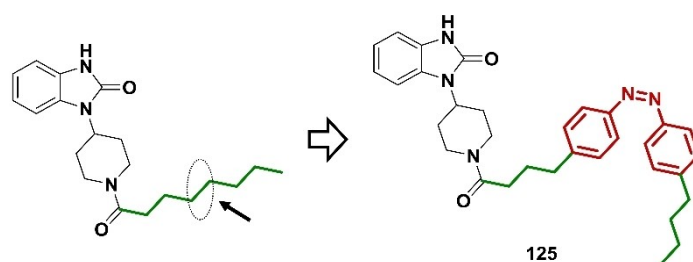


Figure 30. Insertion approach for the design of compound **125**, a (*Z*)-on agonist of lipid-gated TRPC3 channel.^[201]

tuted benzene ring, Miyoshi and co-workers introduced a $-N=N-$ benzene unit between the benzene ring and the alkyl chain (Figure 31). The authors envisioned that (*E,E*)-**126** could orientate its aliphatic chain as the active regioisomer, while the (*Z,Z*)-isomer could resemble the inactive regioisomer. Biological evaluation confirmed the hypothesis, revealing that compound **126** was a dark-active inhibitor, with a $F(Z/E)$ of ≈ 2 . In our opinion, toggling between two states that mimic activity cliffs is an extremely promising approach for achieving large light-induced differences in potency, which should be used more often by molecular designers in photopharmacology.

3.4. Spacer Used to Control the Distance

A great source of inspiration for photopharmacology comes from small molecules that feature spacers in their structure (Table 10). These inert and non-interacting substructures play important roles in several types of ligands, including bivalent ligands for GPCRs,^[203] bifunctional ligands^[204] (e.g., proteolysis targeting chimeras or PROTACs^[205,206]) and DNA binders,^[207] by controlling the interaction of two or more pharmacophores with various binding sites. Since the length of the spacer is typically the most crucial parameter,^[203,204] photoswitchable spacers are particularly attractive due to their geometrical changes upon photoisomerization, especially in terms of end-to-end distance.^[1]

The most straightforward approach to introduce a photoswitchable spacer is to replace an existing spacer in the template ligand with a photoswitch. A pioneering applica-

tion of this design principle involved the alkyl chain of decamethonium, which was substituted with azobenzene to generate the (*E*)-on nAChR agonist **127**.^[172] A second example was reported by our group for the development of photoswitchable mast cell activation inhibitors.^[208] The design was based on disodium cromoglycate, which features two identical chromone groups connected by a flexible unit that allows the binding of both groups to the cromolyn binding protein (CBP). Since the length of the spacer was a key parameter for the original activity, irradiation of an azobenzene-linked analog was expected to influence inhibitory potency, due to the light-induced changes in terms of end-to-end distance. As a result, compound **128** emerged as an (*E*)-on inhibitor, albeit with a moderate $F(Z/E)$ of 1.25.

By contrast, spacer replacement has been reported more frequently in the case of small molecules containing two distinct pharmacophoric units. In the context of GPCR ligands, these compounds are termed heterobivalent ligands, with the further distinction of dualsteric (or bitopic) ligands, when they target orthosteric and allosteric sites simultaneously.^[203] For instance, Agnetta et al. modified a known dualsteric ligand for mAChRs by introducing an azobenzene spacer in place of the original alkyl chain that connected the benzyl quinolone carboxylic acid (allosteric unit) with iperoxo (orthosteric unit).^[209] Compound **129** acted as a photoswitchable dualsteric ligand, with a profile that could be reverted by light (efficacy switch). In fact, the (*E*)-form was characterized as a mAChR agonist, whereas the (*Z*)-form showed antagonist efficacy. An analogous approach was employed to regulate a different subtype of mAChR.^[210] Optical control of cardiac activity in animals

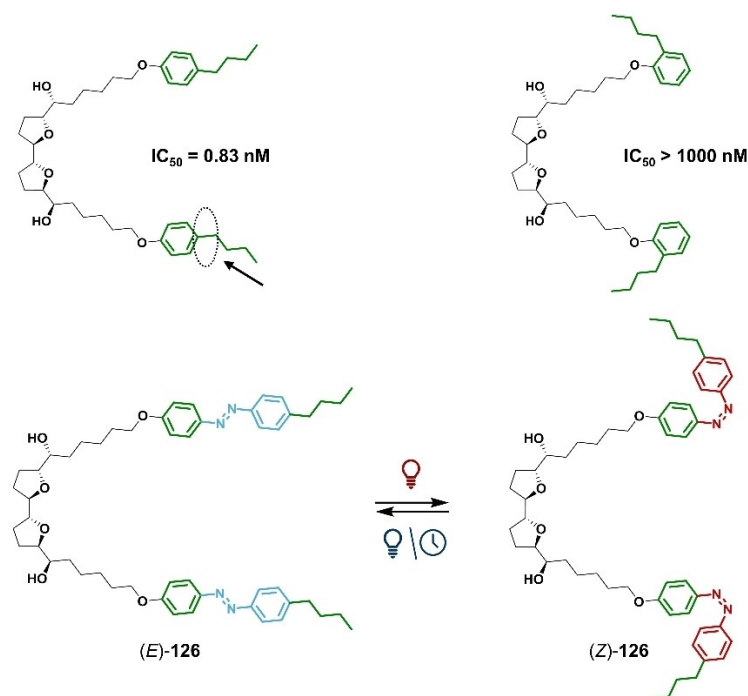


Figure 31. Insertion strategy inspired by an activity cliff for the design of compound **126**, an (*E,E*)-on inhibitor of mitochondrial complex I. Adapted with permission from ref. [202]. Copyright © 2006 American Chemical Society.

Table 10: Overview of the design of photoswitchable spacers (green = original spacer/linker; orange = modifications).

Entry	Compound	Target (ligand)	Parent compound	Photoswitchable derivative (active isomer)	Ref.
1	127	nAChR (agonist)			[172]
2	128	CBP (inhibitor)			[208]
3	129	M ₁ mAChR (antagonist/agonist)			[209]
4	130	M ₂ mAChR (agonist)			[210]
5	131	PROTAC			[211]
6	132	PROTAC			[212]

Table 10: (Continued)

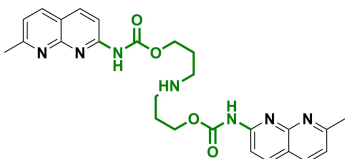
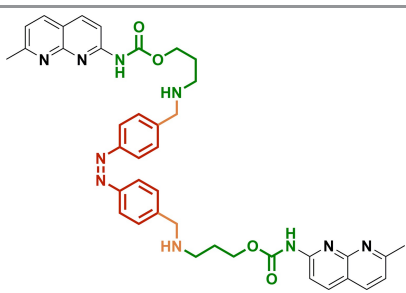
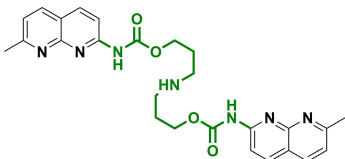
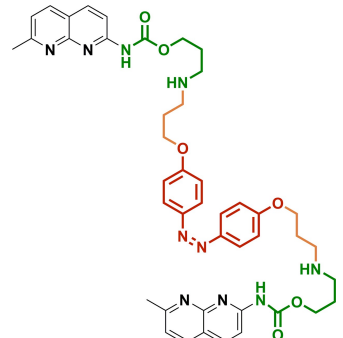
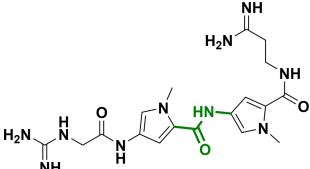
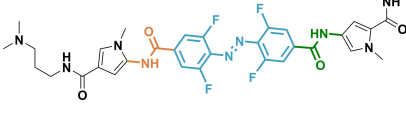
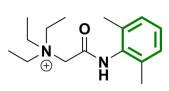
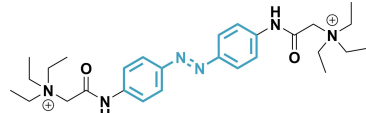
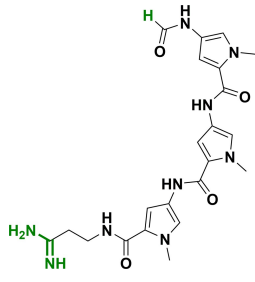
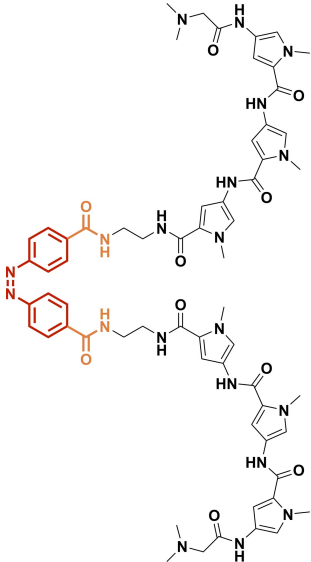
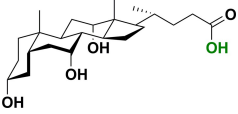
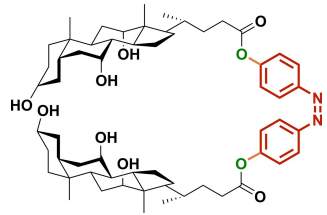
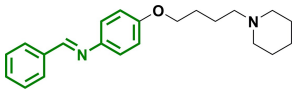
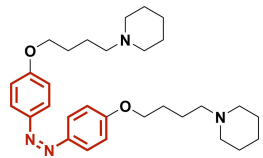
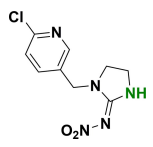
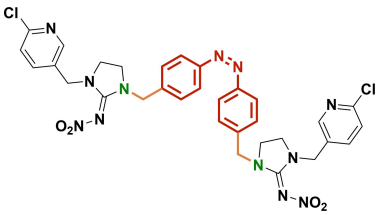
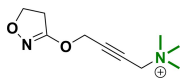
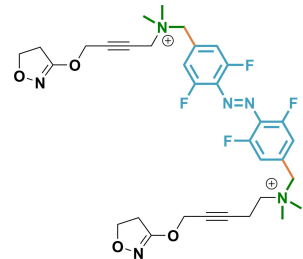
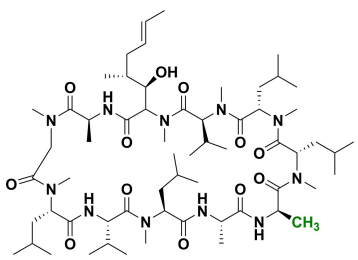
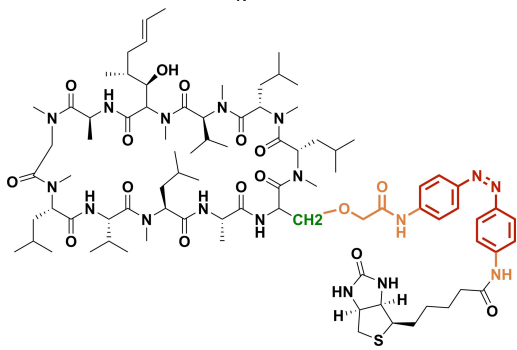
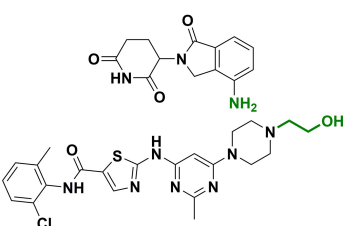
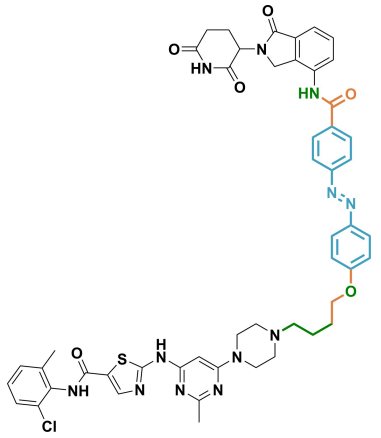
Entry	Compound	Target (ligand)	Parent compound	Photoswitchable derivative (active isomer)	Ref.
7	133	DNA (molecular glue)			[213]
8	134	DNA (molecular glue)			[214]
9	135	DNA (groove binder)			[215]
10	136	K ⁺ channels (blocker)			[216,217]
11	137	DNA (groove binder)			[219]

Table 10: (Continued)

Entry	Compound	Target (ligand)	Parent compound	Photoswitchable derivative (active isomer)	Ref.
12	138	Bacterial membrane (antibiotic)			[220]
13	139	AChE (inhibitor)			[155]
14	140	nAChR (inhibitor)			[221]
15	141	mAChR (agonist)			[93]
16	142	Calcineurin			[97]
17	143	PROTAC			[223]

was achieved with compound **130**, an (*E*)-on mAChR agonist.

Among the pharmacological tools that would benefit from the precise spatiotemporal control offered by photopharmacology, we can also find PROTACs.^[205] These heterobifunctional ligands usually feature an alkyl or polyether spacer that should be long enough for the concomitant binding of two proteins recruited to form a ternary complex. As a result, differences of 3 Å in spacer length can discriminate between active and inactive compounds. Remarkably, such variation corresponds to the change in end-to-end distances between (*E*)- and (*Z*)-azobenzene.^[36] To control protein degradation with light, Carreira and co-workers replaced the oligoether spacer of an existing PROTAC, transposing the amide connectivity.^[211] Keeping the original ligand-to-ligand distance of 11 Å, (*E*)-**131** was designed to be the only form to maintain the activity of the parent compound (Figure 32). Biological evaluation confirmed that the irradiated sample, enriched in the shorter (*Z*)-isomer, was inactive compared to the thermally adapted sample.

Along with the substitution, an additional design strategy is the azo-insertion (see section 3.3) into the original spacer. If one pharmacophore of a bifunctional ligand is linked through an aromatic ring, the latter can be internally extended with an azobenzene. This design is exemplified by the work of Reynnders et al., who devised **132** by the incorporation of azobenzene in the aromatic structure of the lenalidomide subunit of dBET1, after screening several other approaches.^[212] *A posteriori* modeling studies suggested that the (*Z*)-form could be better accommodated in cereblon's binding pocket than the (*E*)-form.

On the other hand, it is possible to insert the photo-switch within an aliphatic spacer. A representative example can be found in the design of photoswitchable molecular glues for DNA by Nakatani and co-workers.^[213] These molecules, also referred to as mismatch-binding ligands, can induce mismatch-containing DNA single strands to hybrid-

ize and form duplex DNA. Taking naphthyridine carbamate dimer as a starting point, compound **133** was obtained by internally extending the flexible chain with azobenzene. In line with its bent, twisted geometry, (*Z*)-**133** stabilized the formation of double-stranded DNA with a 2:1 stoichiometry. In a follow-up study by our group, a variety of computational methods supported the development of compound **134**.^[214] While the enhancement of the photochemical properties was guided by time-dependent DFT (TD-DFT), molecular mechanics (MM) calculations and MD simulations supported the *a posteriori* rationalization of DNA melting experiments and helicity preferences. Besides mismatch-binding ligands, an azobenzene spacer was also used for devising a DNA minor groove binder.^[215] A tetra-*ortho*-fluoroazobenzene was incorporated in the middle of netropsin, and the parent amide linker was repeated on both sides of the photoswitch. The azo-derivative **135** acted as a visible-light-responsive (*E*)-on binder targeting the nucleosome, with a $F(Z/E) \approx 2$.

In addition to substitution and insertion into already existing spacers, photoswitchable spacers were also designed *de novo*. In these cases, the parent ligands were first modified through extension (see section 3.1) or bioisosteric replacement (see section 3.2), but the original pharmacophore was duplicated on the other side of the photoswitch. The application of this design principle is exemplified by the work of Mourot et al., who azo-extended the aromatic core of a lidocaine derivative and repeated its charged quaternary ammonium group on the opposite ring (compound **136**).^[216] In a follow-up study, electrophysiology experiments and computational methods shed more light on the behavior of this voltage-gated K⁺ channel blocker at the molecular level.^[217] Compound **136** was determined to be an (*E*)-on ligand, with a $F(Z/E)$ of 6, and docking calculations were performed into the open channel (PDB ID: 2R9R). The (*E*)-form adopted a similar binding pose to related quaternary ammonium channel blockers, placing one charged headgroup below the selectivity filter and forming hydro-

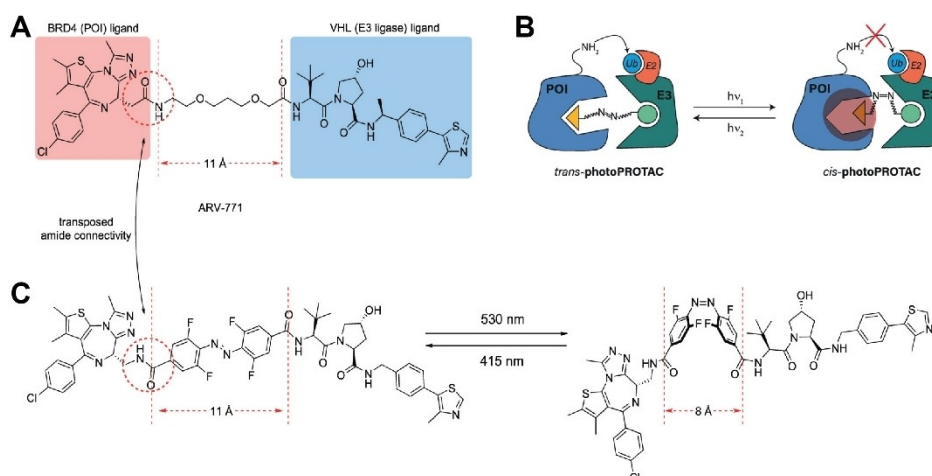


Figure 32. Rational design of compound **131**. The spacer length of the parent PROTAC (A) is mimicked by (*E*)-azobenzene (B), allowing protein degradation only by (*E*)-**131**. Adapted with permission from ref. [211]. Copyright © 2019 American Chemical Society.

phobic interactions with the azobenzene moiety (Figure 33). On the other hand, the less potent (*Z*)-isomer showed a different binding mode, with no quaternary ammonium in the center of the channel. A further computational analysis on similar systems considered simple azobenzene and *para*-diaminoazobenzene as model systems to examine the binding to a Na⁺ channel, albeit only in the (*E*)-forms.^[218] Surprisingly, no calculations were reported for the (*Z*)-isomers, while *para*-diaminoazobenzene is known to exhibit very short half-life of the metastable isomer. However, the authors identified multiple binding pockets for both molecules: near the selectivity filter at the center of the pore, but also in a side fenestration, in lateral cavities and at the gate of the channel.

Besides the previous case of a spacer obtained through *bona fide* extension from an aromatic core, a greater number of photoswitchable spacers were designed through the attachment of azobenzene to diverse functional groups. Again in the context of DNA minor groove binders, an azobenzene spacer was attached to distamycin analogs via an amide linker, followed by the repetition of the distamycin pharmacophore on the other side of the switch.^[219] After exploring both a flexible, longer spacer and a rigid, shorter one, compound **137** emerged as the derivative with the largest difference in DNA binding affinity upon irradiation. *A posteriori* molecular docking suggested that (*Z*)-**137** engages in more hydrogen bond interactions with DNA bases, and that its more rigid spacer granted larger changes in end-to-end distances between the photoisomers.

Instead of targeting specific interactions with receptors or DNA, a different scenario involves the design of a dimer linked by a photoswitch. Such strategy is exemplified by the work of Li and colleagues, who designed the photoswitchable dimer **138** by connecting two units of cholic acid with azobenzene.^[220] Because of their tunable amphiphilic properties, these conjugates were envisioned to act as antibacterial agents, disrupting the bacterial cell walls. Irradiation with UV light triggered a change from an extended to a tweezer-like conformation, which exhibited stronger antimicrobial activity probably due to the reversible formation of hydrophilic pores in phospholipid membranes.

In only one reported example, a bioisosteric replacement was the starting point of a de novo design of a photo-

switchable spacer. Dual AChE inhibitor **139** was designed through the replacement of aza-stilbene with azobenzene, followed by the duplication of the pharmacophore.^[155] The resulting compound **139** displayed a (Z)-on behavior, with a $F(Z/E) \approx 2$. Molecular docking and subsequent MD simulations proposed a crucial contribution of charge-assisted hydrogen bonds between the piperidinium moieties and Asp72.

When a plain azo-extension (see section 3.1) leads to unsatisfactory results, better outcomes can be achieved if the azobenzene group is transformed into the spacer of a bivalent ligand. In the illustrative case of photoswitchable insecticides based on the nAChR agonist imidacloprid, the first attempts of simple extension from the aromatic ring or the aliphatic nitrogen led to inactive compounds.^[221] On the other hand, repeating the pharmacophore on the opposite side of an azobenzene spacer generated the homobivalent ligand **140**, which displayed a promising (*Z*)-on insecticidal activity *in vitro*, with a $F(E/Z)$ of 5 *in vitro*. Moreover, docking into nAChR (PDB ID: 2WNJ) indicated that the second moiety might interact further with the binding pocket only in the (*Z*)-form. In a similar account, mAChR agonist iperoxo was first used as a template for extension, but compound **35** showed limited light-induced effects (see section 3.1.3).^[93] The repetition of the iperoxo pharmacophore also on the other side of the tetra-*ortho*-fluoroazobenzene generated the (*E*)-on homobivalent compound **141**. This dualstereic (or bitopic) ligand showed higher potency than the univalent **35**, with a $F(Z/E) > 4$. Docking poses into a homology model of mAChR indicated that the (*Z*)-isomer could be too bulky for the narrow channel between the orthosteric and allosteric binding sites (Figure 34).

Similarly, unsatisfactory light-induced effects resulting from the azo-extension approach can be improved by designing a heterobifunctional ligand, as demonstrated by Fischer and co-workers for the optical control of immune signaling.^[97] Firstly, compound **39** was obtained through the appendage of azobenzene to a region of cyclosporin A that was not crucial for binding (see section 3.1.4). To enhance the modest light-induced differences in activity, a second ligand (i.e., biotin) was further attached to the azobenzene spacer (compound **142**). Such “protein borrowing” strategy^[222] promoted the simultaneous binding of biotin to

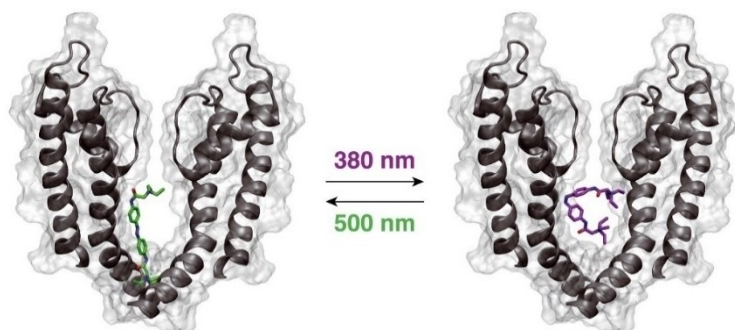


Figure 33. Docking poses of the (E)-isomer (green) and the (Z)-isomer (purple) of compound **136** into the open K⁺ channel (dark gray, PDB ID: 2R9R). Adapted with permission from ref. [217]. Copyright © 2018 Wiley-VCH Verlag GmbH & Co. KGaA.

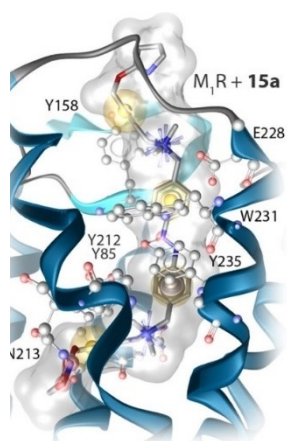


Figure 34. Docking pose of (*E*)-**141** into a homology model of mAChR (blue). Blue stars indicate positive ionizable atoms, and yellow spheres indicate hydrophobic contacts. Adapted with permission from ref. [93]. Copyright © 2019 American Chemical Society.

streptavidin, thereby increasing the structural changes upon photoisomerization.

Finally, the entirely de novo design of a photoswitchable bifunctional ligand was also reported by Jin et al. with the development of PROTAC **143**.^[223] Supported by *a priori* molecular docking, the authors used an azobenzene spacer to conjugate lenalidomide (targeting cereblon) and dasatinib (targeting ABL proteins). The calculations suggested that only (*E*)-**143** could bind to both targets, while (*Z*)-**143** incurred steric clashes that hindered its binding (Figure 35). The biological results confirmed the (*E*)-on character of this azobenzene-containing PROTAC.

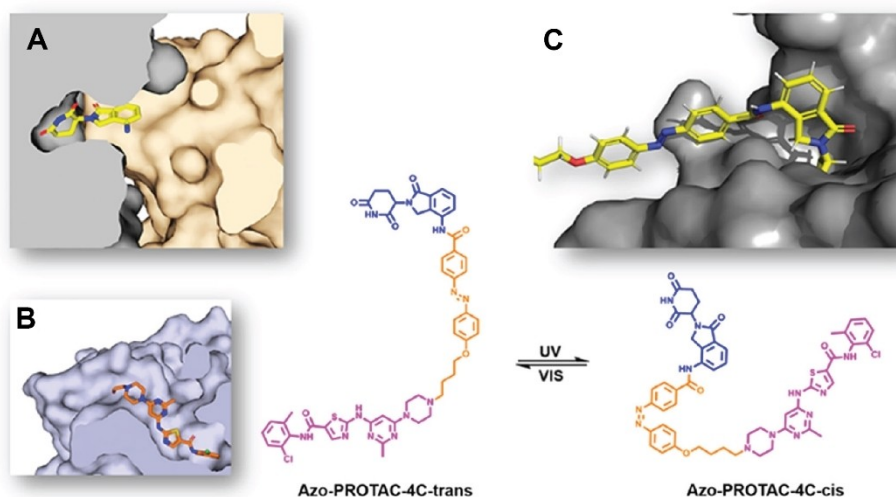


Figure 35. Computer-aided design of a photoswitchable PROTAC. (A, B) Crystal structures of cereblon in complex with lenalidomide (A, PDB ID: 4TZ4), and of ABL protein in complex with dasatinib (B, PDB ID: 2GQG). (C) Docking pose of (*E*)-**143** into cereblon. Adapted with permission from ref. [223]. Copyright © 2020 American Chemical Society.

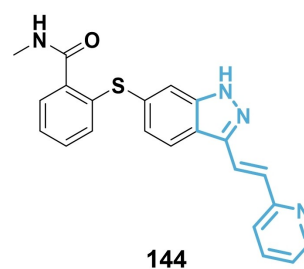


Figure 36. Photo-repurposing of compound **144** (axitinib), an FDA-approved inhibitor of tyrosine kinase. Photoswitchable, stilbene-like substructure highlighted in blue.^[225]

3.5. Photo-Repurposing

Akin to drug repurposing,^[224] we define *photo-repurposing* as the study of the light-induced changes in affinity of a photoswitch-bearing compound that was previously reported outside photopharmacology and has not been evaluated before for its light-induced changes in potency. This approach has been reported for stilbene-like and azobenzene substructures.

A representative example of photo-repurposing was reported by Peifer and co-workers, who recognized the photopharmacological potential of compound **144**, i.e., axitinib (Figure 36).^[225] This FDA-approved inhibitor of tyrosine kinase contains a stilbene-like moiety that can be photoisomerized to the (*Z*)-form. The availability of a crystal structure of vascular endothelial growth factor receptor 2 (VEGFR-2) in complex with (*E*)-**144** (PDB ID: 4AG8) allowed *a priori* docking studies for the other isomer. The computational results indicated that the (*Z*)-isomer would not be able to form important hydrogen bonds with the hinge region, unless it sterically clashed with the target (Figure 37). VEGFR-2 binding assays confirmed that compound **144** could be deactivated upon irradiation with large

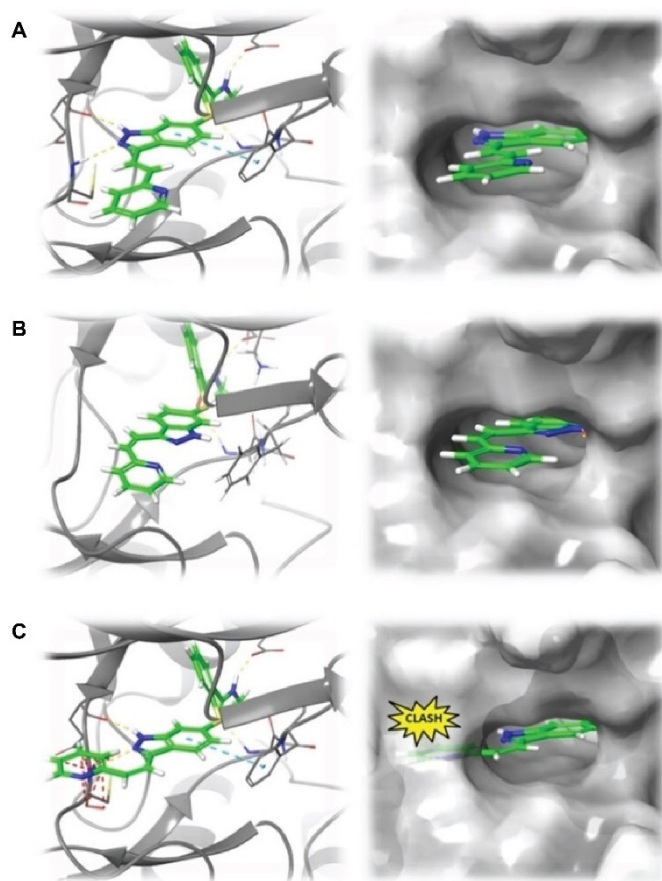


Figure 37. (A) Binding mode of (*E*)-**144** (green) in the binding pocket of VEGFR-2 (gray, PDB ID: 4AG8). Hydrogen bonds are depicted as yellow dashed lines, while π - π interactions are shown as blue dashed lines. (B) Docking pose of (*Z*)-**144** into VEGFR-2, with no hydrogen bonding to the hinge region. (C) The formation of hydrogen bonds between (*Z*)-**144** and the hinge region would result in steric clashes with the protein. Adapted with permission from ref. [225]. Copyright © 2018 Wiley-VCH Verlag GmbH & Co. KGaA.

differences in potency, resulting in a $F(Z/E)$ of 43 *in vitro* and in a $F(Z/E)$ of 31 in human umbilical vein cells. Further improvements of this compound were obtained later via a sign inversion strategy (see section 3.6).

Photo-repurposing can also inspire a lead optimization campaign, especially if structural data are available. Since PPAR α agonist **145** had been reported earlier and co-crystallized with the ligand binding domain of the target (PDB ID: 4CI4),^[226] Willems et al. selected it as a lead compound for the development of photoswitchable derivatives (Figure 38).^[227] In fact, *a priori* molecular docking indicated that the alkoxy spacer of compound **145** had the optimal length for (*E*)-on agonism with significant light-induced differences. With a structure-based design approach, different substituents (i.e., methyl, chlorine, or trifluoromethyl) were evaluated *in silico* in the *ortho*- and *para*-position of the inner or outer ring of azobenzene, respectively. The docking poses suggested that a *para*-methyl-substituted outer ring would generate (*Z*)-on compounds, while a methyl group in the *ortho*-position of the inner ring could occupy a lipophilic subpocket (Figure 39). As a result, the rationally designed (*E*)-on agonist **146** was determined to be >150-fold more potent than the parent compound **145**, with a high $F(Z/E)$ of 35.

In another series of reports, photo-repurposing provided the starting point for further modifications for the improvement of azobenzene-based inhibitors of human carbonic anhydrase II (hCAII). Starting from very similar compounds reported earlier,^[230] Runtsch et al. studied the effects of different substituents on the affinity toward the target.^[231] Even though the library of inhibitors was not analyzed in terms of light-dependent behavior, a crystal structure of compound **147** bound to hCAII was obtained (PDB ID: 5BYI). Inspired by the binding mode of inhibitors containing an (*E*)-azobenzene, Que and co-workers designed a closely related probe (compound **148**), hypothesizing that photoisomerization to the (*Z*)-form could cause steric clashes with the active site.^[228] *in vitro* and *in cellulo* biological characterization confirmed that **148** was an (*E*)-on inhibitor, with a $F(Z/E)$ > 4. In a follow-up study, a posteriori molecular docking was performed to rationalize the larger differences of a tetra-*ortho*-fluoroazobenzene derivative **149**, which showed a high $F(Z/E)$ of ≈ 12 .^[229] In fact, the calculations suggested that the bulkier (*Z*)-isomer could not reach deeper regions of the binding pocket, hindering optimal interactions between the sulfonamide moiety and the Zn^{2+} ion (Figure 40).

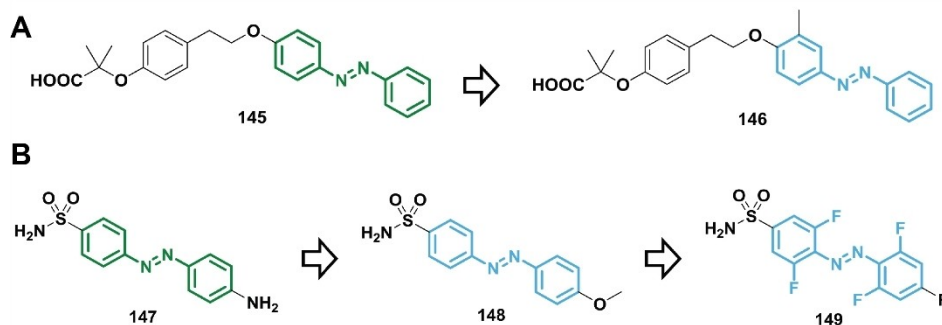


Figure 38. Photo-repurposing and further optimizations of (A) PPAR α agonist **145**,^[227] and of (B) hCAII inhibitor **147**.^[228, 229]

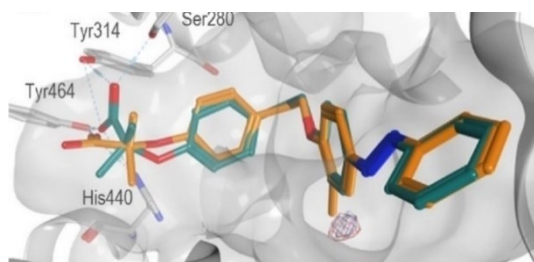


Figure 39. Docking pose of (E)-**146** (orange) into PPAR α (gray, PDB ID: 4CI4), superposed with the co-crystallized binding mode of (E)-**145** (teal). Adapted with permission from ref. [227]. Copyright © 2021 American Chemical Society.

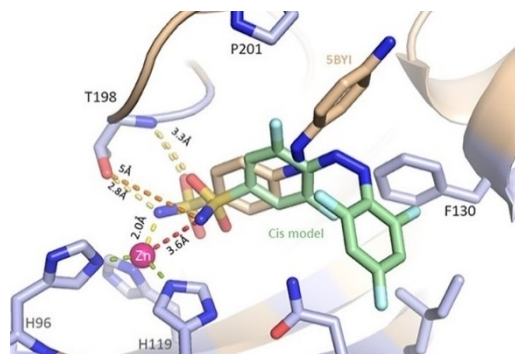


Figure 40. Docking pose of (Z)-**149** (green) into hCAII (violet, PDB ID: 5BYI), superposed with the co-crystallized binding mode of (E)-**147** (beige). Adapted with permission from ref. [229]. Copyright © 2020 American Chemical Society.

Besides the examples described above, we believe that numerous existing ligands contain *E-Z* photoswitches, providing opportunities for more photo-repurposing. Some sources of inspiration include ligands targeting bromodomain-containing protein 4 (BRD4)^[232] and macrophage migration inhibitory factor (MIF).^[233]

3.6. Sign Inversion

Thus far, several strategies for the design of light-active ligands were discussed in this review, ranging from the bioisosteric replacement of (*Z*)-like moieties (see sections 3.2.1.2 and 3.2.2.2) to specific structure-based approaches that highly depend on the target. An additional strategy that emerged recently is the so-called “sign inversion”,^[55,90] which introduces cyclic azobenzenes^[234] (i.e., diazocines) in place of regular azobenzenes (Table 11). These photoswitches have a thermally stable (*Z*)-isomer, while irradiation with visible light generates the metastable (*E*)-isomer. Therefore, the substitution of normal azobenzenes with diazocines reverses the light-dependent changes in geometry and dipole moment, thus enabling the generation of light-active, (*E*)-on compounds from dark-active, (*E*)-on parent compounds.

Taking previous ligands as templates, Ellis-Davies and co-workers described the optical control of ion flow in

neurons.^[235] The NMDAR agonist **150** was based on compound **120**,^[196] while voltage-gated K⁺ channels blocker **151** was based on an earlier reported azobenzene-containing compound.^[236] The latter parent ligand also inspired the study by Trauner and co-workers that introduced the formal definition of sign inversion, leading to the blocker **152**.^[55] Moreover, GIRK channel opener **14**^[71] was the starting point for the design of the cyclic analog **153**. All the examples mentioned above produced the desired outcome: the metastable (*E*)-isomers were more potent, effectively resulting in light-active derivatives.

Remarkably, an application of the scaffold hopping strategy that we described earlier (see section 3.2.1.2.1) is also a key example of sign inversion, with HTI instead of diazocines.^[142] Considering a 2D pharmacophore model, Thorn-Seshold and co-workers took advantage of the asymmetrical geometry of HTI to position the parent phenolic and methoxy substituents for either activation or deactivation upon irradiation. Dark-active (**64**, **65**) or light-active ligands (**66**) were obtained starting from CA-4 and compound **62**.

In addition to ligand-based design, structure-based approaches were employed to further support the similarity of (*E*)-diazocine and (*E*)-azobenzene when bound to the target. Hernando, Gorostiza and co-authors applied *a priori* molecular docking to explore the sign inversion of **120** for the development of GluK2 agonists.^[237] The calculations suggested that **154** could show higher affinity in its (*E*)-isomer, although the interpretation was obfuscated by inaccurate comparisons between the docking scores (see section 3.1.2). Whole-cell experiments confirmed that the light-active, (*E*)-on GluK2 agonist **154** enabled the photo-manipulation of neuronal firing.

Another strategy is the combination of azologization of (*E*)-like bioisosteres (see section 3.2.2.1) with subsequent sign inversion. Such two-step process was described by Trauner and co-workers for the development of photo-switchable covalent inhibitors of the c-Jun N-terminal kinase 3 (JNK3).^[238] Compound **155** was designed through an initial bioisosteric replacement of *N*-aryl benzamide with azobenzene, followed by a sign-inversion approach as well as modification of the electrophile to achieve enhanced solubility and reactivity. The diazocine derivative was found to act as an (*E*)-on inhibitor, with a high *F*(*Z*/*E*) > 15. Furthermore, its mode of action was confirmed by crystal structures of JNK3 with both isomers, which showed that the targeted Cys154 was reached only by the elongated (*E*)-**155** (Figure 41).

Peifer and co-workers used an analogous approach for the design of light-controlled inhibitors of VEGFR-2, in a follow-up study^[239] on compound **144**, i.e., axitinib^[225] (see section 3.5). The original stilbene-like moiety was subjected to terminal substitution (see section 3.2.2) with a heterocyclic azobenzene, but the derivative was immediately discarded because it displayed azo-hydrazone tautomerization that impeded *E-Z* photoisomerization. Consequently, it was necessary to implement the azo-extension strategy (see section 3.1) instead, with a further sign inversion that led to compound **156**. *A priori* molecular docking guided the

Table 11: Overview of sign inversions.

Entry	Compound	Target (ligand)	Parent compound	Photoswitchable derivative (active isomer)	Ref.
1a	150	NMDAR (agonist)			[235]
1b	151	Voltage-gated K ⁺ channels (blocker)			[235]
2a	152	Voltage-gated K ⁺ channels (blocker)			[55]
2b	153	GIRK channel (opener)			[55]
3a	64	Tubulin polymerization (inhibitor)			[142]
3b	66	Tubulin polymerization (inhibitor)			[142]
4	154	GluK2 (agonist)			[237]
5	155	JNK3 (inhibitor)			[238]
6	156	VEGFR-2 (inhibitor)			[239]

maximization of the light-induced differences in binding, even though it was accompanied by misleading comments on the scores (see section 3.1.2). Whereas IFD poses could be obtained for both the (*Z*)- and the (*E*)-isomers of the carbon-bridged diazocine derivative, the sulfur-bridged **156** could be docked only in its (*E*)-isomer (Figure 42B). Such distinct binding was explained through the differences

between the two species in terms of ring angles (Figure 42A). The computational predictions correlated with the experimental results, as compound **156** was determined to be a light-active, (*E*)-on VEGFR-2 inhibitor, with a $F(Z/E) > 40$.

Except an early attempt with little biological activity,^[90] sign inversion proved to be an attractive approach for

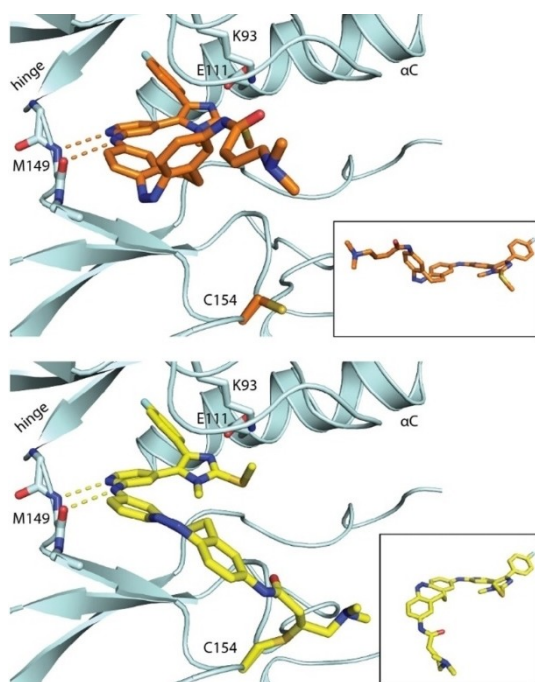


Figure 41. Crystal structures of JNK3 (light blue) in complex with (Z)-155 (orange, PDB ID: 7ORE) and covalently bound to (E)-155 (yellow, PDB ID: 7ORF). Only the (E)-isomer forms a covalent bond with Cys154. Adapted with permission from ref. [238]. Copyright © 2021 Wiley-VCH Verlag GmbH & Co. KGaA.

photopharmacology, despite the fact that the synthesis of diazocines is more challenging than the established preparation of azobenzenes.^[240]

4. Hit Identification

After describing design strategies for photoswitchable analogs, in the following section we present the rare examples that employed strategies for hit identification, which is the first phase of early-stage drug discovery. Photoswitchable

hits have been identified through de novo design and screening methods.

4.1. De Novo Design

According to the recent medicinal chemistry literature, the label “de novo drug design” has mostly referred to the computer-aided design of completely novel bioactive compounds.^[241,242] However, here we use “de novo design” in a broader sense, i.e., as molecular design from scratch that can be also performed by chemists.^[243] As outlined below, photoswitchable bioactive compounds have been devised from scratch only in a handful of examples targeting DNA.

Inspired by the general structure of polyamines, Matczyszyn and co-workers designed the cationic DNA binder **157** (Figure 43).^[244] Interestingly, characterization by circular dichroism suggested that this novel compound could act as a DNA intercalator in its flat (*E*)-form rather than the bulky (*Z*)-form. Moreover, (*E*)-**157** appeared to induce a conformational transition from the canonical B- to the A-DNA form. A follow-up computational study by Zhang et al. further indicated that the ligand could intercalate from the major groove, triggering a DNA deformation that could lower the barrier for the B-to-A transition.^[245]

With a similar strategy, Baigl and co-workers decorated an azobenzene photoswitch with two ethoxy-linked guanidinium moieties, which are known to bind strongly to the phosphate groups of DNA helices.^[246] Compound **158** (Figure 43) was shown to intercalate DNA and significantly increase its melting temperature by up to 18 °C only in the (*E*)-form. In a different application of the same principle, compound **159** (Figure 43) was obtained by attaching two permanently charged, *N*-methyl piperidine groups via a short spacer.^[247] While the (*E*)-isomer promoted the formation of a G-quadruplex secondary structure, the (*Z*)-isomer caused dissociation to an open oligomer. In a subsequent report of DNA-based inhibitors, the light-dependent DNA binding of compound **159** was employed to

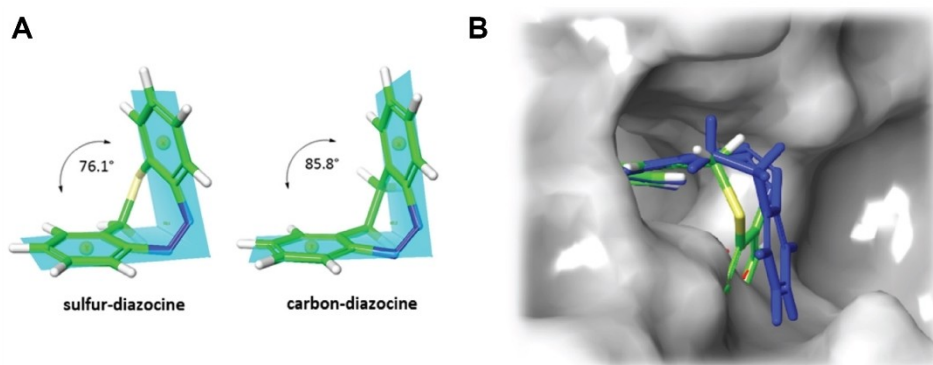


Figure 42. (A) Optimized structures of sulfur- and carbon-bridged diazocines (at the B3LYP/6-31G* level of theory), with measurements of the different ring angles. (B) IFD poses of (Z)-156 (green) into VEGFR-2 (gray surface, PDB ID: 4AG8), superposed with its carbon-bridged analog (blue). Steric clashes arose only with (Z)-156. Adapted with permission from ref. [239]. Copyright © 2020 MDPI.

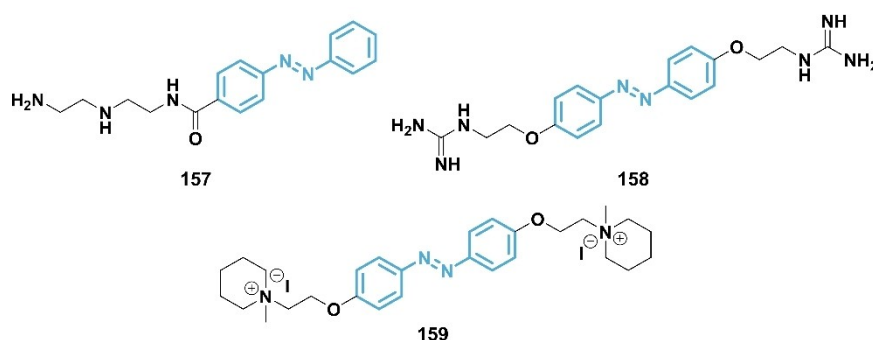


Figure 43. Novel (*E*)-on DNA intercalators designed de novo.

trigger the interconversion of a telomere, toggling between compact and extended forms.^[248]

From the limited number of examples above it appears that de novo design of photoswitchable ligands has more chances of success in the context of DNA intercalators. The design principles for such compounds are simpler, as molecular recognition is mainly guided by electrostatic interactions and π - π interactions with DNA base pairs. Irradiation allows the interconversion between flat and bent geometries, with the former being suitable for DNA intercalation. Nevertheless, an intriguing, structure-based de novo design was reported by Simeth et al. for the development of photoswitchable inhibitors of tryptophan synthase.^[249] Inspired by the binding mode of indole-3-propanol phosphate, the design incorporated important elements of its pharmacophore, namely the hydrogen bond network formed by the phosphate group and the hydrogen bond between the indole NH group and Asp60 (Figure 44). The latter interaction was mimicked by an amide moiety, which served as a handle for the attachment of azobenzene. Biological assays revealed that the inhibitory potencies followed a clearly explicable trend: increasing length of the linker caused stronger inhibition, while it resulted in smaller light-induced differences. However, the compounds surprisingly showed noncompetitive inhibition. To gain insights on the mechanism of (*E*)-on inhibitor **160**, the authors unsuccessfully tried to obtain a co-crystal structure with

tryptophan synthase. In fact, the electron density of the ligand could not be detected, suggesting that it might be too flexible. The abundance of binding modes was further demonstrated with docking studies into a computationally identified, potential allosteric binding site.

4.2. Screening

In a pioneering report, Bellotto et al. developed an *in vitro* evolution method to obtain photoswitchable peptide ligands for streptavidin.^[250] Nevertheless, the application of screening methodologies is challenging for photopharmacology, since photochromic compounds have been classified as pan-assay interference compounds (PAINS).^[251] Addressing the need for different screening strategies, the Fuchter and Peterson groups used a behavior-based platform for the identification of transient receptor potential ankyrin 1 (TRPA1) channel agonist.^[252] After screening a library of 1000 photoswitchable small molecules, compound **161** emerged as a photoswitchable hit due to the induction of motion in zebrafish larvae (Figure 45). Electrophysiology assays confirmed that compound **161** acted as an (*E*)-on agonist of the TRPA1 channel, and subsequent SAR analysis guided the optimization of this initial hit. While the amide group in the *para*-position was determined to be

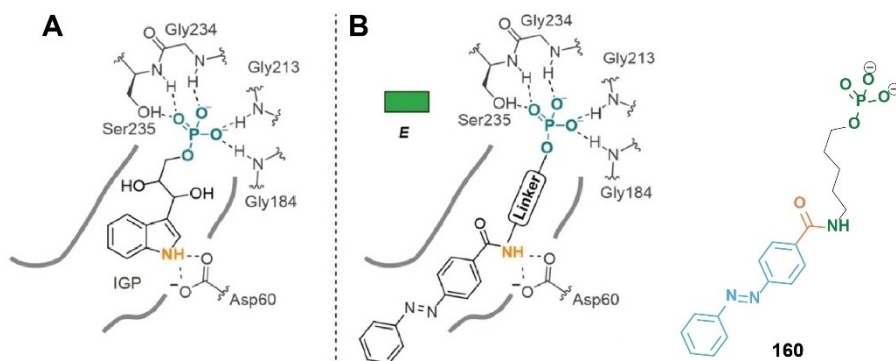


Figure 44. De novo design of tryptophan synthase inhibitor **160**. Adapted with permission from ref. [249]. Copyright © 2020 Wiley-VCH Verlag GmbH & Co. KGaA.

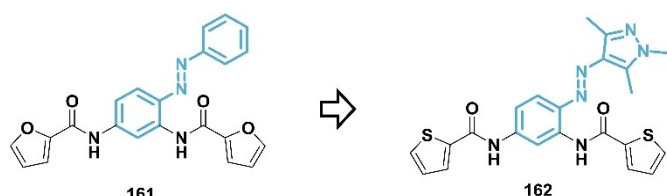


Figure 45. Hit identification and optimization for the optical control of TRPA1 channel.^[252]

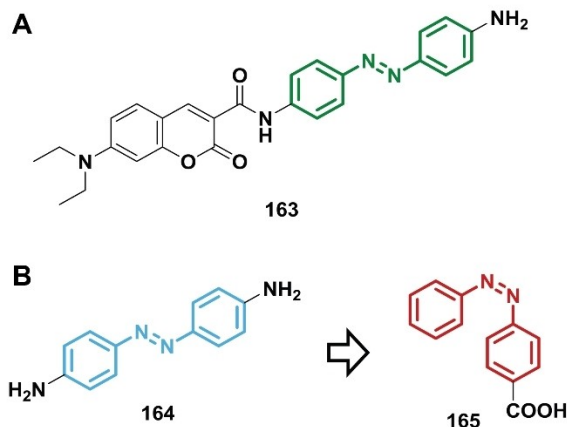


Figure 46. (A) Azobenzene-containing fluorescent probe for the screening of TRPA1 agonist. (B) Hit identification and optimization.^[253, 254]

crucial for the activity, substitution of azobenzene with azopyrazole led to the final compound **162**.

A different approach for the same target was undertaken by Qiao, Qi et al., who reported an azobenzene-based fluorescent probe (compound **163**) for the visualization of TRPA1 channels *in cellulo*.^[253] The design of such tool was inspired by agonist **164**, which was identified in a preliminary screening of active compounds. With probe **163** in hand (Figure 46), the authors systematically explored several modifications of the poorly soluble previous hit structure **164**, identifying compound **165** as a promising (*Z*)-on TRPA1 agonist.^[254]

5. Conclusions and Outlook

Photopharmacology is an exciting, multidisciplinary field that has the potential to revolutionize chemical biology and medicinal chemistry. In a research setting, it enables the unique control over the activity of proteins with unprecedented spatiotemporal precision.^[24] In the biomedical context, it can provide cutting-edge tools to study biological pathways and to limit the side reactions of pharmacological therapies.^[1, 2, 23–25] Concurrently, the light-responsiveness of photoswitchable agents poses additional challenges for ligand design. In fact, a great variety of design strategies has been reported, ranging from straightforward extensions based on trial-and-error approaches to hypothesis-driven iterations of design-make-test-analyze (DMTA) cycles.^[195]

Generally speaking, the introduction of a photoswitch into the scaffold or within the pharmacophore has led to large differences in potency between the photoisomers. On the other hand, attaching a photoswitch in the periphery of a ligand has been shown to affect binding, and thus the overall potency, to a lesser extent.

In addition to the well-known approaches of extension and bioisosteric replacement, molecular design in photopharmacology can take other forms. If intramolecular distance is the key parameter for biological activity, *E-Z* photoswitches can be introduced as spacers to control binding to, e.g., multiple enzymatic binding sites or DNA helices. The recognition of photoswitchable substructures in existing ligands enables the study of their light-dependent behavior. When a known photoswitchable ligand has undesired (*E*)-on behavior, the introduction of diazocine (or HTI) allows for a change in direction from a dark-active to a light-active compound. Conversely, *de novo* design or screening are heavily underexplored for the identification of photoswitchable hits.

With regard to the molecular modeling techniques that have been applied in photopharmacology, molecular docking and MD simulations are prominent. However, although these methods have been mostly used to explain the observed biological activities, they have guided the design only in a limited number of cases.

After examining the literature in detail and realizing the early stage at which this field is, we can identify numerous opportunities for the design approaches taken by photopharmacology. Altogether, considerations that are commonplace in medicinal chemistry, such as ligand efficiency^[25] or Lipinski's rule of five,^[255] are often neglected during the design of photoswitchable ligands.

Especially in earlier photopharmacological endeavors, there is no further rationale behind the design hypothesis besides “hope” (often clearly stated in the text). In our opinion, the fulfillment of “hopes” does not contribute substantial information to the existing scientific knowledge. For this reason, we argue that molecular design in photopharmacology needs to go beyond the lucky outcomes that can derive from blind trial-and-error approaches. Albeit valuable for broadening the horizon of photo-druggable targets,^[23] serendipity^[256] alone does not increase our fundamental understanding of photopharmacology.

Furthermore, knowledge emerging from previous, traditionally obtained SAR analyses should play a bigger role in supporting the design of photoswitchable ligands. One appealing example can be found in the photopharmacological exploitation of activity cliffs^[202] (see section 3.3). Usually, two closely related compounds of a SAR library display only modest differences in affinity. Therefore, a photoswitchable analog that mimics both these compounds with one or the other photoisomer shows an inadequate light-dependent activation. However, a promising strategy for achieving effective photo-activation is to devise a photoswitchable analog that mimics two structurally related compounds with a very large difference in potency. In this case, photoisomerization can be used to toggle between two

states that resemble activity cliffs, i.e., two photoisomers with considerably different biological activities.

Other perfectible points pertain to the computational support of photopharmacology. Rational design could benefit from more frequent evaluations of 3D similarities between the molecular shapes of template ligands and specific isomers of their photoswitchable analogs.^[45,114,116] Similarly, the large light-induced changes in electronic properties (e.g., dipole moment, ESP surfaces) should be exploited to mimic the electrostatic distribution of the parent compounds. In terms of structure-based methodologies, docking scores have been the object of inaccurate correlations in the discussion of photopharmacological results, as we commented earlier (see section 3.1.2).^[41,80,83,84]

Rational, computer-aided drug design for photopharmacology is currently at its infancy. Besides DFT calculations, docking and MD, there is a broad spectrum of computational techniques that still need to be explored for the design and rationalization of photoswitchable ligands, e.g., 3D-QSAR,^[257] 3D pharmacophores,^[47] AI-related methods,^[258] and free energy calculations.^[259]

Methodologies that can greatly inspire future photopharmacology endeavors are virtual screening and fragment-based drug discovery.^[260] Virtual screening of photo-switch-containing libraries could be helpful for generating ideas in silico, aiming at the preferential binding of the (Z)-forms to obtain light-active compounds. We also envision promising applications of fragment-based drug design for the optical control of biological systems. E-Z photoswitches could be the starting point for fragment growing strategies, or they could be used as linkers (see section 3.4) for fragment linking.

In light of the detailed analysis performed in this review, we believe that the assimilation of design terminology and strategies from medicinal chemistry will open extraordinary possibilities for the non-invasive, high-precision control of complex biological systems and beyond.

Acknowledgements

We kindly acknowledge financial support from the EU Horizon 2020 program (ALERT cofund no. 713482 for B.L.F.), the Dutch Scientific Organization (VIDI grant no. 723.014.001 for W.S.). We would like to thank Martyna Komorowska for the design and creation of frontispiece and TOC graphics.

Conflict of Interest

The authors declare no conflict of interest.

Keywords: Drug Design • Medicinal Chemistry • Photopharmacology • Photoswitchable Molecule

- [1] W. A. Velema, W. Szymanski, B. L. Feringa, *J. Am. Chem. Soc.* **2014**, *136*, 2178–2191.

- [2] J. Broichhagen, J. A. Frank, D. Trauner, *Acc. Chem. Res.* **2015**, *48*, 1947–1960.
- [3] C. S. Cleeland, J. D. Allen, S. A. Roberts, J. M. Brell, S. A. Giralt, A. Y. Khakoo, R. A. Kirch, V. E. Kwitkowski, Z. Liao, J. Skillings, *Nat. Rev. Clin. Oncol.* **2012**, *9*, 471–478.
- [4] N. Vasan, J. Baselga, D. M. Hyman, *Nature* **2019**, *575*, 299–309.
- [5] F. Peter Guengerich, *Drug Metab. Pharmacokinet.* **2011**, *26*, 3–14.
- [6] S. Niraula, B. Seruga, A. Ocana, T. Shao, R. Goldstein, I. F. Tannock, E. Amir, *J. Clin. Oncol.* **2012**, *30*, 3012–3019.
- [7] L. Wise, J. Parkinson, J. Raine, A. Breckenridge, *Nat. Rev. Drug Discovery* **2009**, *8*, 779–782.
- [8] K. Strebhardt, A. Ullrich, *Nat. Rev. Cancer* **2008**, *8*, 473–480.
- [9] P. Y. Muller, M. N. Milton, *Nat. Rev. Drug Discovery* **2012**, *11*, 751–761.
- [10] M. W. Tibbitt, J. E. Dahlman, R. Langer, *J. Am. Chem. Soc.* **2016**, *138*, 704–717.
- [11] J. Z. Drago, S. Modi, S. Chandarlapaty, *Nat. Rev. Clin. Oncol.* **2021**, *18*, 327–344.
- [12] J. Rautio, N. A. Meanwell, L. Di, M. J. Hageman, *Nat. Rev. Drug Discovery* **2018**, *17*, 559–587.
- [13] B. N., B. P., *Med. Res. Rev.* **2000**, *20*, 58–101.
- [14] M. Karimi, A. Ghasemi, P. Sahandi Zangabad, R. Rahighi, S. M. Moosavi Basri, H. Mirshekari, M. Amiri, Z. Shafaei Pishabad, A. Aslani, M. Bozorgomid, D. Ghosh, A. Beyzavi, A. Vaseghi, A. R. Aref, L. Haghani, S. Bahrami, M. R. Hamblin, *Chem. Soc. Rev.* **2016**, *45*, 1457–1501.
- [15] P. Buchwald, *Expert Opin. Drug Metab. Toxicol.* **2020**, *16*, 645–650.
- [16] J. F. Liu, B. Jang, D. Issadore, A. Tsourkas, *WIREs Nanomed. Nanobiotechnol.* **2019**, *11*, e1571.
- [17] S. Mitragotri, *Nat. Rev. Drug Discovery* **2005**, *4*, 255–260.
- [18] K. Hüll, J. Morstein, D. Trauner, *Chem. Rev.* **2018**, *118*, 10710–10747.
- [19] B. M. Vickerman, E. M. Zywt, T. K. Tarrant, D. S. Lawrence, *Nat. Chem. Rev.* **2021**, *5*, 816–834.
- [20] S. Kwiatkowski, B. Knap, D. Przystupski, J. Saczko, E. Kędzierska, K. Knap-Czop, J. Kotlińska, O. Michel, K. Kotowski, J. Kulbacka, *Biomed. Pharmacother.* **2018**, *106*, 1098–1107.
- [21] Y. Tao, H. F. Chan, B. Shi, M. Li, K. W. Leong, *Adv. Funct. Mater.* **2020**, *30*, 2005029.
- [22] K. Deisseroth, *Nat. Neurosci.* **2015**, *18*, 1213–1225.
- [23] M. M. Lerch, M. J. Hansen, G. M. van Dam, W. Szymanski, B. L. Feringa, *Angew. Chem. Int. Ed.* **2016**, *55*, 10978–10999.
- [24] M. W. H. Hoorens, W. Szymanski, *Trends Biochem. Sci.* **2018**, *43*, 567–575.
- [25] M. J. Fuchter, *J. Med. Chem.* **2020**, *63*, 11436–11447.
- [26] I. M. Welleman, M. W. H. Hoorens, B. L. Feringa, H. H. Boersma, W. Szymański, *Chem. Sci.* **2020**, *11*, 11672–11691.
- [27] B. L. Feringa, W. R. Browne, *Molecular Switches*, Wiley-VCH, Weinheim, **2011**.
- [28] P. Klán, T. Šolomek, C. G. Bochet, A. Blanc, R. Givens, M. Rubina, V. Popik, A. Kostikov, J. Wirz, *Chem. Rev.* **2013**, *113*, 119–191.
- [29] R. Weinstein, T. Slanina, D. Kand, P. Klán, *Chem. Rev.* **2020**, *120*, 13135–13272.
- [30] M. J. Hansen, W. A. Velema, M. M. Lerch, W. Szymanski, B. L. Feringa, *Chem. Soc. Rev.* **2015**, *44*, 3358–3377.
- [31] A. S. Kozlenko, I. V. Ozhogin, A. D. Pugachev, M. B. Lukyanova, I. M. El-Sewify, B. S. Lukyanov, *A Modern Look at Spiropyrans: From Single Molecules to Smart Materials*, Springer International Publishing, **2023**.
- [32] J. Volarić, W. Szymanski, N. A. Simeth, B. L. Feringa, *Chem. Soc. Rev.* **2021**, *50*, 12377–12449.

- [33] M. M. Lerch, W. Szymański, B. L. Feringa, *Chem. Soc. Rev.* **2018**, *47*, 1910–1937.
- [34] L. Albert, A. Peñalver, N. Djokovic, L. Werel, M. Hoffarth, D. Ruzic, J. Xu, L. O. Essen, K. Nikolic, Y. Dou, O. Vázquez, *ChemBioChem* **2019**, *20*, 1417–1429.
- [35] W. Szymański, J. M. Beierle, H. A. V. Kistemaker, W. A. Velema, B. L. Feringa, *Chem. Rev.* **2013**, *113*, 6114–6178.
- [36] A. A. Beharry, G. A. Woolley, *Chem. Soc. Rev.* **2011**, *40*, 4422–4437.
- [37] S. Crespi, N. A. Simeth, B. König, *Nat. Chem. Rev.* **2019**, *3*, 133–146.
- [38] J. Calbo, C. E. Weston, A. J. P. White, H. S. Rzepa, J. Contreras-García, M. J. Fuchter, *J. Am. Chem. Soc.* **2017**, *139*, 1261–1274.
- [39] S. Wiedbrauk, H. Dube, *Tetrahedron Lett.* **2015**, *56*, 4266–4274.
- [40] C. Matera, A. M. J. Gomila, N. Camarero, M. Libergoli, C. Soler, P. Gorostiza, *J. Am. Chem. Soc.* **2018**, *140*, 15764–15773.
- [41] B. Kuhn, W. Guba, J. Hert, D. Banner, C. Bissantz, S. Ceccarelli, W. Haap, M. Körner, A. Kuglstatter, C. Lerner, P. Mattei, W. Neidhart, E. Pinard, M. G. Rudolph, T. Schulz-Gasch, T. Woltering, M. Stahl, *J. Med. Chem.* **2016**, *59*, 4087–4102.
- [42] C. G. Wermuth, *Drug Discovery Today* **2006**, *11*, 348–354.
- [43] S. P. Leelananda, S. Lindert, *Beilstein J. Org. Chem.* **2016**, *12*, 2694–2718.
- [44] R. A. Lewis, D. Wood, *Wiley Interdiscip. Rev. Comput. Mol. Sci.* **2014**, *4*, 505–522.
- [45] A. Nicholls, G. B. McGaughey, R. P. Sheridan, A. C. Good, G. Warren, M. Mathieu, S. W. Muchmore, S. P. Brown, J. A. Grant, J. A. Haigh, N. Nevins, A. N. Jain, B. Kelley, *J. Med. Chem.* **2010**, *53*, 3862–3886.
- [46] P. C. Rath, R. F. Ludlow, M. L. Verdonk, *J. Med. Chem.* **2020**, *63*, 8778–8790.
- [47] D. Schaller, D. Šribar, T. Noonan, L. Deng, T. N. Nguyen, S. Pach, D. Machalz, M. Bermudez, G. Wolber, *Wiley Interdiscip. Rev. Comput. Mol. Sci.* **2020**, *10*, e1468.
- [48] A. Nin-Hill, N. P. F. Mueller, C. Molteni, C. Rovira, M. Alfonso-Prieto, *Int. J. Mol. Sci.* **2021**, *22*, 12072.
- [49] C. Bissantz, B. Kuhn, M. Stahl, *J. Med. Chem.* **2010**, *53*, 5061–5084.
- [50] M. T. Muhammed, E. Aki-Yalcin, *Chem. Biol. Drug Des.* **2019**, *93*, 12–20.
- [51] P. Śledź, A. Caffisch, *Curr. Opin. Struct. Biol.* **2018**, *48*, 93–102.
- [52] L. Pinzi, G. Rastelli, *Int. J. Mol. Sci.* **2019**, *20*, 4331.
- [53] M. De Vivo, M. Masetti, G. Bottegoni, A. Cavalli, *J. Med. Chem.* **2016**, *59*, 4035–4061.
- [54] M. Schoenberger, A. Damijonaitis, Z. Zhang, D. Nagel, D. Trauner, *ACS Chem. Neurosci.* **2014**, *5*, 514–518.
- [55] J. B. Trads, K. Hüll, B. S. Matsuura, L. Laprell, T. Fehrentz, N. Görlt, K. A. Kozek, C. D. Weaver, N. Klöcker, D. M. Barber, D. Trauner, *Angew. Chem. Int. Ed.* **2019**, *58*, 15421–15428.
- [56] H. Kaufman, S. M. Vratsanos, B. F. Erlanger, *Science* **1968**, *162*, 1487–1489.
- [57] W. J. Deal, B. F. Erlanger, D. Nachmansohn, *Proc. Natl. Acad. Sci. USA* **1969**, *64*, 1230–1234.
- [58] M. Stein, S. J. Middendorp, V. Carta, E. Pejo, D. E. Raines, S. A. Forman, E. Sigel, D. Trauner, *Angew. Chem. Int. Ed.* **2012**, *51*, 10500–10504.
- [59] M. Schönberger, D. Trauner, *Angew. Chem. Int. Ed.* **2014**, *53*, 3264–3267.
- [60] M. Schönberger, M. Althaus, M. Fronius, W. Clauss, D. Trauner, *Nat. Chem.* **2014**, *6*, 712–719.
- [61] P. Stawski, M. Sumser, D. Trauner, *Angew. Chem. Int. Ed.* **2012**, *51*, 5748–5751.
- [62] T. Wolter, T. Steinbrecher, D. Trauner, M. Elstner, *PLoS One* **2014**, *9*, e92716.
- [63] A. Müller-Deku, J. C. M. Meiring, K. Loy, Y. Kraus, C. Heise, R. Bingham, K. I. Jansen, X. Qu, F. Bartolini, L. C. Kapitein, A. Akhmanova, J. Ahlfeld, D. Trauner, O. Thorn-Seshold, *Nat. Commun.* **2020**, *11*, 4640.
- [64] S. B. Vogensen, K. Frydenvang, J. R. Greenwood, G. Postorino, B. Nielsen, D. S. Pickering, B. Ebert, U. Bølcho, J. Egebjerg, M. Gajhede, J. S. Kastrup, T. N. Johansen, R. P. Clausen, P. Krogsgaard-Larsen, *J. Med. Chem.* **2007**, *50*, 2408–2414.
- [65] M. J. Hansen, W. A. Velema, G. De Bruin, H. S. Overkleef, W. Szymanski, B. L. Feringa, *ChemBioChem* **2015**, *16*, 2053–2057.
- [66] B. Blanco, K. A. Palasis, A. Adwal, D. F. Callen, A. D. Abell, *Bioorg. Med. Chem.* **2017**, *25*, 5050–5054.
- [67] M. R. Cunha, R. Bhardwaj, S. Linder, C. Butorac, C. Romanin, M. A. Hediger, J. L. Reymond, *ACS Med. Chem. Lett.* **2019**, *10*, 1341–1345.
- [68] W. Szymanski, M. E. Ourailidou, W. A. Velema, F. J. Dekker, B. L. Feringa, *Chem. Eur. J.* **2015**, *21*, 16517–16524.
- [69] A. J. Harvey, A. D. Abell, *Tetrahedron* **2000**, *56*, 9763–9771.
- [70] K. Rustler, M. J. Mickert, J. Nazet, R. Merkl, H. H. Gorris, B. König, *Org. Biomol. Chem.* **2018**, *16*, 7430–7437.
- [71] D. M. Barber, M. Schönberger, J. Burgstaller, J. Levitz, C. D. Weaver, E. Y. Isacoff, H. Baier, D. Trauner, *Chem. Sci.* **2016**, *7*, 2347–2352.
- [72] M. Stein, A. Breit, T. Fehrentz, T. Gudermann, D. Trauner, *Angew. Chem. Int. Ed.* **2013**, *52*, 9845–9848.
- [73] N. Perur, M. Yahara, T. Kamei, N. Tamaoki, *Chem. Commun.* **2013**, *49*, 9935–9937.
- [74] D. Kolarski, C. Miró-Vinyals, A. Sugiyama, A. Srivastava, D. Ono, Y. Nagai, M. Iida, K. Itami, F. Tama, W. Szymanski, T. Hirota, B. L. Feringa, *Nat. Commun.* **2021**, *12*, 3164.
- [75] B. G. Dwyer, C. Wang, D. Abegg, B. Racioppo, N. Qiu, Z. Zhao, D. Pechalieu, A. Shuster, D. G. Hoch, A. Adibekian, *Angew. Chem. Int. Ed.* **2021**, *60*, 3071–3079.
- [76] W. A. Velema, J. P. Van Der Berg, M. J. Hansen, W. Szymanski, A. J. M. Driessen, B. L. Feringa, *Nat. Chem.* **2013**, *5*, 924–928.
- [77] E. Contreras-García, D. Martínez-López, C. A. Alonso, C. Lozano, C. Torres, M. A. Rodríguez, P. J. Campos, D. Sampedro, *Eur. J. Org. Chem.* **2017**, 4719–4725.
- [78] S. A. Reis, B. Ghosh, J. A. Hendricks, D. M. Szantai-Kis, L. Törk, K. N. Ross, J. Lamb, W. Read-Button, B. Zheng, H. Wang, C. Salthouse, S. J. Haggarty, R. Mazitschek, *Nat. Chem. Biol.* **2016**, *12*, 317–323.
- [79] D. M. Barber, S. A. Liu, K. Gottschling, M. Sumser, M. Hollmann, D. Trauner, *Chem. Sci.* **2017**, *8*, 611–615.
- [80] A. Fischer, M. Smieško, M. Sellner, M. A. Lill, *J. Med. Chem.* **2021**, *64*, 2489–2500.
- [81] A. D. Abell, M. A. Jones, A. T. Neffe, S. G. Aitken, T. P. Cain, R. J. Payne, S. B. McNabb, J. M. Coxon, B. G. Stuart, D. Pearson, H. Y. Y. Lee, J. D. Morton, *J. Med. Chem.* **2007**, *50*, 2916–2920.
- [82] R. C. Sarott, A. E. G. Viray, P. Pfaff, A. Sadybekov, G. Rajic, V. Katritch, E. M. Carreira, J. A. Frank, *J. Am. Chem. Soc.* **2021**, *143*, 736–743.
- [83] Z. Wang, H. Sun, X. Yao, D. Li, L. Xu, Y. Li, S. Tian, T. Hou, *Phys. Chem. Chem. Phys.* **2016**, *18*, 12964–12975.
- [84] B. J. Bender, S. Gahbauer, A. Luttens, J. Lyu, C. M. Webb, R. M. Stein, E. A. Fink, T. E. Balias, J. Carlsson, J. J. Irwin, B. K. Shoichet, *Nat. Protoc.* **2021**, *16*, 4799–4832.
- [85] G. Maleeva, D. Wutz, K. Rustler, A. Nin-Hill, C. Rovira, E. Petukhova, A. Bautista-Barrufet, A. Gomila-Juaneda, P.

- Scholze, F. Peiretti, M. Alfonso-Prieto, B. König, P. Gorostiza, P. Bregestovski, *Br. J. Pharmacol.* **2019**, *176*, 2661–2677.
- [86] A. M. J. Gomila, K. Rustler, G. Maleeva, A. Nin-Hill, D. Wutz, A. Bautista-Barrufet, X. Rovira, M. Bosch, E. Mukhametova, E. Petukhova, D. Ponomareva, M. Mukhamedyarov, F. Peiretti, M. Alfonso-Prieto, C. Rovira, B. König, P. Bregestovski, P. Gorostiza, *Cell Chem. Biol.* **2020**, *27*, 1425–1433.
- [87] G. Maleeva, A. Nin-Hill, K. Rustler, E. Petukhova, D. Ponomareva, E. Mukhametova, A. M. Gomila, D. Wutz, M. Alfonso-Prieto, B. König, P. Gorostiza, P. Bregestovski, *eNeuro* **2020**, *8*, ENEURO.0294-20.2020.
- [88] D. Dolles, A. Strasser, H. J. Wittmann, O. Marinelli, M. Nabissi, R. G. Pertwee, M. Decker, *Adv. Ther.* **2018**, *1*, 1700032.
- [89] D. Pagé, E. Balaux, L. Boisvert, Z. Liu, C. Milburn, M. Tremblay, Z. Wei, S. Woo, X. Luo, Y. X. Cheng, H. Yang, S. Srivastava, F. Zhou, W. Brown, M. Tomaszewski, C. Walpole, L. Hodzic, S. St-Onge, C. Godbout, D. Salois, K. Payza, *Bioorg. Med. Chem. Lett.* **2008**, *18*, 3695–3700.
- [90] M. Schehr, C. Ianes, J. Weisner, L. Heintze, M. P. Müller, C. Pichlo, J. Charl, E. Brunstein, J. Ewert, M. Lehr, U. Baumann, D. Rauh, U. Knippschild, C. Peifer, R. Herges, *Photochem. Photobiol. Sci.* **2019**, *18*, 1398–1407.
- [91] M. Wegener, M. J. Hansen, A. J. M. Driessen, W. Szymanski, B. L. Feringa, *J. Am. Chem. Soc.* **2017**, *139*, 17979–17986.
- [92] A. Impastato, A. Shemet, N. Veprek, G. Saper, H. Hess, L. Rao, A. Gennerich, D. Trauner, *Angew. Chem. Int. Ed.* **2022**, *61*, e202115846.
- [93] L. Agnetta, M. Bermudez, F. Riefolo, C. Matera, E. Claro, R. Messerer, T. Littmann, G. Wolber, U. Holzgrabe, M. Decker, *J. Med. Chem.* **2019**, *62*, 3009–3020.
- [94] T. Kamei, T. Fukaminato, N. Tamaoki, *Chem. Commun.* **2012**, *48*, 7625–7627.
- [95] W. A. Velema, M. J. Hansen, M. M. Lerch, A. J. M. Driessen, W. Szymanski, B. L. Feringa, *Bioconjugate Chem.* **2015**, *26*, 2592–2597.
- [96] L. Laprell, E. Repak, V. Franckevicius, F. Hartrampf, J. Terhag, M. Hollmann, M. Sumser, N. Rebola, D. A. DiGregorio, D. Trauner, *Nat. Commun.* **2015**, *6*, 8076.
- [97] Y. Zhang, F. Erdmann, G. Fischer, *Nat. Chem. Biol.* **2009**, *5*, 724–726.
- [98] J. Broichhagen, I. Jurastow, K. Iwan, W. Kummer, D. Trauner, *Angew. Chem. Int. Ed.* **2014**, *53*, 7657–7660.
- [99] L. Yue, M. Pawlowski, S. S. Dellal, A. Xie, F. Feng, T. S. Otis, K. S. Bruzik, H. Qian, D. R. Pepperberg, *Nat. Commun.* **2012**, *3*, 1095.
- [100] T. Fehrentz, F. M. E. Huber, N. Hartrampf, T. Bruegmann, J. A. Frank, N. H. F. Fine, D. Malan, J. G. Danzl, D. B. Tikhonov, M. Sumser, P. Sasse, D. J. Hodson, B. S. Zhorov, N. Klöcker, D. Trauner, *Nat. Chem. Biol.* **2018**, *14*, 764–767.
- [101] E. R. Thapaliya, L. Mony, R. Sanchez, B. Serraz, P. Paoletti, G. C. R. Ellis-Davies, *ChemPhotoChem* **2021**, *5*, 445–454.
- [102] P. Dunkel, J. Ilaš, *Cancers* **2021**, *13*, 3237.
- [103] D. A. Rodríguez-Soacha, J. Fender, Y. A. Ramírez, J. A. Collado, E. Muñoz, R. Maitra, C. Sottriffer, K. Lorenz, M. Decker, *ACS Chem. Neurosci.* **2021**, *12*, 1632–1647.
- [104] M. Borowiak, F. Küllmer, F. Gegenfurtner, S. Peil, V. Nasufovic, S. Zahler, O. Thorn-Seshold, D. Trauner, H. D. Arndt, *J. Am. Chem. Soc.* **2020**, *142*, 9240–9249.
- [105] S. Pospich, F. Küllmer, V. Nasufović, J. Funk, A. Belyy, P. Bieling, H. D. Arndt, S. Raunser, *Angew. Chem. Int. Ed.* **2021**, *60*, 8678–8682.
- [106] N. Brown, in *Bioisosteres in Medicinal Chemistry* (Eds.: R. Mannhold, H. Kubinyi, G. Folkers, N. Brown), Wiley-VCH, Weinheim, **2012**, pp. 1–14.
- [107] C. W. Thornber, *Chem. Soc. Rev.* **1979**, *8*, 563–580.
- [108] H. Sun, G. Tawa, A. Wallqvist, *Drug Discovery Today* **2012**, *17*, 310–324.
- [109] N. Brown, in *Scaffold Hopping in Medicinal Chemistry* (Ed.: N. Brown), Wiley-VCH, Weinheim, **2013**, pp. 1–14.
- [110] Y. Hu, D. Stumpfe, J. Bajorath, *J. Med. Chem.* **2017**, *60*, 1238–1246.
- [111] F. A. Jerca, V. V. Jerca, R. Hoogenboom, *Nat. Chem. Rev.* **2022**, *6*, 51–69.
- [112] G. A. Patani, E. J. LaVoie, *Chem. Rev.* **1996**, *96*, 3147–3176.
- [113] N. A. Meanwell, *J. Med. Chem.* **2011**, *54*, 2529–2591.
- [114] J. Morstein, M. Awale, J. L. Reymond, D. Trauner, *ACS Cent. Sci.* **2019**, *5*, 607–618.
- [115] S. R. Langdon, P. Ertl, N. Brown, *Mol. Inf.* **2010**, *29*, 366–385.
- [116] P. Kobauri, W. Szymanski, F. Cao, S. Thallmair, S. J. Marrink, M. D. Witte, F. J. Dekker, B. L. Feringa, *Chem. Commun.* **2021**, *57*, 4126–4129.
- [117] T. Hu, G. Zheng, D. Xue, S. Zhao, F. Li, F. Zhou, F. Zhao, L. Xie, C. Tian, T. Hua, S. Zhao, Y. Xu, G. Zhong, Z.-J. Liu, A. Makriyannis, R. C. Stevens, H. Tao, *J. Med. Chem.* **2021**, *64*, 13752–13765.
- [118] Y. Hu, D. Stumpfe, J. Bajorath, *J. Med. Chem.* **2016**, *59*, 4062–4076.
- [119] L. D. Pennington, D. T. Moustakas, *J. Med. Chem.* **2017**, *60*, 3552–3579.
- [120] B. Eisel, F. W. W. Hartrampf, T. Meier, D. Trauner, *FEBS Lett.* **2018**, *592*, 343–355.
- [121] C. W. Grathwol, N. Wössner, S. Behnisch-Cornwell, L. Schulig, L. Zhang, O. Einsle, M. Jung, A. Link, *ChemMedChem* **2020**, *15*, 1480–1489.
- [122] C. Brown, S. K. Rastogi, S. L. Barrett, H. E. Anderson, E. Twichell, S. Gralinski, A. McDonald, W. J. Brittain, *J. Photochem. Photobiol. A* **2017**, *336*, 140–145.
- [123] A. I. Khalaf, N. Anthony, D. Breen, G. Donoghue, S. P. MacKay, F. J. Scott, C. J. Suckling, *Eur. J. Med. Chem.* **2011**, *46*, 5343–5355.
- [124] S. Pittolo, X. Gómez-Santacana, K. Eckelt, X. Rovira, J. Dalton, C. Goudet, J. P. Pin, A. Llobet, J. Giraldo, A. Llebaria, P. Gorostiza, *Nat. Chem. Biol.* **2014**, *10*, 813–815.
- [125] C. Nasrallah, G. Cannone, J. Briot, K. Rottier, A. E. Berizzi, C. Y. Huang, R. B. Quast, F. Hoh, J. L. Banères, F. Malhaire, L. Berto, A. Dumazer, J. Font-Ingles, X. Gómez-Santacana, J. Catena, J. Kniazeff, C. Goudet, A. Llebaria, J. P. Pin, K. R. Vinothkumar, G. Lebon, *Cell Rep.* **2021**, *36*, 109648.
- [126] X. Yang, G. Ma, S. Zheng, X. Qin, X. Li, L. Du, Y. Wang, Y. Zhou, M. Li, *J. Am. Chem. Soc.* **2020**, *142*, 9460–9470.
- [127] K. Matsuo, S. Thayyil, M. Kawaguchi, H. Nakagawa, N. Tamaoki, *Chem. Commun.* **2021**, *57*, 12500–12503.
- [128] K. Rustler, G. Maleeva, P. Bregestovski, B. König, *Beilstein J. Org. Chem.* **2019**, *15*, 780–788.
- [129] J. A. Frank, D. A. Yushchenko, N. H. F. Fine, M. Duca, M. Citir, J. Broichhagen, D. J. Hodson, C. Schultz, D. Trauner, *Chem. Sci.* **2017**, *8*, 7604–7610.
- [130] D. Kolarski, A. Sugiyama, T. Rodat, A. Schulte, C. Peifer, K. Itami, T. Hirota, B. L. Feringa, W. Szymanski, *Org. Biomol. Chem.* **2021**, *19*, 2312–2321.
- [131] P. Donthamsetti, D. B. Konrad, B. Hetzler, Z. Fu, D. Trauner, E. Y. Isacoff, *J. Am. Chem. Soc.* **2021**, *143*, 8951–8956.
- [132] K. Lu, Q. Chen, X. F. Xu, Y. Meng, J. Lin, W. M. Chen, *J. Antibiot.* **2020**, *73*, 82–90.
- [133] S. Wategaonkar, A. Bhattacharjee, *J. Phys. Chem. A* **2018**, *122*, 4313–4321.
- [134] Y. Xu, C. Gao, L. Håversen, T. Lundbäck, J. Andréasson, M. Grøtli, *Chem. Commun.* **2021**, *57*, 10043–10046.
- [135] R. Ferreira, J. R. Nilsson, C. Solano, J. Andréasson, M. Grøtli, *Sci. Rep.* **2015**, *5*, 9769.

- [136] S. Herre, T. Schadendorf, I. Ivanov, C. Herrberger, W. Steinle, K. Rück-Braun, R. Preissner, H. Kuhn, *ChemBioChem* **2006**, *7*, 1089–1095.
- [137] A. Cebrián-Prats, T. Rovira, P. Saura, À. González-Lafont, J. M. Lluch, *J. Phys. Chem. A* **2017**, *121*, 9752–9763.
- [138] F. Wages, P. Lentes, T. Griebenow, R. Herges, C. Peifer, E. Maser, *Chem.-Biol. Interact.* **2022**, *354*, 109822.
- [139] J. E. Sheldon, M. M. Dcona, C. E. Lyons, J. C. Hackett, M. C. T. Hartman, *Org. Biomol. Chem.* **2016**, *14*, 40–49.
- [140] M. Borowiak, W. Nahaboo, M. Reynders, K. Nekolla, P. Jalinot, J. Hasserodt, M. Rehberg, M. Delattre, S. Zahler, A. Vollmar, D. Trauner, O. Thorn-Seshold, *Cell* **2015**, *162*, 403–411.
- [141] A. J. Engdahl, E. A. Torres, S. E. Lock, T. B. Engdahl, P. S. Mertz, C. N. Streu, *Org. Lett.* **2015**, *17*, 4546–4549.
- [142] A. Sailer, F. Ermer, Y. Kraus, F. H. Lutter, C. Donau, M. Bremerich, J. Ahlfeld, O. Thorn-Seshold, *ChemBioChem* **2019**, *20*, 1305–1314.
- [143] A. Sailer, F. Ermer, Y. Kraus, R. Bingham, F. H. Lutter, J. Ahlfeld, O. Thorn-Seshold, *Beilstein J. Org. Chem.* **2020**, *16*, 125–134.
- [144] A. Sailer, J. C. M. Meiring, C. Heise, L. N. Pettersson, A. Akhmanova, J. Thorn-Seshold, O. Thorn-Seshold, *Angew. Chem. Int. Ed.* **2021**, *60*, 23695–23704.
- [145] S. K. Rastogi, Z. Zhao, S. L. Barrett, S. D. Shelton, M. Zafferani, H. E. Anderson, M. O. Blumenthal, L. R. Jones, L. Wang, X. Li, C. N. Streu, L. Du, W. J. Brittain, *Eur. J. Med. Chem.* **2018**, *143*, 1–7.
- [146] J. Garcia-Amorós, A. Sánchez-Ferrer, W. A. Massad, S. Nonell, D. Velasco, *Phys. Chem. Chem. Phys.* **2010**, *12*, 13238–13242.
- [147] L. Gao, J. C. M. Meiring, Y. Kraus, M. Wranik, T. Weinert, S. D. Pritzl, R. Bingham, E. Ntoulou, K. I. Jansen, N. Olieric, J. Standfuss, L. C. Kapitein, T. Lohmüller, J. Ahlfeld, A. Akhmanova, M. O. Steinmetz, O. Thorn-Seshold, *Cell Chem. Biol.* **2021**, *28*, 228–241.
- [148] T. Mashita, T. Kowada, H. Takahashi, T. Matsui, S. Mizukami, *ChemBioChem* **2019**, *20*, 1382–1386.
- [149] K. A. Brameld, B. Kuhn, D. C. Reuter, M. Stahl, *J. Chem. Inf. Model.* **2008**, *48*, 1–24.
- [150] D. Prischich, A. M. J. Gomila, S. Milla-Navarro, G. Sangüesa, R. Díez-Alarcia, B. Preda, C. Matera, M. Batlle, L. Ramírez, E. Giralt, J. Hernando, E. Guasch, J. J. Meana, P. de la Villa, P. Gorostiza, *Angew. Chem. Int. Ed.* **2021**, *60*, 3625–3631.
- [151] K. Tsuchiya, T. Umeno, G. Tsuji, H. Yokoo, M. Tanaka, K. Fukuhara, Y. Demizu, T. Misawa, *Chem. Pharm. Bull.* **2020**, *68*, 398–402.
- [152] F. Riefole, R. Sortino, C. Matera, E. Claro, B. Preda, S. Vitiello, S. Traserra, M. Jiménez, P. Gorostiza, *J. Med. Chem.* **2021**, *64*, 9259–9270.
- [153] N. J. Hauwert, T. A. M. Mocking, D. Da Costa Pereira, A. J. Kooistra, L. M. Wijnen, G. C. M. Vreeker, E. W. E. Verweij, A. H. De Boer, M. J. Smit, C. De Graaf, H. F. Vischer, I. J. P. De Esch, M. Wijtmans, R. Leurs, *J. Am. Chem. Soc.* **2018**, *140*, 4232–4243.
- [154] J. Tirado-Rives, W. L. Jorgensen, *J. Med. Chem.* **2006**, *49*, 5880–5884.
- [155] B. Biscussi, M. A. Sequeira, V. Richmond, P. Arroyo Mañez, A. P. Murray, *J. Photochem. Photobiol. A* **2021**, *418*, 113375.
- [156] A. Damijonaitis, J. Broichhagen, T. Urushima, K. Hüll, J. Nagpal, L. Laprell, M. Schönberger, D. H. Woodmansee, A. Rafiq, M. P. Sumser, W. Kummer, A. Gottschalk, D. Trauner, *ACS Chem. Neurosci.* **2015**, *6*, 701–707.
- [157] B. Cheng, J. Morstein, L. K. Ladefoged, J. B. Maesen, B. Schjøtt, S. Sinning, D. Trauner, *ACS Chem. Neurosci.* **2020**, *11*, 1231–1237.
- [158] J. Morstein, J. B. Trads, K. Hinnah, S. Willems, D. M. Barber, M. Trauner, D. Merk, D. Trauner, *Chem. Sci.* **2020**, *11*, 429–434.
- [159] B. Cheng, D. Shchepakin, M. P. Kavanaugh, D. Trauner, *ACS Chem. Neurosci.* **2017**, *8*, 1668–1672.
- [160] M. W. H. Hoorens, H. Fu, R. H. Duurkens, G. Trinco, V. Arkhipova, B. L. Feringa, G. J. Poelarends, D. J. Slotboom, W. Szymanski, *Adv. Ther.* **2018**, *1*, 1800028.
- [161] V. Arkhipova, H. Fu, M. W. H. Hoorens, G. Trinco, L. N. Lameijer, E. Marin, B. L. Feringa, G. J. Poelarends, W. Szymanski, D. J. Slotboom, A. Guskov, *J. Am. Chem. Soc.* **2021**, *143*, 1513–1520.
- [162] R. Huckvale, M. Mortensen, D. Pryde, T. G. Smart, J. R. Baker, *Org. Biomol. Chem.* **2016**, *14*, 6676–6678.
- [163] S. N. Mostyn, S. Sarker, P. Muthuraman, A. Raja, S. Shimon, T. Rawling, C. L. Cioffi, R. J. Vandenberg, *ACS Chem. Neurosci.* **2020**, *11*, 1250–1258.
- [164] J. Broichhagen, N. R. Johnston, Y. Von Ohlen, H. Meyer-Berg, B. J. Jones, S. R. Bloom, G. A. Rutter, D. Trauner, D. J. Hodson, *Angew. Chem. Int. Ed.* **2016**, *55*, 5865–5868.
- [165] B. J. Jones, R. Scopelliti, A. Tomas, S. R. Bloom, D. J. Hodson, J. Broichhagen, *ChemistryOpen* **2017**, *6*, 501–505.
- [166] K. Hinnah, S. Willems, J. Morstein, J. Heering, F. W. W. Hartrampf, J. Broichhagen, P. Leippe, D. Merk, D. Trauner, *J. Med. Chem.* **2020**, *63*, 10908–10920.
- [167] N. J. Hauwert, T. A. M. Mocking, D. Da Costa Pereira, K. Lion, Y. Huppelschoten, H. F. Vischer, I. J. P. De Esch, M. Wijtmans, R. Leurs, *Angew. Chem. Int. Ed.* **2019**, *58*, 4531–4535.
- [168] M. Ikura, S. Nakatani, S. Yamamoto, H. Habashita, T. Sugiura, K. Takahashi, K. Ogawa, H. Ohno, H. Nakai, M. Toda, *Bioorg. Med. Chem.* **2006**, *14*, 4241–4252.
- [169] F. W. W. Hartrampf, D. M. Barber, K. Gottschling, P. Leippe, M. Hollmann, D. Trauner, *Tetrahedron* **2017**, *73*, 4905–4912.
- [170] T. Chen, H. Xiong, J. F. Yang, X. L. Zhu, R. Y. Qu, G. F. Yang, *J. Agric. Food Chem.* **2020**, *68*, 9839–9877.
- [171] G. Quandt, G. Höfner, J. Pabel, J. Dine, M. Eder, K. T. Wanner, *J. Med. Chem.* **2014**, *57*, 6809–6821.
- [172] E. Bartels, N. H. Wassermann, B. F. Erlanger, *Proc. Natl. Acad. Sci. USA* **1971**, *68*, 1820–1823.
- [173] J. P. Van Der Berg, W. A. Velema, W. Szymanski, A. J. M. Driessen, B. L. Feringa, *Chem. Sci.* **2015**, *6*, 3593–3598.
- [174] M. J. Hansen, J. I. C. Hille, W. Szymanski, A. J. M. Driessen, B. L. Feringa, *Chem* **2019**, *5*, 1293–1301.
- [175] M. V. Westphal, M. A. Schafroth, R. C. Sarott, M. A. Imhof, C. P. Bold, P. Leippe, A. Dhopeswarkar, J. M. Grandner, V. Katritch, K. Mackie, D. Trauner, E. M. Carreira, J. A. Frank, *J. Am. Chem. Soc.* **2017**, *139*, 18206–18212.
- [176] J. Morstein, R. Z. Hill, A. J. E. Novak, S. Feng, D. D. Norman, P. C. Donthamsetti, J. A. Frank, T. Harayama, B. M. Williams, A. L. Parrill, G. J. Tigyi, H. Riezman, E. Y. Isacoff, D. M. Bautista, D. Trauner, *Nat. Chem. Biol.* **2019**, *15*, 623–631.
- [177] J. A. Frank, H. G. Franquelim, P. Schwille, D. Trauner, *J. Am. Chem. Soc.* **2016**, *138*, 12981–12986.
- [178] N. Hartrampf, T. Seki, A. Baumann, P. Watson, N. A. Vepřek, B. E. Hetzler, A. Hoffmann-Röder, M. Tsuji, D. Trauner, *Chem. Eur. J.* **2020**, *26*, 4476–4479.
- [179] M. W. H. Hoorens, M. E. Ourailidou, T. Rodat, P. E. van der Wouden, P. Kobauri, M. Kriegs, C. Peifer, B. L. Feringa, F. J. Dekker, W. Szymanski, *Eur. J. Med. Chem.* **2019**, *179*, 133–146.
- [180] D. Kolarski, S. Miller, T. Oshima, Y. Nagai, Y. Aoki, P. Kobauri, A. Srivastava, A. Sugiyama, K. Amaike, A. Sato, F. Tama, W. Szymanski, B. L. Feringa, K. Itami, T. Hirota, *J. Am. Chem. Soc.* **2021**, *143*, 2078–2087.

- [181] J. A. Frank, M. Moroni, R. Moshourab, M. Sumser, G. R. Lewin, D. Trauner, *Nat. Commun.* **2015**, *6*, 7118.
- [182] J. A. Frank, D. A. Yushchenko, D. J. Hodson, N. Lipstein, J. Nagpal, G. A. Rutter, J. S. Rhee, A. Gottschalk, N. Brose, C. Schultz, D. Trauner, *Nat. Chem. Biol.* **2016**, *12*, 755–762.
- [183] R. Tei, J. Morstein, A. Shemet, D. Trauner, J. M. Baskin, *ACS Cent. Sci.* **2021**, *7*, 1205–1215.
- [184] J. Morstein, M. A. Dacheux, D. D. Norman, A. Shemet, P. C. Donthamsetti, M. Citir, J. A. Frank, C. Schultz, E. Y. Isacoff, A. L. Parrill, G. J. Tigyi, D. Trauner, *J. Am. Chem. Soc.* **2020**, *142*, 10612–10616.
- [185] J. Broichhagen, M. Schönberger, S. C. Cork, J. A. Frank, P. Marchetti, M. Bugliani, A. M. J. Shapiro, S. Trapp, G. A. Rutter, D. J. Hodson, D. Trauner, *Nat. Commun.* **2014**, *5*, 5116.
- [186] C. E. Weston, A. Krämer, F. Colin, Ö. Yildiz, M. G. J. Baud, F. J. Meyer-Almes, M. J. Fuchter, *ACS Infect. Dis.* **2017**, *3*, 152–161.
- [187] L. Yet, *Privileged Structures in Drug Discovery: Medicinal Chemistry and Synthesis*, Wiley, Hoboken, **2018**, pp. 83–154.
- [188] X. Gómez-Santacana, S. M. de Munnik, P. Vijayachandran, D. Da Costa Pereira, J. P. M. Bebelman, I. J. P. de Esch, H. F. Vischer, M. Wijtmans, R. Leurs, *Angew. Chem. Int. Ed.* **2018**, *57*, 11608–11612.
- [189] X. Gómez-Santacana, S. M. De Munnik, T. A. M. Mocking, N. J. Hauwert, S. Sun, P. Vijayachandran, I. J. P. De Esch, H. F. Vischer, M. Wijtmans, R. Leurs, *Beilstein J. Org. Chem.* **2019**, *15*, 2509–2523.
- [190] D. Stumpfe, H. Hu, J. Bajorath, *ACS Omega* **2019**, *4*, 14360–14368.
- [191] N. N. Mafy, K. Matsuo, S. Hiruma, R. Uehara, N. Tamaoki, *J. Am. Chem. Soc.* **2020**, *142*, 1763–1767.
- [192] K. Matsuo, N. Tamaoki, *Org. Biomol. Chem.* **2021**, *19*, 6979–6984.
- [193] S. Mondal, S. S. Parekar, M. Nagar, P. R. Thompson, *ACS Chem. Biol.* **2018**, *13*, 1057–1065.
- [194] T. Lutz, T. Wein, G. Höfner, J. Pabel, M. Eder, J. Dine, K. T. Wanner, *J. Med. Chem.* **2018**, *61*, 6211–6235.
- [195] P. Kobauri, N. S. Galenkamp, A. M. Schulte, J. de Vries, N. A. Simeth, G. Maglia, S. Thallmair, D. Kolarski, W. Szymanski, B. L. Feringa, *J. Med. Chem.* **2022**, *65*, 4798–4817.
- [196] M. Volgraf, P. Gorostiza, S. Szobota, M. R. Helix, E. Y. Isacoff, D. Trauner, *J. Am. Chem. Soc.* **2007**, *129*, 260–261.
- [197] A. Reiter, A. Skerra, D. Trauner, A. Schiefner, *Biochemistry* **2013**, *52*, 8972–8974.
- [198] Y. Guo, T. Wolter, T. Kubař, M. Sumser, D. Trauner, M. Elstner, *PLoS One* **2015**, *10*, e0135399.
- [199] A. Duran-Corbera, J. Catena, M. Otero-Viñas, A. Llebaria, X. Rovira, *J. Med. Chem.* **2020**, *63*, 8458–8470.
- [200] J. Liu, D. Obando, V. Liao, T. Lifa, R. Codd, *Eur. J. Med. Chem.* **2011**, *46*, 1949–1963.
- [201] O. Tiapko, N. Shrestha, S. Lindinger, G. Guedes De La Cruz, A. Graziani, C. Klec, C. Butorac, W. F. Graier, H. Kubista, M. Freichel, L. Birnbaumer, C. Romanin, T. Glasnov, K. Groschner, *Chem. Sci.* **2019**, *10*, 2837–2842.
- [202] D. Fujita, M. Murai, T. Nishioka, H. Miyoshi, *Biochemistry* **2006**, *45*, 6581–6586.
- [203] J. Shonberg, P. J. Scammells, B. Capuano, *ChemMedChem* **2011**, *6*, 963–974.
- [204] T. W. Corson, N. Aberle, C. M. Crews, *ACS Chem. Biol.* **2008**, *3*, 677–692.
- [205] X. Sun, H. Gao, Y. Yang, M. He, Y. Wu, Y. Song, Y. Tong, Y. Rao, *Signal Transduction Targeted Ther.* **2019**, *4*, 64.
- [206] M. Békés, D. R. Langley, C. M. Crews, *Nat. Rev. Drug Discovery* **2022**, *21*, 181–200.
- [207] S. Bhaduri, N. Ranjan, D. P. Arya, *Beilstein J. Org. Chem.* **2018**, *14*, 1051–1086.
- [208] W. A. Velema, M. Van Der Toorn, W. Szymanski, B. L. Feringa, *J. Med. Chem.* **2013**, *56*, 4456–4464.
- [209] L. Agnetta, M. Kauk, M. C. A. Canizal, R. Messerer, U. Holzgrabe, C. Hoffmann, M. Decker, *Angew. Chem. Int. Ed.* **2017**, *56*, 7282–7287.
- [210] F. Riefolo, C. Matera, A. Garrido-Charles, A. M. J. Gomila, R. Sortino, L. Agnetta, E. Claro, R. Masgrau, U. Holzgrabe, M. Batlle, M. Decker, E. Guasch, P. Gorostiza, *J. Am. Chem. Soc.* **2019**, *141*, 7628–7636.
- [211] P. Pfaff, K. T. G. Samarasinghe, C. M. Crews, E. M. Carreira, *ACS Cent. Sci.* **2019**, *5*, 1682–1690.
- [212] M. Reynders, B. S. Matsuura, M. Bérouti, D. Simoneschi, A. Marzio, M. Pagano, D. Trauner, *Sci. Adv.* **2020**, *6*, eaay5064.
- [213] C. Dohno, S. N. Uno, K. Nakatani, *J. Am. Chem. Soc.* **2007**, *129*, 11898–11899.
- [214] N. A. Simeth, S. Kobayashi, P. Kobauri, S. Crespi, W. Szymanski, K. Nakatani, C. Dohno, B. L. Feringa, *Chem. Sci.* **2021**, *12*, 9207–9220.
- [215] B. Heinrich, K. Bouazoune, M. Wojcik, U. Bakowsky, O. Vázquez, *Org. Biomol. Chem.* **2019**, *17*, 1827–1833.
- [216] A. Mourot, T. Fehrentz, Y. Le Feuvre, C. M. Smith, C. Herold, D. Dalkara, F. Nagy, D. Trauner, R. H. Kramer, *Nat. Methods* **2012**, *9*, 396–402.
- [217] A. Mourot, C. Herold, M. A. Kienzler, R. H. Kramer, *Br. J. Pharmacol.* **2018**, *175*, 2296–2311.
- [218] V. F. Palmisano, C. Gómez-Rodellar, H. Pollak, G. Cárdenas, B. Corry, S. Faraji, J. J. Nogueira, *Phys. Chem. Chem. Phys.* **2021**, *23*, 3552–3564.
- [219] S. Ghosh, D. Usharani, A. Paul, S. De, E. D. Jemmis, S. Bhattacharya, *Bioconjugate Chem.* **2008**, *19*, 2332–2345.
- [220] W. Li, Y. Li, X. Yin, Y. Liang, J. Li, C. Wang, Y. Lan, H. Wang, Y. Ju, G. Li, *Tetrahedron Lett.* **2016**, *57*, 2539–2543.
- [221] Z. Xu, L. Shi, D. Jiang, J. Cheng, X. Shao, Z. Li, *Sci. Rep.* **2015**, *5*, 13962.
- [222] J. E. Gestwicki, G. R. Crabtree, I. A. Graef, *Science* **2004**, *306*, 865–869.
- [223] Y. H. Jin, M.-C. Lu, Y. Wang, W. X. Shan, X. Y. Wang, Q. D. You, Z. Y. Jiang, *J. Med. Chem.* **2020**, *63*, 4644–4654.
- [224] S. Pushpakom, F. Iorio, P. A. Eyers, K. J. Escott, S. Hopper, A. Wells, A. Doig, T. Williams, J. Latimer, C. McNamee, A. Norris, P. Sanseau, D. Cavalla, M. Pirmohamed, *Nat. Rev. Drug Discovery* **2019**, *18*, 41–58.
- [225] D. Schmidt, T. Rodat, L. Heintze, J. Weber, R. Horbert, U. Girreser, T. Raeker, L. Bußmann, M. Kriegs, B. Hartke, C. Peifer, *ChemMedChem* **2018**, *13*, 2415–2426.
- [226] J. C. dos Santos, A. Bernardes, L. Giampietro, A. Ammazalorso, B. De Filippis, R. Amoroso, I. Polikarpov, *J. Struct. Biol.* **2015**, *191*, 332–340.
- [227] S. Willems, J. Morstein, K. Hinnah, D. Trauner, D. Merk, *J. Med. Chem.* **2021**, *64*, 10393–10402.
- [228] K. Aggarwal, M. Banik, B. Medellin, E. L. Que, *Biochemistry* **2019**, *58*, 48–53.
- [229] K. Aggarwal, T. P. Kuka, M. Banik, B. P. Medellin, C. Q. Ngo, D. Xie, Y. Fernandes, T. L. Dangerfield, E. Ye, B. Bouley, K. A. Johnson, Y. J. Zhang, J. K. Eberhart, E. L. Que, *J. Am. Chem. Soc.* **2020**, *142*, 14522–14531.
- [230] A. Maresca, F. Carta, D. Vullo, A. Scozzafava, C. T. Supuran, *Bioorg. Med. Chem. Lett.* **2009**, *19*, 4929–4932.
- [231] L. S. Runtsch, D. M. Barber, P. Mayer, M. Groll, D. Trauner, J. Broichhagen, *Beilstein J. Org. Chem.* **2015**, *11*, 1129–1135.
- [232] G. Zhang, A. N. Plotnikov, E. Rusinova, T. Shen, K. Morohashi, J. Joshua, L. Zeng, S. Mujtaba, M. Ohlmeyer, M. M. Zhou, *J. Med. Chem.* **2013**, *56*, 9251–9264.
- [233] P. F. Cirillo, O. A. Asojo, U. Khire, Y. Lee, S. Mootien, P. Hegan, A. G. Sutherland, E. Peterson-Roth, M. Ledizet, R. A. Koski, K. G. Anthony, *ACS Med. Chem. Lett.* **2020**, *11*, 1843–1847.

- [234] R. Siewertsen, H. Neumann, B. Buchheim-Stehn, R. Herges, C. Näther, F. Renth, F. Temps, *J. Am. Chem. Soc.* **2009**, *131*, 15594–15595.
- [235] E. R. Thapaliya, J. Zhao, G. C. R. Ellis-Davies, *ACS Chem. Neurosci.* **2019**, *10*, 2481–2488.
- [236] M. R. Banghart, A. Mourrot, D. L. Fortin, J. Z. Yao, R. H. Kramer, D. Trauner, *Angew. Chem. Int. Ed.* **2009**, *48*, 9097–9101.
- [237] G. Cabré, A. Garrido-Charles, À. González-Lafont, W. Moormann, D. Langbehn, D. Egea, J. M. Lluch, R. Herges, R. Alibés, F. Busqué, P. Gorostiza, J. Hernando, *Org. Lett.* **2019**, *21*, 3780–3784.
- [238] M. Reynders, A. Chaikuad, B. Berger, K. Bauer, P. Koch, S. Laufer, S. Knapp, D. Trauner, *Angew. Chem. Int. Ed.* **2021**, *60*, 20178–20183.
- [239] L. Heintze, D. Schmidt, T. Rodat, L. Witt, J. Ewert, M. Kriegs, R. Herges, C. Peifer, *Int. J. Mol. Sci.* **2020**, *21*, 8961.
- [240] S. Li, N. Eleya, A. Staubitz, *Org. Lett.* **2020**, *22*, 1624–1627.
- [241] G. Schneider, U. Fechner, *Nat. Rev. Drug Discovery* **2005**, *4*, 649–663.
- [242] P. Schneider, G. Schneider, *J. Med. Chem.* **2016**, *59*, 4077–4086.
- [243] G. Schneider, D. E. Clark, *Angew. Chem. Int. Ed.* **2019**, *58*, 10792–10803.
- [244] M. Deiana, Z. Pokladek, J. Olesiak-Banska, P. Młynarz, M. Samoc, K. Matczyszyn, *Sci. Rep.* **2016**, *6*, 28605.
- [245] H. Zhang, H. Fu, X. Shao, C. Chipot, A. Monari, F. Dehez, W. Cai, *Phys. Chem. Chem. Phys.* **2018**, *20*, 22645–22651.
- [246] A. Bergen, S. Rudiuk, M. Morel, T. Le Saux, H. Ihmels, D. Baigl, *Nano Lett.* **2016**, *16*, 773–780.
- [247] X. Wang, J. Huang, Y. Zhou, S. Yan, X. Weng, X. Wu, M. Deng, X. Zhou, *Angew. Chem. Int. Ed.* **2010**, *49*, 5305–5309.
- [248] T. Tian, Y. Song, J. Wang, B. Fu, Z. He, X. Xu, A. Li, X. Zhou, S. Wang, X. Zhou, *J. Am. Chem. Soc.* **2016**, *138*, 955–961.
- [249] N. A. Simeth, T. Kinateter, C. Rajendran, J. Nazet, R. Merkl, R. Sterner, B. König, A. C. Kneutinger, *Chem. Eur. J.* **2021**, *27*, 2439–2451.
- [250] S. Bellotto, S. Chen, I. Rentero Rebollo, H. A. Wegner, C. Heinis, *J. Am. Chem. Soc.* **2014**, *136*, 5880–5883.
- [251] J. B. Baell, G. A. Holloway, *J. Med. Chem.* **2010**, *53*, 2719–2740.
- [252] P. Y. Lam, A. R. Thawani, E. Balderas, A. J. P. White, D. Chaudhuri, M. J. Fuchter, R. T. Peterson, *J. Am. Chem. Soc.* **2020**, *142*, 17457–17468.
- [253] Z. Qiao, H. Qi, H. Zhang, Q. Zhou, N. Wei, Y. Zhang, K. Wang, *Anal. Chem.* **2020**, *92*, 1934–1939.
- [254] Z. Qiao, J. Luo, Y.-Q. Tang, Q. Zhou, H. Qi, Z. Yin, X. Tang, W. Zhu, Y. Zhang, N. Wei, K. Wang, *J. Med. Chem.* **2021**, *64*, 16282–16292.
- [255] C. A. Lipinski, F. Lombardo, B. W. Dominy, P. J. Feeney, *Adv. Drug Delivery Rev.* **1997**, *23*, 3–25.
- [256] H. Kubinyi, *J. Recept. Signal Transduction* **1999**, *19*, 15–39.
- [257] J. Verma, M. V. Khedkar, C. E. Coutinho, *Curr. Top. Med. Chem.* **2010**, *10*, 95–115.
- [258] D. Paul, G. Sanap, S. Shenoy, D. Kalyane, K. Kalia, R. K. Tekade, *Drug Discovery Today* **2021**, *26*, 80–93.
- [259] Z. Cournia, B. Allen, W. Sherman, *J. Chem. Inf. Model.* **2017**, *57*, 2911–2937.
- [260] D. A. Erlanson, S. W. Fesik, R. E. Hubbard, W. Jahnke, H. Jhoti, *Nat. Rev. Drug Discovery* **2016**, *15*, 605–619.

Manuscript received: January 13, 2023

Accepted manuscript online: April 7, 2023

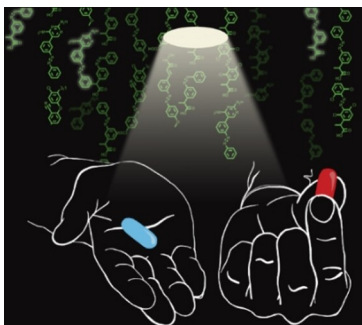
Version of record online: ■■■, ■■■

Reviews

Photoswitches

P. Kobauri, F. J. Dekker, W. Szymanski,*
B. L. Feringa* ————— **e202300681**

Rational Design in Photopharmacology
with Molecular Photoswitches



The state of the art of rational design in photopharmacology is analyzed with a focus on *E-Z* molecular photoswitches and on computer-aided approaches. By meticulously examining the design strategies of photopharmacology through the lens of medicinal chemistry, this review identifies existing trends and novel opportunities for the development of photoswitchable ligands.